3D-printed Microfluidic Control Systems

Yuan-Sheng Lee

A thesis

submitted in partial fulfillment of the

requirements for the degree of

Master of Science

University of Washington

2018

Committee:

Albert Folch, Chair

Jae-Hyun Chung

Jonathan Posner

Program Authorized to Offer Degree:

Mechanical Engineering

University of Washington

Abstract

3D-printed Microfluidic Control Systems

Yuan-Sheng Lee

Chair of the Supervisory Committee:
Associate Professor Albert Folch
Mechanical Engineering

Microfluidic devices are tools for manipulating fluids in microchannels to achieve a variety of functions, for instance, sample mixing, analytes testing and detection, dispensing, etc. These functions provided by microfluidic devices can be applied to different fields such as biology and medicine. Although microfluidic devices have revolutionized the research and development in drug delivery, oncology studies, cell culture and so on, fluids in the current devices are still not well automatically controlled. The devices are required to be either manipulated with complicated and time-consuming pipetting processes or connected with external control elements which make the whole system even larger (compared to the conventional devices or instruments lacking microfluidic technologies). Therefore, the integration of control systems into microfluidic devices is essential for improving their functionality, efficacy, and effectiveness.

3D printing is a new method for fabricating microfluidic devices and some of the advantages provided by 3D printing may not exist in the conventional approach to microfluidic device manufacturing. Well-trained personnel is not required to conduct the fabrication and the manufacturing time is shortened dramatically, from ~24 hours (soft lithography) to ~ 2 hours (3D printing). Here we demonstrate one of the most important components in a microfluidic control system, which is a 3D-printable microvalve that is transparent, built with a biocompatible resin, and has a simple architecture that can be easily scaled up into large arrays.[1] The open-at-rest valve design is derived from Quake's PDMS valve design. We used a stereolithographic (SL) 3D printer to print a thin (25 or 10 μm-thick) membrane (1200 or 500 μm-diam.) that is pneumatically pressed (~3–6 psi) over a bowl-shaped seat to close the valve. We used poly(ethylene glycol diacrylate) (MW = 258) (PEG-DA-258) as the resin because it

yields transparent cytocompatible prints. Although the flexibility of PEG-DA-258 is inferior to that of other microvalve fabrication materials such as PDMS, the valve benefits from the bowl design and the membrane's high restoring force since it does not need a negative pressure to re-open. We also 3D-printed a micropump by combining three Quake-style valves in series. The micropump only requires positive pressure for its operation and profits from the fast return to the valves' open states. Moreover, we printed a 64-valve array constructed with 500 μm-diam. valves to demonstrate the reliability and scalability of the valves. Overall, we demonstrate the 3D-printing of compact microvalves and micropumps using a process that precludes the need for specialized, time-consuming labor.

In this thesis, the control system device development process and the related experimental characterizations and setups are introduced, including the membrane (in the 3D printed Quake-style valve) thickness testing with resin study, membrane deflection simulation, 3D printer setup and optimization, design flow and device performance examination. Future work is placed in the last part of the thesis to suggest some potential work that can be done for improving the printing quality and functionality of the device.

Acknowledgements

I am indebted to a great number of people who help me complete this research successfully. First, I want to thank Prof. Albert Folch for his guidance, instructions and encouragement in every stage of my research work. This work would not have been done without his vision and critical decisions. I am also thankful to Dr. Nirveek Bhattacharjee for mentoring me, helping me and giving me advice. I have learnt so many things including research methods, problem solving skills and broad knowledge in this field when working with him. Not to mention his is literally a walking encyclopedia in our lab who always provides super useful clues and solutions and answers a variety of questions regarding physics, chemistry, biology, and engineering to explain the results and phenomena. I am grateful for his help. I also thank Kurt Castro, who is one of my best friends in my graduate school life. He supported my initial 3D printing work and research by teaching me how to use the Phoenix 3D printer and making some laser-cut pieces for me. We always share things no matter in our research, work, life, helping each other by providing suggestions and sometimes critiquing one another during practicing presentations.

I am also thankful to Dr. YongTae Kim for his guidance in the chemistry and biology part of this research. I thank Alex Kuo and Arman Naderi for their supports in 3D printing material development and 3D design counseling throughout the course of this research work. I thank to Dr. Lisa Horowitz, Adan Rodriguez, Vidhya Balaji and all the undergraduate students in the Folch lab as well. The financial support through research and teaching assistantship from University of Washington and Prof. Albert Folch are also acknowledged.

I thank all my friends for always being there for me, especially my Taiwanese friends here and my roommates in Mercer Court D408. You are my family here in Seattle and you support my life by encouraging me when I face difficulties and being happy for me when I share my joy and accomplishments. Finally, I thank my beloved parents for everything that they have done for me, I would not have grown up so much without the assistance and support across from the ocean from them!

Table of Contents

List of Figures

List of Tables

1. Overview- Introduction

1.1. Motivation and Significance

Microfabricated devices are ubiquitous in our lives. Smartphones, tablets (tablet computers), wearable instruments, point-of-care devices, and tire-pressure monitoring sensors (TPMS) for example, benefit from the technology of miniaturization. Therefore, they have experienced tremendous growth and evolution in the market. These devices are tiny, mass-producible, relatively affordable and because of the Micro Electrical Mechanical System (MEMS) technology. Microfluidic devices were introduced due to with this "miniaturization" trend and have been developed with some of the MEMS fabrication processes, such as processing fluid samples with feature sizes down to at least a "micro" level. Nowadays, microfluidics is always emphasized with a broad range of biomedical applications. The existence of microfluidic devices dramatically alters the fields of DNA sequencing, cell biology, and medical devices, enabling the testing and experiments to be done within a small cheap and thus reducing the cost from installing huge workflow systems and labor.

During the development of microfluidic devices, prototypes are usually made of plastic by utilizing hot-embossing, injection molding, or polydimethylsiloxane (PDMS) molding. Currently, PDMS is the most common material used in microfluidic devices because of its favorable mechanical properties (e.g. flexibility), optical transparency, and high biocompatibility. However, these fabrication methods require cleanroom microfabrication of molds using photolithography by well-trained individuals, especially when making a device containing multiple layers that need to be aligned and bonded. In addition, this process is time-consuming (e.g. bonding and alignment time for a 2-layer device can add up to more than 3 hours[2], and photomask manufacturing can take up to a few days). Since the process is based on manual labor, the device quality is highly dependent on personal skills. Although there are a great number of sophisticated microfluidic devices which have been presented with excellent engineering, the application and integration of microfluidic devices by non-engineering researchers are still low. For example, we need to spend a long period of time training biologists and biochemists until they are familiar with using photolithography related instruments to make their own devices.

To overcome the obstacles that accompany traditional microfluidic fabrication processes, 3D printing might be an alternative to avoid time-consuming and labor-demanding problems. 3D printing could provide a faster prototyping process including easy and direct 3D design steps compared to soft lithography, simple preparation processes (no need for photomasks, silicon wafers, a clean room, etc.), shorter fabrication time, and a simpler post-manufacturing procedure (no complicated connection between tubing and microchannels and further assembly)[3].

1.2. Background

This thesis tries to address two main problems in microfluidic device fabrication: 1) The high cost of soft lithographic processes, and 2) The high real-estate consumption of microfluidic automation components. While the cost is difficult to assess because every device is different, it helps to study it in simplified situations, as argued by Au. et al[4]. who looked at the cost of a simple, very small "canonical" soft lithographic device that can be made in one day. The total cost then includes the one-day wage of a research assistant, $160 + the cost of a silicon wafer, $10 + a high resolution photomask, $30 + 50 g of PDMS, $5 + 10 mL of SU-8 and 50 mL of SU-8 developer, $10 = $ 215. Note that the cost of this canonical device is 25% materials and 75 % labor, where the high cost of labor is caused by the long fabrication time of a device. In contrast, making the same device using 3D printers, the total cost is only $30 (1.5 hours of 3D printer setup and printing time) + $1 (resin including the photoinitiator + photosensitizer) = $31. As a result, the total cost of this canonical microfluidic device using 3D printing is ~7 times less than soft lithography, where the cost is significantly reduced by savings in fabrication time.

The second problem that this thesis is trying to address is the microfluidic device testing setup. As Fig. 1 shows, the setup of the whole microfluidic operation can be very bulky compared to the microfluidic chip itself. With all the combinations of external control components including valves, pumps, liquid bottles (reservoirs) and tubing, the microfluidic device loses the merits of being compact and thus the cost is higher than the ones which have internal components embedded. The complex setup with a number of external control objects also limits the potential of scaling microfluidic chips up into large arrays to conduct parallel experiments. Even though the design of the 3D printed Quake style valve cannot completely save the room for the device setup (we still need an outer air source to run our devices), we hope that we can

decrease the size of each component gradually. I believe that we are in the progress of truly miniaturizing microfluidic devices and making these devices fully portable.

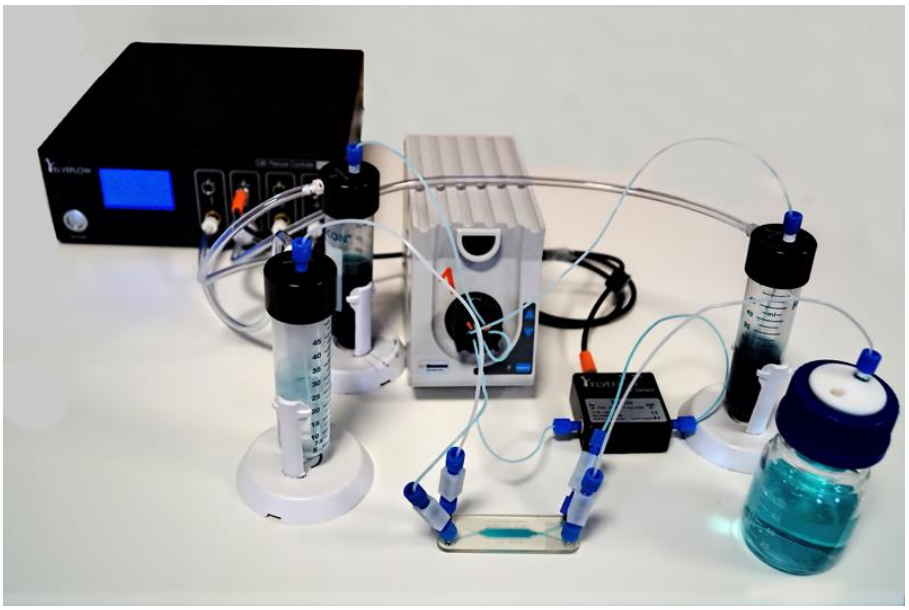

Figure 1: The traditional microfluidic device operation setup with external tubing, liquid bottles, valves and pumps.[5]

Microfluidic devices are important tools for researchers to approach the world of fluid volumes at the microscale. To efficiently conduct the tasks related to micro fluids, it is crucial to create an interface between macroscale and microscale fluid volumes that is able to contain complicated fluidic control systems, is well-established with visible channels and is simple to manipulate. Researchers have exhibited some great microfluidic devices with PDMS. However, some real-world problems need to be solved before entering the market that require low cost, short fabrication time and easy application, which PDMS devices do not offer. The other issue is the inability to be integrated with different systems, such as the connection interface between driving sources and channels in a microfluidic device. Therefore, we have been looking for alternatives to solve or bypass these problems. We hope that the new method that we explore can truly provide the necessary solutions and meet the demand of the real biomedical/biochemical market.

1.3. Approach

The development of 3D-printed microfluidic control systems in this thesis focuses on the design and manufacturing of the Quake style valve using SLA 3D printers. The membrane and bowl shape structure of the valve seat are two major factors in the valve design that directly

influence the performance of the valve. The thickness of the membrane and critical dimensions of the bowl-shape valve seat are studied and tested to improve the valve operation. The settings of the manufacturing process, which are the printing parameters of the 3D printer, are also crucial issues in the course of valve development. PEG-DA resins are mixed with different concentrations of photoinitiator and photosensitizer to gain better mechanical properties such as high flexibility. The settings of the 3D printer and its features are investigated and tested to achieve higher yield and quality of printed devices. To sum up, the goal of this research is to accelerate the fabrication process of microfluidic devices and lower the need of labor and cost with maintaining the same performance of these devices as the previous ones made with PDMS.

1.4. Summary

In chapter 2, the background, history, and purposes of building microfluidic devices are discussed. Chapter 2 also introduces the most popular fabrication method and material for making microfluidic devices- soft lithography and PDMS. In chapter 3, we introduce a variety of components in microfluidic devices such as microvalves and micropumps. This chapter also covers the development of 3D printed components in microfluidics. Chapter 4 elaborates the preliminary work of building 3D printed microfluidic control systems which includes resin selection and characterization, the first-used 3D printer (Phoenix Touch Pro) of this work, membrane thickness testing and membrane deflection simulations. In chapter 5, the design and development of the 3D printed Quake style valve are presented. The design processes of the 3D printed Quake style valve using a 3D modeling software, Inventor, are simply illustrated in chapter 6 as well. Chapter 6 demonstrates the functions, performances, and applications of the 3D printed Quake style valve by showing the flow rate and electrical current versus applied pressures experiments, dynamic behavior of the valve with different valve closing frequencies, the 3D printed Quake style pump design and its pumping performance, and the scalability of a 500-μm valve array. Chapter 7 explains the 3D printing setup including the material for 3D printing, features, and settings of the 3D printer. It also covers valve/pump device fabrication, flow rate measurements, current measurements to visualize the behavior of the 3D printed Quake style valve and the pump flow rate measurements. Finally, chapter 8 summarizes the 3D printing research that I have accomplished and provides the direction of potential research and development of 3D printing in the future.

2. Lab on a chip- microfluidic device fabrication

2.1. Introduction

Microfluidics, which have feature dimensions in the 1-500 μm range and volumes around microliter to nanoliters, is one of the core technologies in various micromachine systems that are developed for mechanical, chemical, biological and medical applications[6]. Fluid control systems have dramatically reduced in size due to the demand for small volume, portable, fast and mass-producible devices and equipment. An analogous example can be found in the development of personal computers. In the first half of 20th century, computers were developed with basic computational functions, but they also took much more room for installation and assembly. To set up a computer, three classrooms worth of space were required to contain all relays, valves, and tubes to perform a fundamental computing function. As shown in Fig. 2, a computer setup requires parallel connections of each enormous processor, however, the function is limited, and the processing speed is low. Compared to the computer that was developed in the early 20th century, a modern personal computer is at least ~1000 times smaller and has a more powerful computing ability with miscellaneous applications.

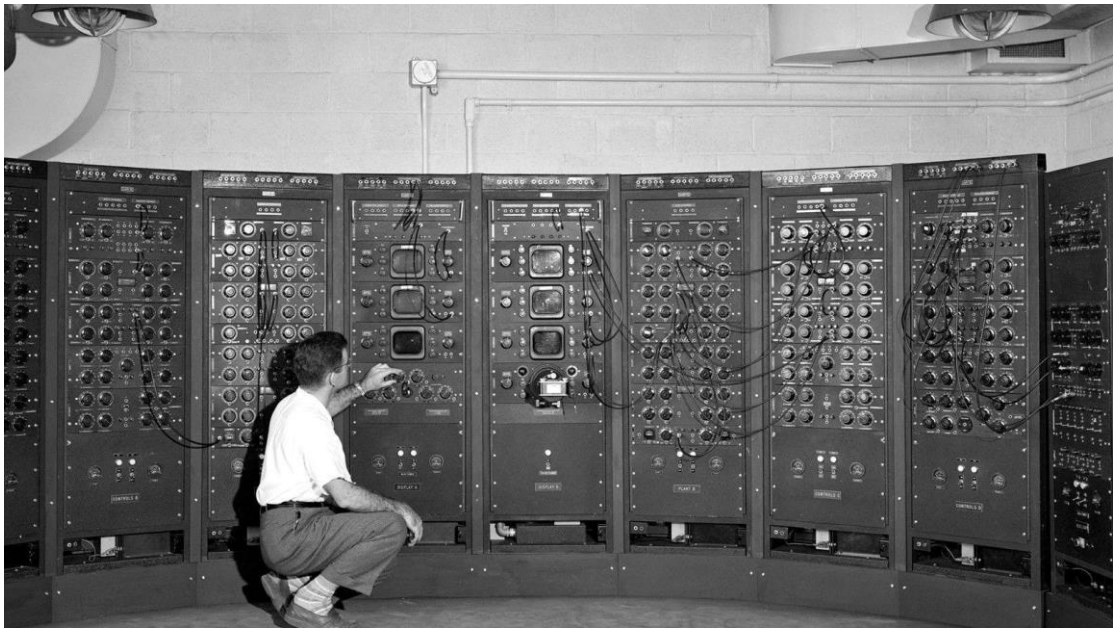

Figure 2: The setup of a huge computer in early the early 20th century[7]

There are also many microfluidic applications currently facing the same situation as the personal computer did 100 years ago. A bulky workflow contains many features and functions like biomedical analysis and data processing, and is able to work on multiple tasks at the same

time. Although it can handle complex processes and cover the needs of a high throughput laboratory with well-designed custom programming, the volume and cost are so high that most normal laboratories (e.g. laboratories in a school) cannot afford it. As the photo of Roche's product- cobas 8100 automated workflow series that is shown in Fig.3, the workflow is huge and takes much space to install it. Normally, it can only be found in large research institutes and hospitals owing to their sufficient budget and space. This bulky platform has already provided the solution to conducting experiments without intense labor but it does not have the properties of being inexpensive and portable. To achieve the goal of fabricating a low-cost, easily-manipulated and miniature device, many research groups in the field of mechanical engineering, electrical engineering, chemistry (chemical engineering), material science engineering and bioengineering have been developing a so-called "Lab-on-a-chip" device (Fig. 4) The concept of "Lab-on-a-chip" is to use a "miniature" (or at least portable) chip (device) to execute multiple processes and finish the testing within a chip in a short period of time.

Figure 3: Roche cobas® 8100 automated workflow series[8]

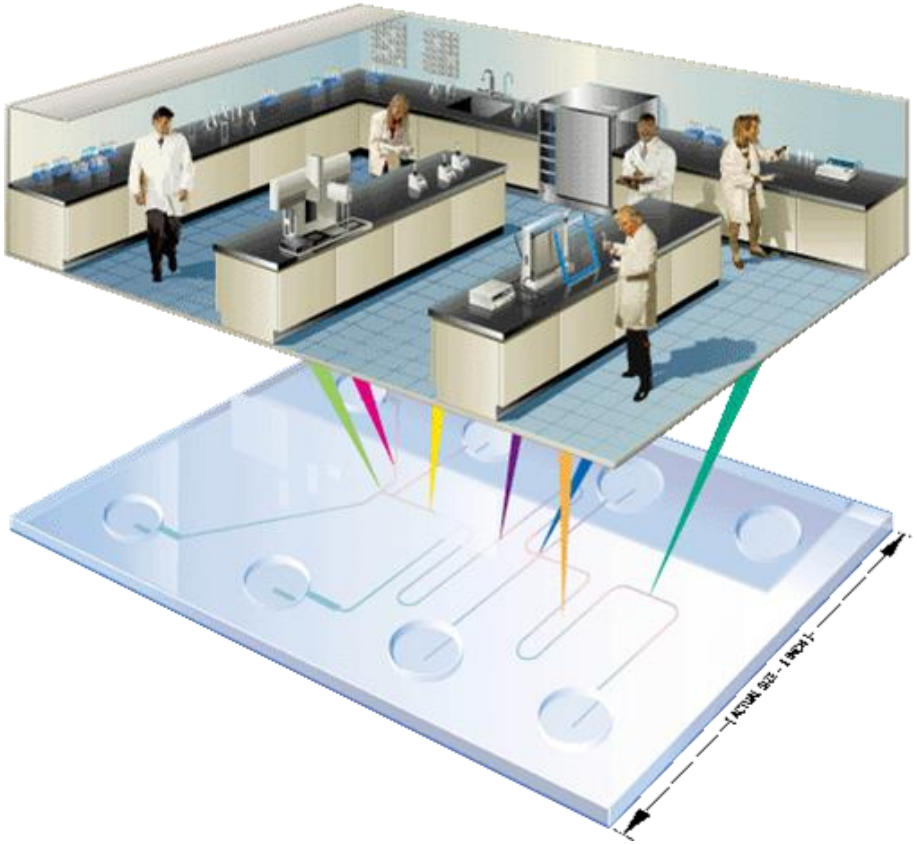

Figure 4: A conceptual schematic of a Lab-on-a-chip device[9]

2.2. Lab on a chip – the scope and applications

The definition of Lab on a chip is a device with an integration of several laboratory functions on a chip which has a size from millimeters to a few square centimeters and that are able to process exceedingly little amount of fluid volumes down to 10^{-15} liters. The demand for lab on a chip is followed by some advantages listed below[9]-

1. A low dosage of reagent, due to the small volume of chips (devices) (ex. Blood testing, instead of drawing a tube of blood and testing with a large corresponding amount of reagent, a blood droplet can be taken from the tip of a finger and mixed with a low dosage of regents and buffer, minimizing cost and usage of liquid.)
2. A high control speed and better analysis because of fast heating and cooling time (high surface to volume ratio and small heat capacities) and short mixing time (a short distance of diffusion).
3. A faster response to the system, leading to better process control.
4. Generates a more high-throughput analysis since it is compact enough to create massive

parallelization.

5. The ability to contain large integration of functionality owing to systems' small volume and compactness.
6. The small volume allows for mass production, fabrication of cost-effective disposable chips and low cost

Lab on a chip devices, which are also called "Micro Total analysis systems" (μTAS), are one of the branches under MEMS. The scope of lab on a chip devices can range from semiconductors, which have the earliest application in pressure sensor with Complementary metal–oxide–semiconductor (CMOS) embedded, to a blooming research in genomics and DNA-sequencing in the biochemical/medical field, which is the most common application in Lab on a chip nowadays. Due to the rise of the biomedical research and development, microfluidics have become one of the indispensable technologies in the development of Lab on a chip. The critical functions of a lab on a chip device, including liquid delivery, sample preparation, separation, detection, and reagent mixing, require the assistance from microfluidics. Besides the construction of microchannels, lab on a chip devices also need some mechanical flow control and analysis components like pumps and valves or sensors like flowmeters or viscometers. Without the study and development of microfluidics, we are not capable of applying bio/genomics-related research and experiments on lab to a chip devices.[10,11]

2.3. Microfluidic device fabrication method- soft lithography

There are several considerations when choosing designs or materials for microfluidic systems: needed functions, conditions accompanied by the functions, and applications. Silicon and glass substrates were first introduced in the initial stage of microfluidic device development. Nonetheless, neither has become the mainstream of microfluidic device manufacturing methods. Even though the patterns of micro-components can be well-defined by physical or chemical vapor deposition (PVD or CVD, additive methods) and wet or dry etching (subtractive methods), the material properties, stiffness and transparency, are the biggest hindrances when using this kind of device. The utilization of glass has somewhat reduced the difficulty of observation when compared to silicon, but its characteristics such as non-gas permeability and low nonspecific adsorption cause another problem when integrating with some biological applications. Moreover, fabrication with silicon and glass is too expensive due to the requirements of etching and deposition. In the late 1990s, Dr. George Whitesides' group

from Harvard first showcased the fabrication and procedure of Poly-dimethyl-siloxane (PDMS) based microfluidic devices that were integrated with water-based and biological applications.[6] After the first demonstration of the PDMS-based microfluidic device, more than 10,000 studies have been published with the use of PDMS in different research fields. The fabrication of PDMS microfluidic devices has been standardized because of the wide use of this material. Microfluidic devices are manufactured using the "Soft Lithography" process. The basic concept is to make a mold with microfluidic patterns which can firmly attach to the substrate, which is created using the technique of photolithography, then continue to use the same mold to replicate the same device (patterns) repeatedly until the mold is unusable due to wear and tear or the need for design change.[12]

There are five main steps in the soft lithographic microfabrication process-

1. Design of photomasks

   Photomask design is the first step in the soft lithography process. Designs are usually designed using 2D CAD software: AutoCAD. The function of the mask is to create differentiated UV-exposure in the step of photolithography, which is an optical process in microfabrication that projects and transfers patterns onto a substrate. A photolithographic mask is typically made of transparent fused silica, which consists of blanks and non-transparent patterns on it.
2. Fabrication of photomasks

   The design will be exported and sent to the fabrication process after the design process is done and checked. There are some methods to fabricate photomasks for photolithography like exposing or writing. The most common type of masks is a piece of soda lime glass with a layer of Chrome film and the patterns on it are created using a laser writer at 20,000 dpi. The pattern is transferred to the Chrome film when the resist layer is removed from the surface of the film.
3. Fabrication of the soft-lithographic mold using photolithography

   A three-dimensional pattern is created with the coating of a thin layer of photoresist (PR) by spin-coating and a UV-exposure step with a photomask sitting between a UV-light source and a photomask. The most common negative photoresist- SU-8 is coated on a silicon wafer. The photoresist on a wafer is then exposed when UV light passes through a photomask. The photoresist will be solidified when UV light penetrates through transparent regions on a photomask and the rest will remain the same since it is not exposed to UV. After a series of post-processing procedures including baking and

development, the solidified photoresist strongly attaches on the photomask and the rest is removed and washed away. The patterned silicon wafer is ready to serve as a master mold and we can pour PDMS on the mold to make microchannel structures. Fig. 5 shows the solidified SU-8 patterns on a silicon wafer.

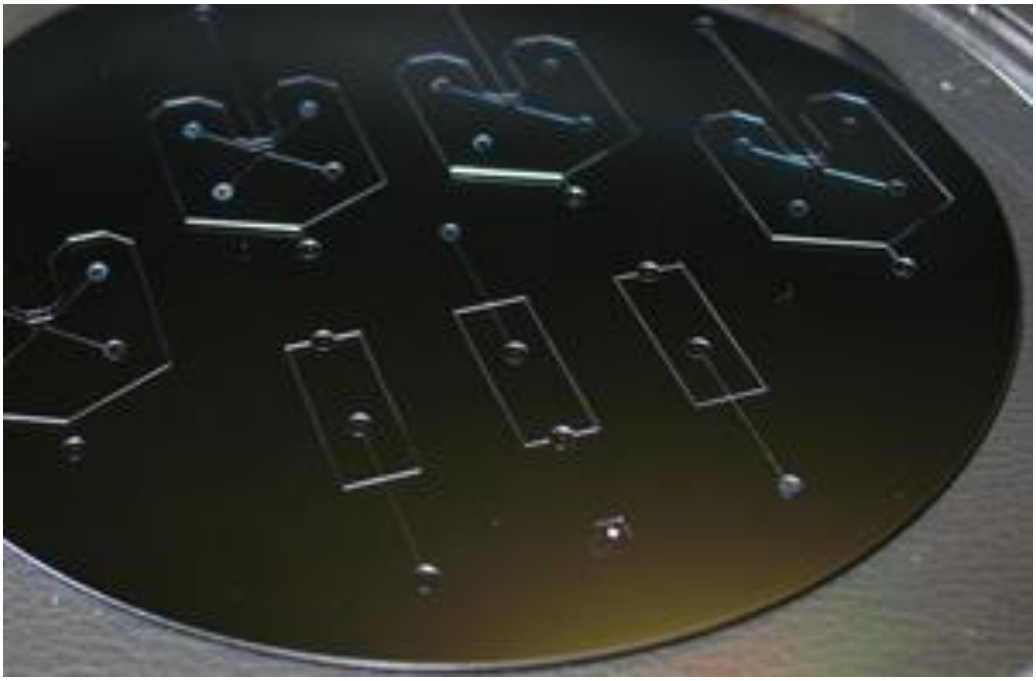

Figure 5: Patterns created on a master mold (Si wafer) using photolithography[13]

4. PDMS molding from the master mold

   The surface of the master mold is treated with Trimethylsilyl chloride (TMSCI) vapor to prevent the adhesion between the mold and PDMS. The base of PDMS is mixed with the curing reagent of PDMS in a ratio of 10:1 to start the curing process. After one-minute deposition of TMSCI, PDMS is then poured onto the silicon master mold and degassed in a desiccator for about an hour to remove all the bubbles in it. After the degassing process, the mold with PDMS is then put in the oven at 70 ˚C overnight to accelerate the curing process. PDMS can be peeled off from the wafer after the curing process is done.

5. Assembly/Bonding of layers

   The channels created with the master mold are open and therefore need a cover or roof to be closed. The open channels are usually bonded to a glass slide or a non-patterned PDMS layer. The bonding between glass/PDMS and PDMS happens when two

components are treated with Oxygen plasma and kept on a hot plate at 70 ˚C for 15 minutes.

2.4. Properties of PDMS

PDMS is a mineral organic polymer, which consists of carbon and silicon, of the siloxane family (a combination of silicon, oxygen, and alkane, the formula is shown in Fig. 6). It is also used as a food additive (E900), an anti-foaming agent in beverages or lubricating oils and in shampoo. For the applications in microfluidic devices, PDMS base is mixed with the cross-linking agent, then poured into a master mold and heated up to ~70 ˚C to obtain an elastomeric replica of the mold. There are three major reasons that PDMS is so famous and widely-used in the biomedical/chemical field: transparency, flexibility, and biocompatibility. It is also copy-right free, gas-permeable, easily-prepared, cheap, and water-impermeable (hydrophobic). PDMS is available as Sylgard 184 (Dow Corning) with two types of silicone elastomeric material in a kit. For making PDMS from liquid type to solid, the base which has Dimethyl siloxane terminated by dimethyl vinyl groups is mixed with a curing agent, which is dimethyl methyl hydrogen siloxane in a ratio of 10: 1. With this mixing ratio, the Young's Modulus of PDMS ranges from 0.36 MPa to 2.97 MPa.[51415] Table. 1. shows 8 properties of PDMS with its characteristics and consequences.

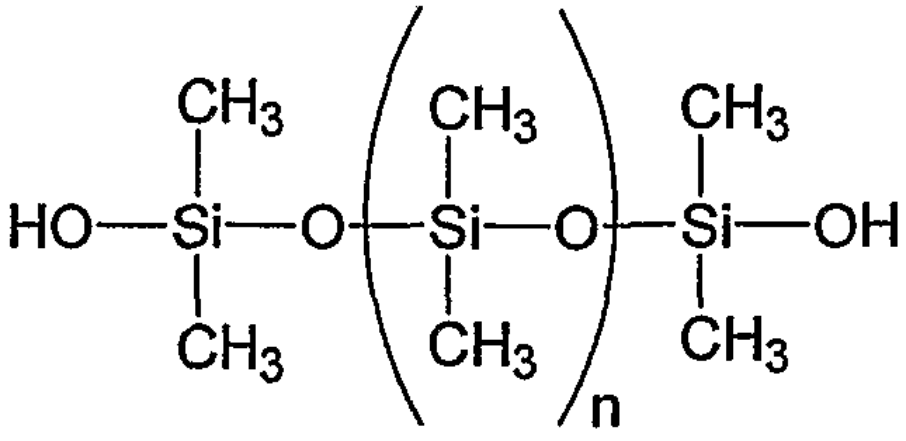

Figure 6: The structural formula of PDMS, the empirical formula of PDMS is $(C_2HO_6Si)_n$ and the fragmented formula is $CH_3[Si(CH_3)_2O]_nSi(CH_3)_3$, where n is the repetition number of monomers. PDMS will be in liquid type when the value of n is low and semi-solid type when the value of n is high. The siloxane bonds result in a flexible polymer

chain with high viscoelasticity.[15]

Property	Characteristic	Consequence
Optical	Transparent; UV cutoff, 240 nm	Optical detection from 240 to 1100 nm
Electrical	Insulating; breakdown voltage, 2 × 107 V/m	Allows embedded circuits; intentional breakdown to open connections
Mechanical	Elastomeric; tunable Young's modulus, typical value of ~750 kPa	Conforms to surfaces; allows actuation by reversible deformation; facilitates release from molds
Thermal	Insulating; thermal conductivity, 0.2 W/(m,K); coefficient of thermal expansion, 310 µm/(m,°C)	Can be used to insulate heated solutions; does not allow dissipation of resistive heating from electrophoretic separation
Interfacial	Low surface free energy ~ 20 erg/ cm	Replicas release easily from molds; can be reversibly sealed to materials
Permeability	Impermeable to liquid water; permeable to gases and nonpolar organic solvents	Contains aqueous solutions in channels; allows gas transport through the bulk material; incompatible with many organic solvents
Reactivity	Inert; can be oxidized by exposure to a plasma; Bu4N+F-((TBA)F)	Unreactive toward most reagents; the surface can be etched; can be modified to be hydrophilic and also reactive toward silanes; etching with (TBA)F can alter the topography of surfaces
Toxicity	Nontoxic	Can be implanted in vivo; supports mammalian cell growth

Table 1: Physical and Chemical Properties of PDMS[6]

2.5. The application and commercialization of using stereolithography and PDMS

As mentioned in Sec. 2.4, PDMS has several merits such as transparency (it helps the observation of channels and components in the device under a microscope), low autofluorescence and biocompatibility. PDMS has a number of applications including screening conditions for protein crystallization, laboratory demonstrations such as high-throughput screening in drug development, bioanalysis, examination and single cells/molecules manipulations, control of multiphase flows, cell biology, chemical synthesis and microanalytical systems for bioanalysis. PDMS microfluidic devices can be classified into two categories- Passive and active devices. Passive devices are flow channels, chambers mixers, generators and so on, which are not "moving" parts in microfluidic devices. Active devices consist of pumps, valves, and multiplexers. Professor Stephen Quake from California Institute of Technology showed a powerful application of PDMS and soft lithography in microfluidics by inventing a so-called "Quake valve", which is a structure of multiple PDMS layers stacked together. The basic concept of the valve is to have 3 layers combined as a sandwich structure with one control channel lying perpendicularly on one flow channel with a thin layer of membrane in between. The Quake group has taken advantage of this simple structure and successfully improved the technology and broadened the applications in the field of Integrated Fluidic Circuits (IFCs). This technology has been commercialized and brought into the market with the establishment of the company- Fluidigm Corporation. They utilized microfluidic related technologies derived from Integrated Fluidic Circuit to integrate valves into their device for controlling flow in different channels. The development of IFCs allows for rapid, high-throughput and reproducible analysis of genetic markers across thousands of DNA samples in a very short amount of time[16]. This amazing development in the field of DNA analysis shows a high potential of growth in microfluidic devices with the integration of miniature active components. It can be expected that more and more biomedical/biochemical experiments and testing like cell/drug sorting, affinity measurement of substances, and immunoassays will be done within a microfluidic device and be widespread in the market. Nevertheless, Fluidigm is facing some hurdles due to high costs of the chips despite the fact that it has a dramatic impact in genomics, biophysics, and biochemistry. This example casts doubts on whether startups focusing on microfluidics have the ability to produce PDMS devices with such a heavy burden.

2.6. Limitations of using PDMS with soft lithography

Although PDMS has become one of the most popular materials in the field of microfluidics due to its advantageous properties: flexible, transparent, biocompatible, inexpensive, etc., it has some significant downsides leading some research groups to transition from PDMS and soft lithography to other fabrication methods, like 3D printing. Current focuses on translation and low-cost microfluidic devices create some problems for PDMS and soft lithography. PDMS molding and related processes such as curing, assembly, bonding and inlet/outlet punching require a tedious manual process, preventing these microfluidic devices from being automated. This implies that the fabrication is expensive, and cannot meet the requirements to be inexpensive in the market. For example, a 3D or multi-layer structure needs to be produced with well-trained, intensive labor and tedious, repetitive lithographic processes. As we can see, it limits the complexity of designs in the Z-direction substantially. Not only does the fabrication process hinder the construction in the Z-direction, but the channel itself, made with a master mold does not appear closed, so a piece of glass or PDMS needs to be bonded and sealed on the opening side. Many devices fail in the bonding stage due to misalignment, structure limitations and inappropriate treatments. Furthermore, the user interfaces, which are inlets and outlets, of PDMS devices are apt to leakage and inconvenient connection. The control systems of microfluidic devices, including computer software, fluid driving equipment, and pressure sources, need some engineering skills and instruments that are not usually seen in biomedical labs. Therefore, some alternative solutions like stereolithography have emerged for microfabrication applications. Table. 2 shows the comparison of microfluidic device fabrication strategies [14]. According to this table, we can see that the setup cost of PDMS is around 4-80 times higher than 3D printing. Additionally, the turn-around time (device fabrication time) can be reduced ~12 times if we use 3D printing to make microfluidic devices instead of soft lithography. As far as I am concerned, time and cost are the two major focuses in the development and manufacturing of microfluidic devices. We can help non-engineering researchers and developers come across the device fabrication barriers as long as both time and cost can minimize.

	Soft lithography	*Injection molding*	*Paper microfluidics*	*3D printing*
Setup cost	~$80k	>$50k	<$1k	$1–20k
Cost per print/materials	High	Low	Low	High
Turn-around time	~24 h	3 weeks	<2 h	<2 h
3D capability	Layered 2D designs	Layered 2D designs	Layered 2D designs	3D digital designs
Fluid automation	Routine	Difficult	Rudimentary	Demonstrated
Throughput	Low	Very high	High	Medium
Manufacturability	Poor	Poor	Good	Good

Table 2: The comparison among 4 main microfluidic device manufacturing methods[3]

2.7. Introducing 3D-printing to microfluidic device fabrication

3D printing has been chosen for one of the fabrication methods to improve the manufacturability of microfluidic devices. Its characteristics of rapid manufacturing and simple fabrication processes are favorable for people in the biomedical field, especially for those who do not have a strong engineering background. There are three major types of 3D printing approaches- Stereolithography (SL or SLA), Multi Jet Molding (MJM), and Fused Deposition Molding (FDM). The schematic of each printing technique is shown in Fig. 7.

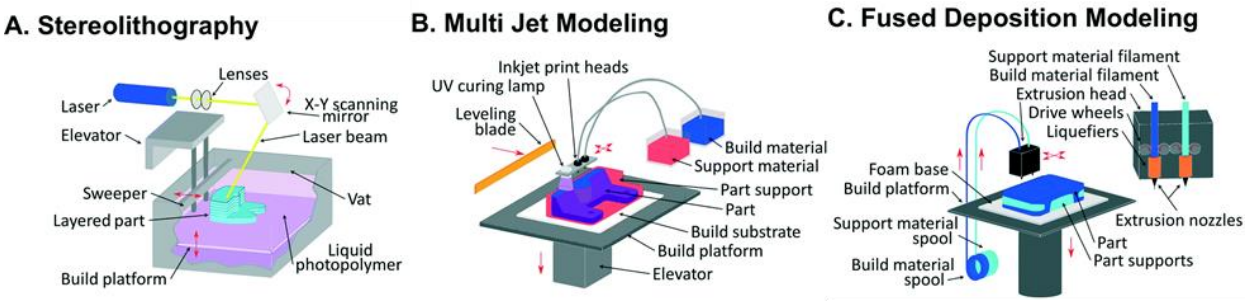

Figure 7: Different types of 3D-printing techniques (A) Stereolithography (SL) (B) Multi Jet Molding (MJM) (C) Fused Deposition Molding (FDM) - Image reproduced from Ref 3 with the permission from Royal Society of Chemistry.

I use Stereolithographic Digital Light Processing printing (SLA-DLP) to print my microfluidic

devices (Fig. 8) owing to various reasons such as the most rapid prototyping speed among the three printing techniques mentioned above, allowing for using custom resin and its simple control system. Stereolithography is quite similar to photolithography except for the need for photomasks. The liquid polymer resin is stored in a resin tray (a vat) and the pattern of each 2D layer in the 3D structure is created by shining UV light to the unpolymerized resin[17]. Stereolithographic 3D printers build a 3D device by generating different shapes/patterns for each layer with UV light and the uncured resin will be polymerized and thus solidified after being exposed to the UV light. The polymerization process is the same as the solidification process of photoresist in photolithography. However, the bonding process is not needed in 3D printing when building multilayer (3D) structures, each layer adheres to the previous layer directly. Thus, alignment and bonding are not required to construct 3D objects, as a result, the complexity and time spent of the fabrication process are reduced considerably. All cavities, channels, and walls are built by changing the UV pattern for each layer. Stereolithography is a powerful automation fabrication technique that can generate or print almost any kind of structures and shapes at medium-volume throughputs. Every feature in the design can be done by direct laser writing or digital light processing (DLP) by controlling the on and off of each micromirror. There are also many designs and fabrication methods that we can choose from, including generating 3D designs by using CAD software and print it out using personal printers or ordering by mail (sending the design to manufacturing service companies without making on our own).

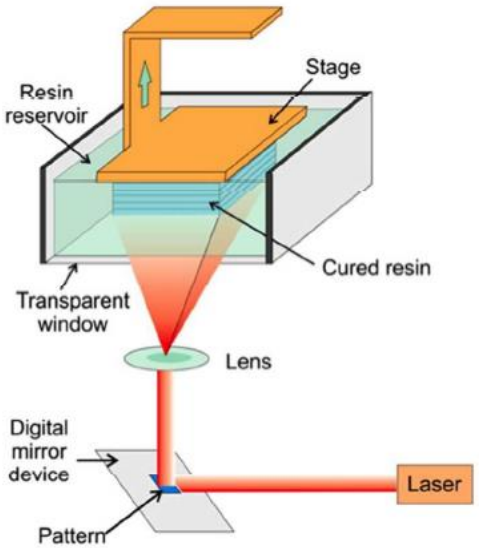

Figure 8: The configuration of an SLA-DLP printer.[18] Image reproduced from Ref 18 with the permission from American Chemical Society

3. Components in microfluidic devices

3.1. Introduction

There are several essential components in microfluidic systems. For example, channels, pillars, connectors, reservoirs, mixers, valves, and pumps are basic elements in miscellaneous types of microfluidic devices. These types of components, as described above, are classified into two main groups- active and passive components. The development of fabrication in passive parts such as channels, pillars, reservoirs, is already mature. On the contrary, the design and manufacturing of active parts are not as simple as passive parts. For instance, active parts need to be integrated with different actuation mechanisms including electroosmotic, electrochemical, pneumatic and etc. The automation of microfluidic systems requires a strong combination and integration of both active parts and passive parts. To truly invent and make a portable, easily-control and low-cost microfluidic device, we need to shrink down the size of components in the system. Without the direct integration of these components, the significance of these applications will be unapparent or it will even create new problems in a system. If channels are the only microfluidic component in the device without any internal control unit, they will need to be connected to external control systems such as valves and pumps to achieve "automation" of the device. However, the external systems are normally too large for a microfluidic device. As shown in Fig. 9, the pump itself is already much larger than the microfluidic device. The application of the microfluidic device that is shown in Fig. 9 only saves the consumption of liquid and reagents and eliminates the need of pipetting but not the space. The miniaturization of microfluidics devices is not accomplished without the integration of control systems. A similar case can be also found in the design of a smartphone. All features including a speaker, microphone, keyboard or even a camera are combined in a small case without falling apart or connected externally. If we can integrate a valve or a pump into a small microfluidic chip, the space that is taken by the whole system will be little and the number and complexity of connections between each component by means of tubing, wires and cable can be reduced. Therefore, the integration of all miniaturized passive and active parts in a confined volume is essential in the development of microfluidic devices.

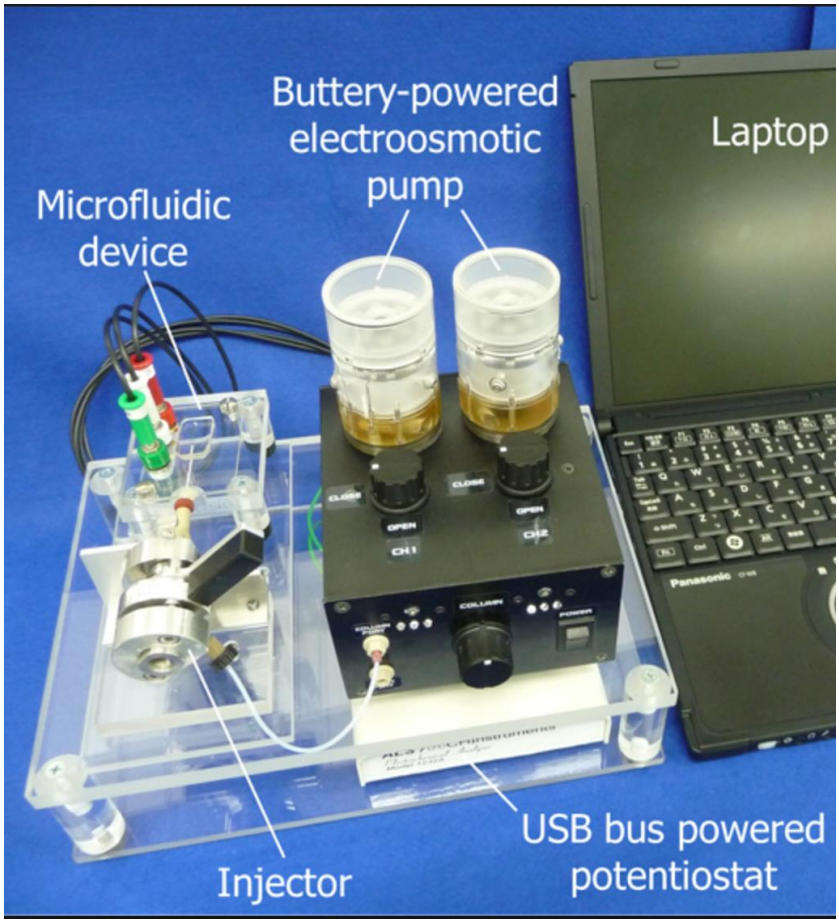

Figure 9: The system setup of a microfluidic device with external control systems, pumps and a laptop.[19]

3.2. Control dynamic behaviors within microfluidic devices

The control systems in microfluidic can be simply sorted into two categories- active and passive. Active components, as the name implies, are usually movable and not always fixed to a certain position or location in a device. With a certain type of control, such as applying current or air pressure to a component or object, some actions will take place in a device like deflection or deformation. Unlike passive components, which do not change its position and shape or sometimes do not generate thrust or disturbance spontaneously (e.g. channels and pillars), active parts provide driving force or potential for liquid and particles to move in a system or device. In this section, active valves and pumps are the two major focuses and will be introduced with the functions and working mechanisms in detail. Microvalves and micropumps are crucial and basic in many different types of microfluidic systems. Microvalves allow for fluid flow control including liquid movement and flow direction in microchannels by changing different macroscopic parameters. Valves can be actuated and controlled mechanically,

electrokinetically, and pneumatically by changing phases or by utilizing external forces. All active valves need an external energy for actuation so the control interface between the internal components and the external source is also very important. A micropump is also one of the critical components as well because it provides the driving force and controls liquid movements in microfluidic networks. There are several types of micropumps which can be categorized into two main types- active and passive. Integration of micropumps into microfluidic devices is also the main task in the microfluidic device development since it helps reduce the need for external equipment and decrease dead volumes between the pump connection interface.[20,21]

3.3. Microvalves

A valve is a device that regulates, directs or controls the flow of a fluid by opening or closing passageways. When a valve is open, fluid flows from a higher-pressure side to a lower pressure side. When a valve is closed, fluid is obstructed and stalls. A microvalve is a small valve which is in the scale of typically submillimeter or even smaller, controlling routing, timing, and separation of fluids within a microfluidic device. It is a vital component for integrating complex designs or functionality into a microfluidic device. There are five major types of active microvalves which are pneumatic, burst, electrokinetic, phase change, and pinch. Except for electrokinetic valves, the rest of four types of valves basically exploit the displacement or deformation of a membrane to control flows.[22] (An example is shown in Fig. 10) Pneumatic valves are normally actuated by controlling a soft, bendable membrane so that it can change the behavior of a flow in the flow channel. Burst valves are opened when a flow overcomes a certain resistance in the channel or when a temporary membrane collapses due to the thrust of the flow, therefore it can only be used one time. Electrokinetic valves serve as fluid routers which are operated in continuous flow systems, using electroosmotic flow to change the path of fluids from one channel to another. Phase-change valves regulate flow by alternating different phases of materials such as paraffin, hydrogels or aqueous solutions. Pinch valves, which are similar to pneumatic valves, manipulate the deformation of PDMS physically using mechanical pressure.

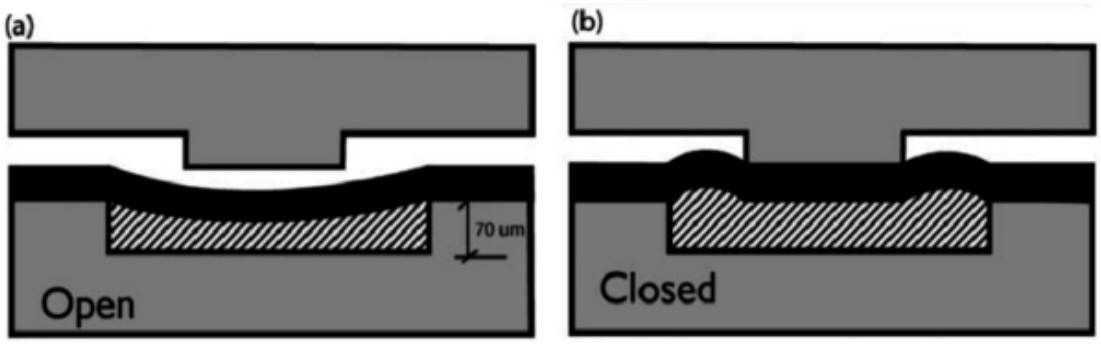

Figure 10: A thermal expansion microvalve, (a) shows the open state of the valve, (b) shows the closed state of the valve. The membrane which is dark black in the figure deflects when heat is applied to it.[22] Image reproduced from Ref 22 with the permission from American Chemical Society.

3.3.1. Pneumatic microvalves

Pneumatic microvalves take advantage of the easily-deflecting, high ductility and malleability properties of PDMS to stop or interrupt flows. This idea was brought out by Stephen Quake's group from Caltech. in 2000, which is demonstrated in the paper "Monolithic Microfabricated Valves and Pumps by Multilayer Soft Lithography" and has a notable name "Quake valve". The working principle of pneumatic valves is to apply air pressure on a piece of flexible membrane, which then seals against the flow channel (the valve seat) and blocks the pass way of fluid when it deflects. Air pressure is generated within a closed chamber or channel through connecting air source to the inlet of this closed region. In the design of Quake valves, a channel which is filled with air pressure is termed "control line" or "control channel". A control channel lies on the top of a flow channel and is separated by a barrier, which is a piece of thin membrane. Typically, a membrane is actuated by controlling air pressure in a control channel via an outer-connected air pressure. Sometimes a control channel is also filled with fluid if air permeation through the membrane needs to be prevented. This design is so widely-adopted in microfluidic devices since it can be integrated with standard soft lithography processes, which a great number of laboratories are familiar with. Basically, there are three types of pneumatic microvalves: Normally-open, normally-closed and lateral deflection valves.

Normally open valves are also called open-at-rest valves. The membrane does not deflect and block the flow channel until it is actuated by an outer force. When positive pressure is applied to a control channel, the force generated by the air pressure pushes the membrane to close the valve and thus the flow in the flow channel is halted. Quake valves and plunger valves are the

most seen normally open membrane microvalves. Quake valves are composed of three different layers- control, flow and membrane layers, which liquid flows in one plane. Whereas plunger valves have four layers and liquid flows between two of the planes.[2]

The Quake microvalves consist of a control channel that overlaps partial of a flow channel perpendicularly (Fig. 11). The overlapping section defines the shape of the membrane, which is usually 5-15 µm thick and separates the control and flow channels. The first version of the Quake valve was a push-down structure where a rectangular-cross-section control channel was placed on top of a semicircular-cross-section flow channel. Noted that the cross-section of the flow channel needs to be semicircular; otherwise, the membrane cannot seal against the valve seat perfectly due to the gaps in the corner of walls. The size of the flow channel is 100 µm wide and 10 µm high with 40 kPa actuation pressure to seal the flow channel at zero back pressure. The second generation of the Quake valve was invented by the same group, which is a push-up design and has a lower closing pressure compared to the first version. They swapped the configuration of the flow and control channels, which a semicircular flow channel is on top of a rectangular control channel. In this design, the thickness of the membrane is uniform and the air pressure coming from the bottom control channel shoves the membrane up to seal against the valve seat. Due to the design of this planar membrane, flow channels are allowed to be made higher (from 10 µm to 55 µm) and the required closing pressure is lower as well (from 40 kPa to 15 kPa).

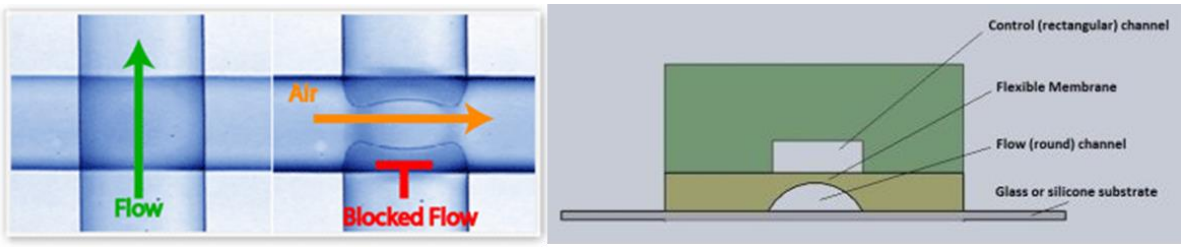

Figure 11: The configuration and working mechanism of the first version Quake valve, which has a flow channel lying beneath a control channel. The overlapping area is the position and shape of the membrane, which is 30 µm thick in this case (vertical gap between the flow and control channels).[23,24]

Plunger valves (Fig. 12) are derived from a common valve design that has a rubber plunger set against a circular orifice. The valve consists of four layers- the pneumatic layer, membrane

layer, hole layer and flow layer. Fluid flows through from one layer to another through a small hole in the elastomeric substrate (the hole layer). A flexible membrane is actuated by a pneumatic chamber, which closes and seals the through-hole when air pressure is applied to the pneumatic layer. One of the plunger valve applications combines a rigid SU-8 disk with a PDMS membrane so that a higher pressure gain can be achieved.

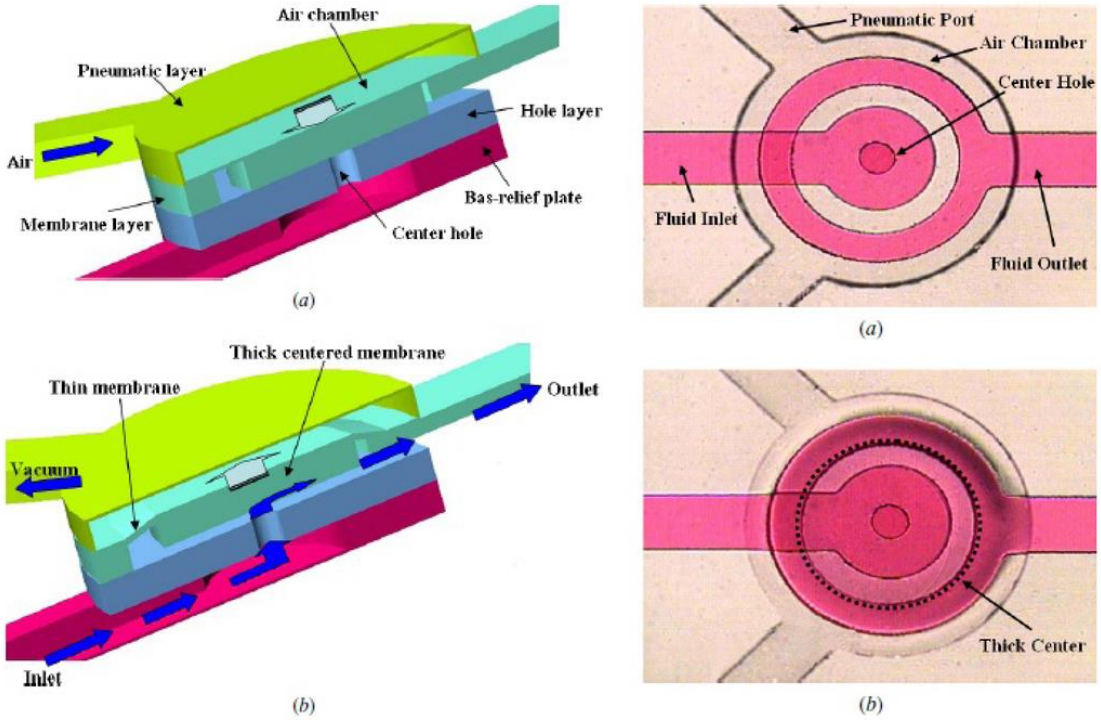

Figure 12: Schematic diagrams and micrographs of a (a) closed and (b) open micro plunger valve.[25] Image reproduced from Ref 25 with the permission from Journal of micromechanics and microengineering.

Normally closed valves

In contrast to the valve type mentioned above, normally closed valves are closed-at-rest valves. There are no external forces required to close the valves; however, negative pressure (vacuum) needs to apply to open the path for flows. The fabrication process is easier compared to normally open valves since only one type of photoresist is needed and reflow of photoresist is not necessary. Prevention of permanent bonding between PDMS is the most important issue in the fabrication process. However, the bonding issue can be avoided by adding a sacrificial barrier on the membrane in the bonding process or by using a non-PDMS valve seat.

The first normally-closed valve was developed by Hosokawa and Maeda. The PDMS membrane is contact-transferred as a film and sandwiched between the control and the flow

channel (Fig. 13). The arrangement of the valve is to have a control chamber which is connected to a vacuum source on the bottom, a thin piece of PDMS in the middle and a disconnected flow channel separated by a wall on top. When negative pressure is applied to the control channel, the membrane deflects downward so that there is a small space for fluid to pass under the wall.[26]

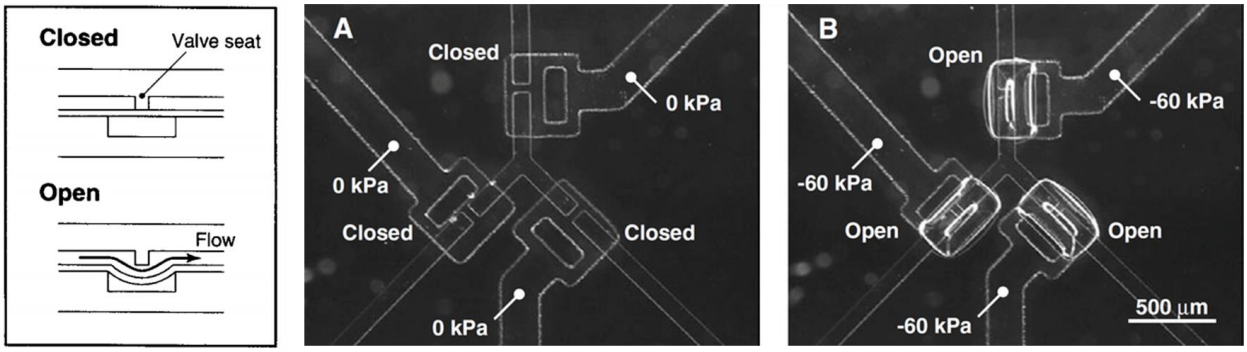

Figure 13: The working mechanism of the doormat valves. (A) and (B) show the open state and the closed state, respectively.[26] Image reproduced from Ref 26 with the permission from Journal of micromechanics and microengineering.

3.3.2. Electrokinetic microvalves

Electrokinetic microvalves control flow directions, which is a router essentially and works with continuous flows. In 1993, Andreas Manz reported that electroosmotic flows can be routed from one channel to another swiftly in a capillary electrophoresis system. A group from Oak Ridge National Laboratory also used this technique to control flows, where the sample fluid and buffer are both attracted by the anode (550 V) in the chip. The buffer fluid is cut off and the sample fluid is free to flow when the buffer is disconnected from the cathode. The buffer then occupies the flow channel when it is connected to the cathode again. (Fig. 14)[27]

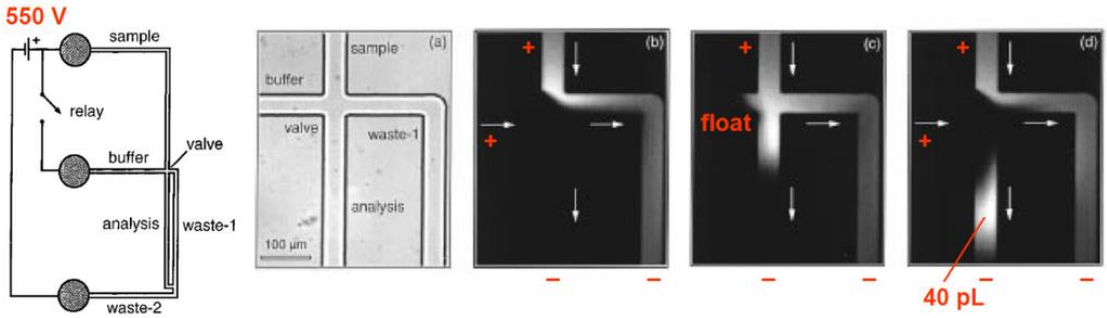

Figure 14: Schematic of the electrokinetic valving microchip. (a) is the bright field image of the valve (b) loading mode, (c) dispensing mode and (d) analysis mode.[27] Reprinted

with permission from Ref 27. Copyright (1999) American Chemical Society.

3.3.3. Pinch valves

Pinch valves are quite similar to PDMS Quake valves and doormat valves, which utilize the deformation of materials (normally PDMS) to create a barrier to stop flows. However, there are two major differences between pinch valves and normal PDMS valves: 1. Pinch valves stop flows with the deformation of the bulk of PDMS that forms the device instead of the deformation of a thin layer of PDMS which lays between a control channel and a flow channel. 2. The source of pressure which causes the deformation is based on the adjacent mechanical generation of pressure instead of a distant connection to air pressure source.

Braille pinch microvalves are one of the examples of pinch valves. The valve control relies on the physical contact between a Braille pin and a piston. When a Braille pin pokes the piston, the deformation of the touching point leads to a pressure change in the piston, which creates the deformation of the piston on the top of the flow channel and stops the flow. The illustration of the valve working principle is shown in Fig. 15.[28]

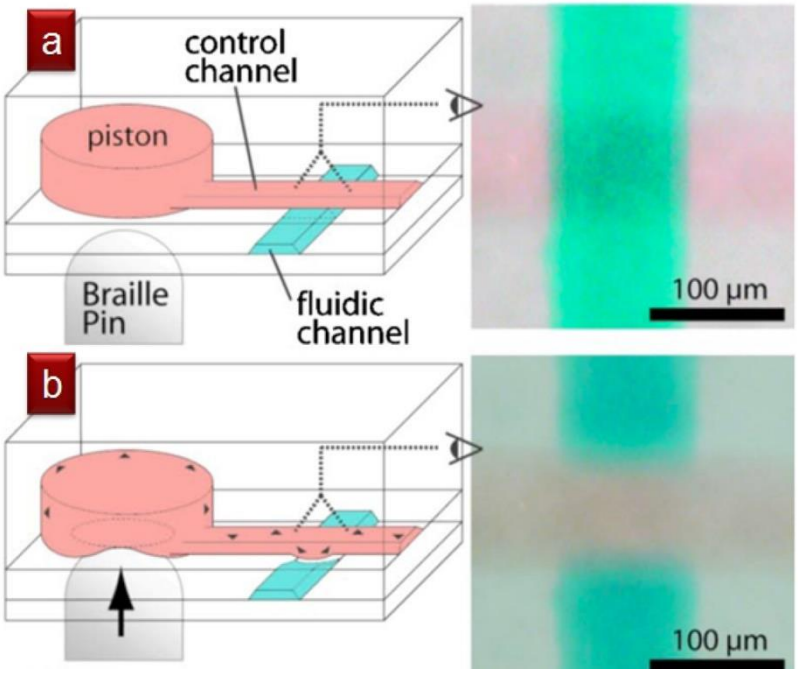

Figure 15: A Braille valve in its (a) open state and (b) close state.[28] Image reproduced from Ref 28 with the permission from Applied Physics Letters.

3.4. Micropumps

The most fundamental function of a pump is to move fluids by mechanical actions. Micropumps play an important role in the miniaturization of a microfluidic device. It has raised an interest in microfluidic research and provides several important functions such as fluid movement, mixing and separation. Micropumps also assist the development of biomedicine, biochemistry and biology. For example, biological specimens have to be moved through the components of miniature assay systems and coolant must me forced through a micro heat exchanger. Transportation in microfluidic devices can be done by utilizing passive mechanisms, which the most notable one is the change of surface tension. However, an element which is an active source, a self-contained object, and the size of which is comparable to the volume of fluid to be pumped, is necessary and highly desirable for a microfluidic system. Therefore, integrated and miniaturized pumps have become a hot topic in the microfluidic field. The target of the integration of micropumps does not only help save real estate on a chip, it also aims to eliminate the use of pipettes. On one hand, micropumps reduce the dead volume and the size of the device so that the cost can be minimized. On the other hand, the pumping in a chip technique lowers the cost of labor by achieving real automation. Some miniaturized and novel pump designs will be introduced in the following paragraphs.[29]

3.4.1. Pneumatic membrane micropumps

The design of the pneumatic micropumps basically follows the existing membrane microvalves design. By connecting several valves in series, a pump can generate peristalsis in microchannels with different actuation phases of each valve. A fluid volume, which is defined by the space between the membrane and valve seat, moves unidirectionally through a sequential actuation of valves. Therefore, the volume is moved away from its original position, which generates a volume displacement in microchannels. Same as pneumatic membrane microvalves, this type of pump can be categorized into two groups: the normally-open and normally-closed pumps.

The Quake micropumps were developed by the Quake group in 2000 with the first publishing of the Quake valve (Fig. 16). The pump was constructed by connecting 3 in-line pneumatic valves in series with separate control lines. Each control channel is connected to different air

source channels and controls each valve independently. The initial design has a flow channel which is 100 µm wide and 10 µm tall and is separated by a 30- µm thick membrane from the control lines. With 50 kPa pneumatic pressure, the flow rate can reach the maximum of 2.35 nL/s at 75 Hz actuation frequency. This design is the only normally-open pump design that can seal the valve seat and remove the fluid volume in the valve completely since the shape of the valve seat is semicircular. Thus, the dead volume in the pump is significantly small (~100 pL).[2]

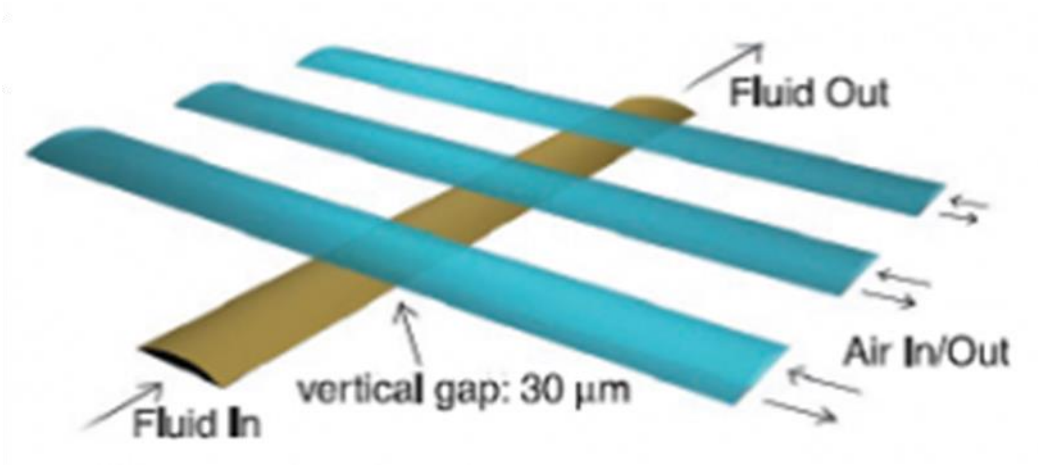

Figure 16: Schematic of the Quake micropump[2] Image reproduced from Ref 2 with the permission from Science.

The other type of micropump is the doormat micropump (Fig. 17). A doormat micropump can be made with the integration of doormat microvalves, which are normally closed valves. In this design, valve seats create gaps between segments of the flow channel. Grover et al. produced a doormat pump that has a 254 µm thick PDMS membrane between the flow channel (layer) and the control channel (layer). There are two types of actuation chambers which are a circular shape of 6 mm diameter and a hexagonal shape of 1 mm diameter. The volume of the circular and the hexagonal chambers are 2050 nL and 67.1 nL, respectively. For each pumping step, the actuation time was between 1.5 s and 10 s, depending on the phase, to make complete filling of each chamber.[30]

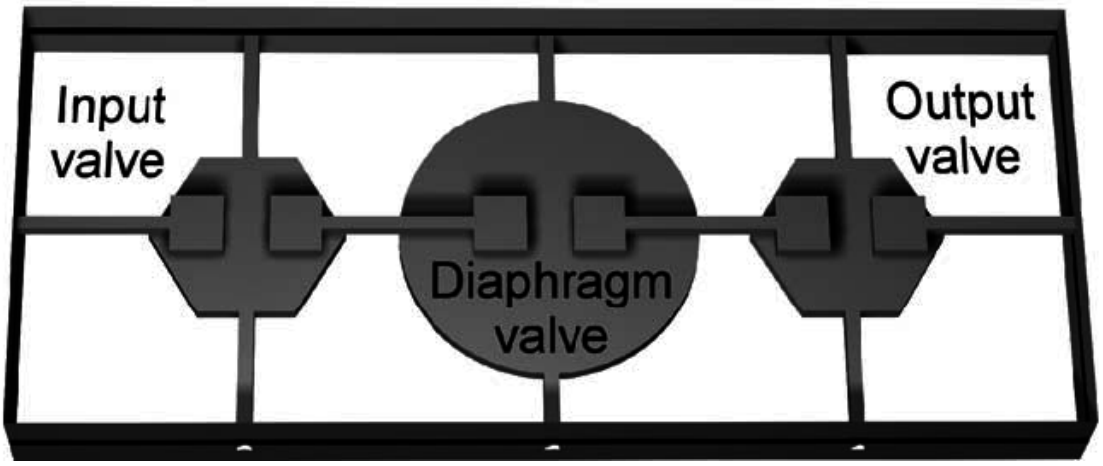

Figure 17: The schematic of the doormat micropump which consists of three diaphragm microvalves.[30] Image reproduced from Ref 30 with the permission from Elsevier.

3.5. Manufacturing valves and pumps using 3D printing

Microvalves and micropumps are crucial components to help achieve device automation. A large number of biomedical/biochemical devices require repetitive and complex fluid manipulation, such as fluid transportation from one space to another, mixing of two or more different types of fluids in a closed chamber or channel. In the past, researchers used to handle fluid using manually-operated pipettes, which the process is usually complex and tedious, liable to err, time-consuming, and expensive. For research and product development in industrial laboratories, robotic dispensers have been largely used to replace humans, but the installation and maintenance fees are usually extremely high. On the contrary, microfluidic technology has been introduced and developed for manipulating and processing small volumes of fluids within a miniaturized chip with a much lower cost compared to automatic, robotic control systems. This technology allows for massive parallelization, low reagent costs, and short reaction time in fluid processing. Although microfluidic devices have been well-developed and reached a certain maturity in biological related fields, the manufacturing process is still a big obstacle in terms of time and complexity. When talking about the integration of moving parts in a microfluidic device, the most obvious issue is the fabrication time and craftsmanship. For instance, PDMS-made microfluidic moving parts like microvalves and micropumps need a long fabrication time for each different layer (at least three), not to mention that these layers still have to be assembled after they are made. In the last 5 years, some microfluidic researchers have been starting to utilize another method to fabricate microfluidic devices, such as 3D printing and laser-cutting. These methods provide some merits that

traditional manufacturing processes do not possess- rapid prototyping, easy design, low cost, and assembly-free. 3D printing has demonstrated all the merits that are mentioned above. The design can be easily done using 3D modeling software, which directly gives the visualization of device's structure and makes the design processes more intuitive. The printing process is fast and simple as well. Unlike PDMS microfluidic devices, the finished design can be easily transferred to a specific type of file that a 3D printer can read and does not need to be sent for photomasks fabrication, which typically takes a long time to be made and is expensive. The 3D printing process is totally continuous if the whole device is made of a single material. Take membrane type valve fabrication for example, all the control layers, membrane layers, and the flow layers are continuously in one print task. As a result, the time need for alignment and special surface treatment for bonding and assembly are shortened.

One of the initial 3D-printed valves was made by Au et al. in 2014, which was a diaphragm/nozzle valve made of Watershed (Fig. 18 A). The design was made with a 3D modeling software- Inventor and sent to a commercial printing service provider. The 3D printer type he chose was stereolithography. The valve was operated by applying air pressure to the control chamber which causes the 10 mm-diam, 100 μm thick watershed membrane to deflect. With this dimension of the membrane, it could deflect up to ~ 200 μm and seal the valve seat at ~6 psi. The valve was totally closed without leakage at the 6 psi closing pressure and could be operated more than 15,000 cycles at 7 Hz between 0 and 3 psi. Using the same valve design, he was able to combine several valves together to perform a pumping and switching function for controlling multiple channels. The pump design was also shown in this paper by connecting three valves in series (Fig. 18 B). By controlling the open and phase of each valve (the open and closed state of individual valves), fluid in the flow channel could be driven in an assigned direction peristaltically. Moreover, a four-way switch could be made by combining four valves together with sharing a common outlet channel. Each flow line with different types of fluids could be chosen to move to the downstream and outlet by opening the selected valve and closing the rest (Fig. 18 C).[31]

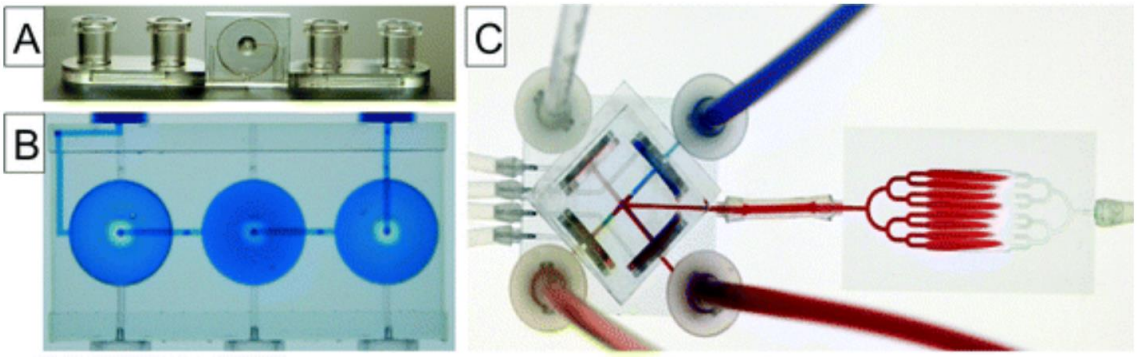

Figure 18: (A) A SL-printed single membrane valve that is made with the Watershed resin. (B) A peristaltic pump with three membrane valves connected in series (the one in the middle is open and two on the sides are closed) (C) An illustration of an actuating switch that is connected to a cell-culture chamber. Only the valve for red dye is open.[31] Image reproduced from Ref 31 with the permission from Royal Society of Chemistry.

Another valve type which is also a membrane valve was published by Sochol et al. using the Multi-Jet Modeling (MJM) printer. Instead of making the membrane flat, they redesigned the shape of the membrane, which is a diaphragm with a sinusoidal cross-section (so the surface is wavy) as a dynamic microfluidic element. The sinusoidal cross-section design can increase the displacement of the membrane by applying the same air pressure into the control chamber. They also extended the application of the valve by generating different microfluidic circuitries such as a fluidic capacitor, diode, rectifier and transistor (Fig. 19 & 20). Noted that the diode in the fluidic circuitry design can be seen as a check valve, which only allows fluid to flow in one direction. A fluidic rectifier can be easily made by combining four diodes (check valves) together with an arrangement of specific orientation of each valve (Fig. 20). A tidal wave, for example, can be rectified into one flow direction, which is the same concept as the conversion from AC to DC.[32]

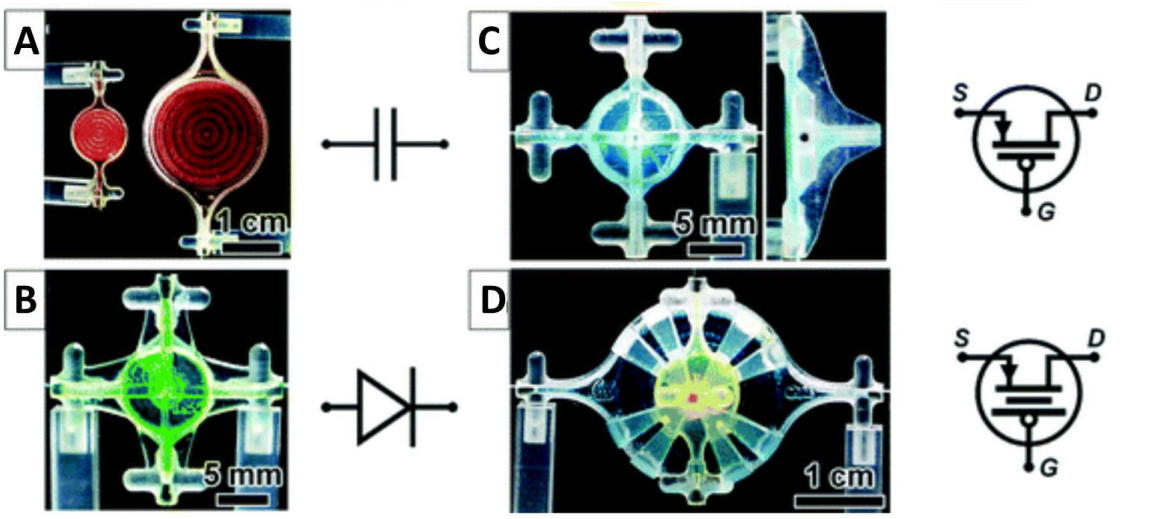

Figure 19: Fluidic circuit control elements which filled with dye and their respective analogous electrical symbols. (A) Fluidic capacitors (B) Fluidic diode (C) Fluidic transistor and (D) Enhanced-gain fluidic transistor.[32] Image reproduced from Ref 32 with the permission from Royal Society of Chemistry.

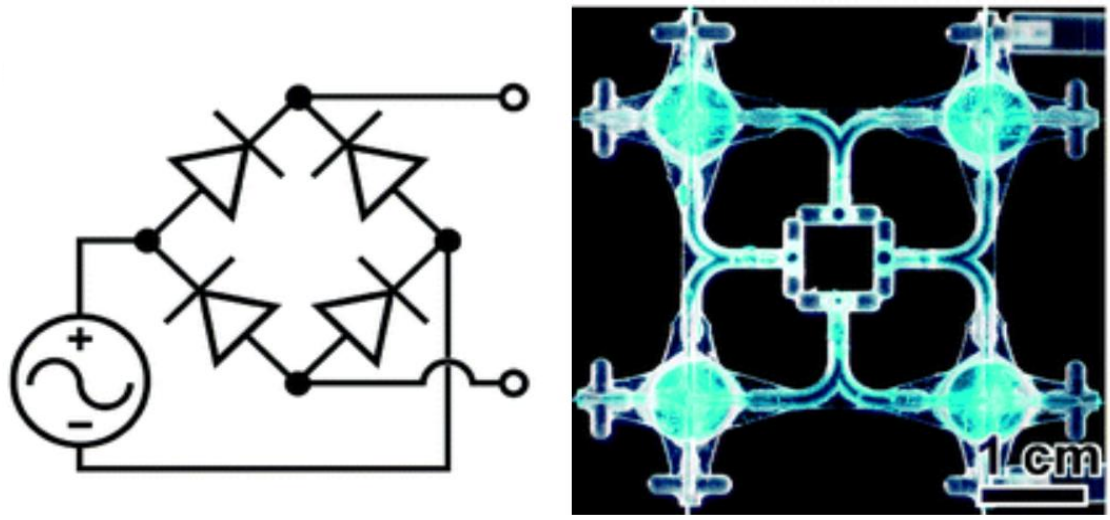

Figure 20: A analogous electrical symbol of a rectifier and the photograph of a fluidic rectifier.[32] Image reproduced from Ref 32 with the permission from Royal Society of Chemistry.

4. 3D printed microfluidic devices

4.1. Introduction & Automation

As mentioned above, there are some “manufacturability barriers” in the PDMS modeling approach so that researchers and developers are currently looking for alternative solutions. Main issues such as rapid fabrication and prototyping processes, cost of the device and instrument, and the skill requirement of labors are the focuses in the microfluidic device manufacturing field. 3D-printing has become one of the alternatives in these manufacturing methods and processes. It provides a number of advantages and solutions to the roadblocks that PDMS microfluidic devices are facing. The differences between the two manufacturing methods and the reasons of choosing 3D printing instead of PDMS molding are shown in Table. 3.

PDMS microfluidic devices	3D printed microfluidic devices
Molding process (curing, assembly, bonding, and inlet construction) is highly labor-demanding and hard to be completely automated.	Less manual process (curing, assembly, etc. are fully done in the 3D printing process. The molding process is totally automated.
The connection interface (inlets and outlets) requires punching or molded holes, which leads to an easy leakage at the junction.	All kinds of connectors (Luer-lock, barb) can be printed with the bulk of the device together. The interface of tubing and microchannels is smooth and continuous. It is totally leak-free.
Control systems such as computer, pressure source control interface that control valves and pumps require solid engineering background or expertise for connections and operations between the device and control panel.	The design and operation are simple and intuitive. It only needs the plugin process of different sources (liquid and air for example).
Fabrication is expensive and almost impossible to achieve mass production like batch-fabricated MEMS devices	All elements compared to PDMS fabrication process are cheap (instruments, materials, etc.). It is

	possible to achieve mass production by operating numerous 3D printers simultaneously.

Table 3: Comparison of PDMS and 3D printing techniques in terms of microfluidic devices.

There are three major types of 3D printers that can be used for microfluidic devices fabrication- Stereolithography (SL or SLA), Fused Deposition Modeling (FDM) and Multi-Jet Modeling (MJM). We chose SL as our printing method due to its fastest production speed among the three printing types above and high accessibility to customizable printing materials (resins). Before starting to build real 3D printed devices, we have done the testing of resin's characteristic, printing parameters optimization and testing of printing qualities.

The main goal of this thesis is to build a flow control system in microfluidic devices using SLA 3D printers. One of the most important components in a microfluidic control system is valves. According to the introduction of valves in the above section, we know that there are many well-developed valves that have been integrated with microfluidic systems perfectly. Additionally, some of the valves were shown to be printed with 3D printers and capable of being operated successfully. However, the existing 3D printed valves are either too large or too hard to be made. We believed that optimizing the size and structure of 3D printed valves can help create a more delicate and compact microfluidic device. Therefore, we decided to develop the Quake style valve design with 3D printing, which has great properties among all kinds of valve designs: simple components and structures in a valve unit, easy to design, and the ability to be scaled down to small volumes.

4.2. Resin selection and characterization

The first made 3D printed microfluidic control component in this paper is a "Quake" style 3D printed valve, which has a sandwich structure with a control channel on top, a flow channel on the bottom and a thin layer of membrane in between. A normal sub-millimeter channel was able to be well-printed with the initial formula of the printing material and basic printer settings. As a consequence, the most critical element in this design is the membrane layer. Here, the key goal of resin characterization is to find out the best material composition and printing settings for printing a "soft, flexible and thin" membrane. To obtain the properties listed above, we

focus on the development of the printing material, which is the resin for 3D printers, in this section.

The resin we use for our 3D printed device is poly(ethylene glycol) diacrylate (MW = 258) (PEG-DA-258, Sigma-Aldrich, MO) mixed with photoinitiator- Irgacure 819 and photosensitizer- 2- Isopropyl thioxanthone (ITX). PEG-DA-258 is the base of the resin and polymerizable at a certain range of light wavelength when mixed with photoinitiators. PEG-DA is one type of a hydrogel and usually used as a medium for cell culture or tissue culture with different cell arrangements. The molecular weight of PEG-DA ranges from several hundred to thousands, depending on the number of the CH_2CH_2O repetitive (ethylene glycol) groups in the middle (Fig. 21). The molecular weight is higher when the repetitive CH_2CH_2O group is longer, which turns out being a more viscous liquid type under room temperature without UV treatment. The molecular weight of PEG-DA we chose is 258, which has the shortest CH_2CH_2O chain and lower viscosity among all series of PEG-DA. PEG-DA 258 has the highest stiffness and the lowest porosity compared to higher molecular weight PEG-DAs after it is UV cured. The property of having the lowest porosity makes PEG-DA 258 the best candidate for making membranes, nonetheless, we also need to minimize the thickness of the membrane to compensate for its low flexibility.

Irgacure 819 is the photoinitiator in our PEG-DA resin (Fig. 22). It is a molecule that generates reactive products upon exposure to radiation of specific wavelengths. Irgacure 819 is photosensitive and has the highest light absorption close to wavelength 385 nm (Fig. 23), which matches the light source wavelength of the printer we are currently using- Phoenix Touch Pro and Asiga PICO 2 HD. Irgacure 819 absorbs the UV light generated by 3D printers and decomposes into two groups following with two radicals (floating electrons). The energy provided by the radicals can activate PEG-DA monomers to crosslink with each other and become solidified. The shorter chain of PEG-DA indicates that there are more PEG-DA molecules crosslinked within a unit weight. Therefore, PEG-DA with lower molecular weights will have a higher stiffness compared to the higher molecular weight of PEG-DA (more porous and gel-like).

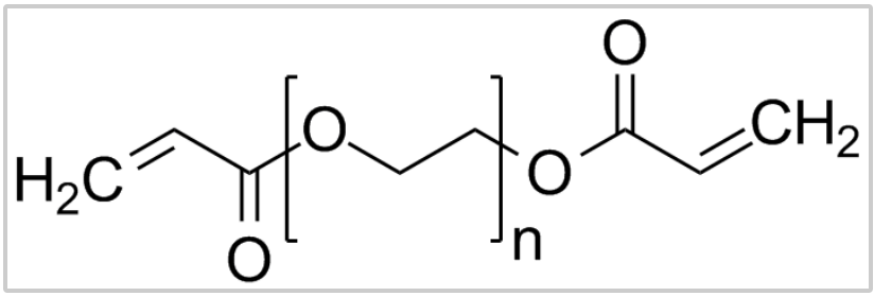

Figure 21: Structural formula of PEG-DA. The number of n decides the molecular weight of PEG-DA (e.g. In PEG-DA-258, n=3).[33]

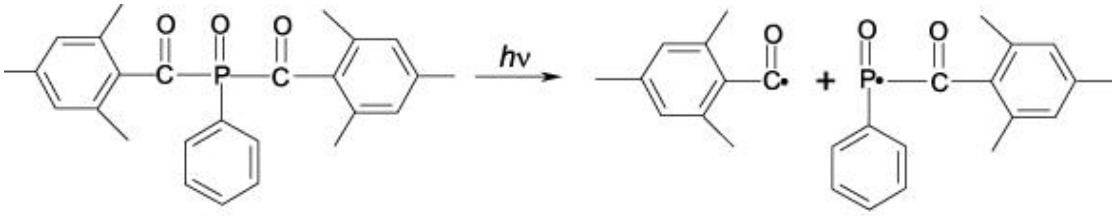

Figure 22: Structural formula of Irgacure 819. It is separated into two groups after being exposed to UV light, which provides the energy to break the chemical bond between carbon and phosphorous.[34]

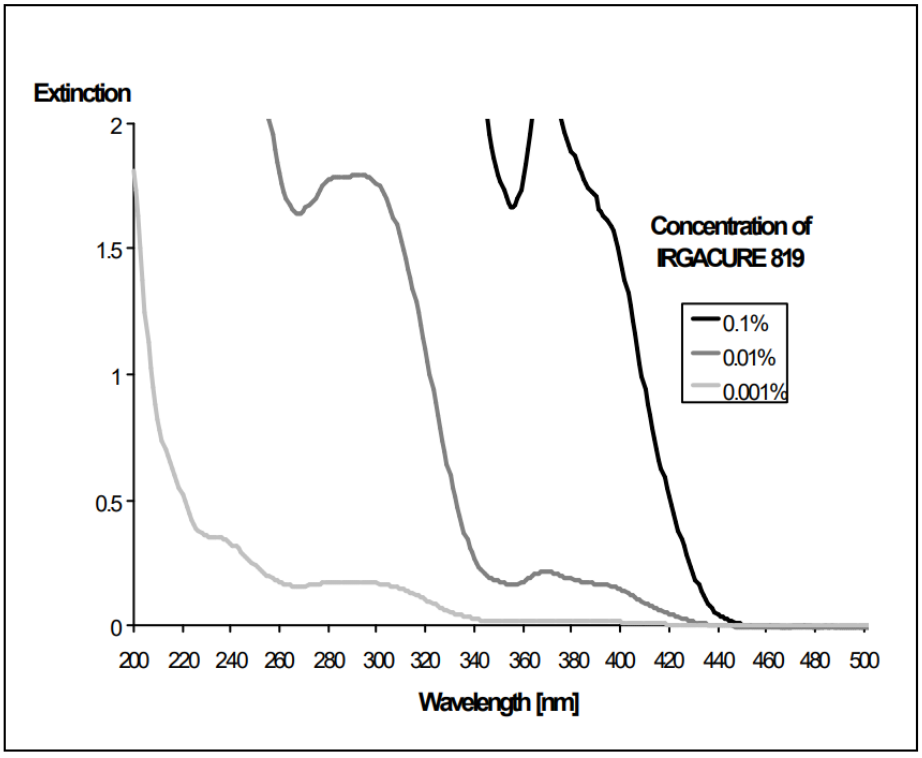

Figure 23: Absorption spectrum of Irgacure 819. It has the highest excitation around 385

nm when the concentration is above 0.1 %.[35]

ITX (Fig. 24) plays an important role in SL 3D printing as a photosensitizer (as known as UV absorber). A photosensitizer usually conducts a chemical change in another material (usually molecules) in a photochemical process. Although ITX does not directly affect the chemical reaction between PEG-DA and Irgacure 819, it can prevent PEG-DA molecules from over-curing. In order to control layer thicknesses of the device precisely (Z resolution), ITX is added to the resin for absorbing excessive UV energy. Especially when making complex 3D structures such as tiny holes, extremely thin membranes or shallow channels, ITX helps absorb extra UV energy and inhibit the UV light from penetrating through a certain layer thickness. Thus, the residue liquid PEG-DA in the previous layers will be able to be removed after the whole printing process is done rather than being cured.

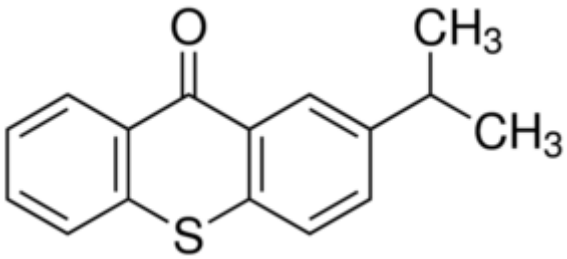

Figure 24: Structural formula of ITX.[36]

The initial concentration of Irgacure 819 and ITX was 0.2% w/w and 0.2% w/w, respectively. 40 g of PEG-DA-258 (stored in a 4 ˚C refrigerator) was added into a tube with a piece of aluminum foil wrapped on the tube's surface. 0.08 g of Irgacure and ITX were then added to the PEG-DA solution and agitated. Finally, it was put in a 70 ˚C oven for 30 minutes for complete dissolution before being used.[37]

We quickly realized that 0.2% of Igacure 819 and 0.2% of ITX is not the best concentration for making thin and soft membranes after we observed some prints of roofs with different thicknesses (details are addressed in section 4.3). Before starting to change the concentration of Irgacure 819 and ITX, it is important to understand the optical properties of light and exposed matters. We know that the intensity of light becomes lower as it passes through the resin (or any kinds of liquid). This behavior is governed by the Beer-Lambert Law (eq. 1). According to this law, we can roughly see the relationship between penetration depths of light and printed results after polymerization (Fig. 25).[38]

$$\boldsymbol{log_{10}\left(\frac{I_0}{I}\right) = \varepsilon lc = A} \qquad (\boldsymbol{eq.1})$$

In this equation, I_0 is the received radiation power with no analyte, I is the received radiation power with the analyte at concentration c, ε is the molar absorption coefficient, c is the analyte concentration, l is the optical path length and A is the absorbance.[39]

The other expression of Beer-Lambert Law is:

$$\boldsymbol{I = I_0 e^{-\alpha z}} \qquad \textbf{(eq. 2)}$$

where α is the absorption coefficient and z is the penetration depth. α is also defined as $1/h_a$, where h_a is the penetration depth of light in a material when the intensity of the radiation inside the material falls to 1/e (~ 37 %) of its original value at the surface.

By combining eq.1 and eq. 2 together, we can get the relationship between the penetration depth and the concentration of the analyte.

$$\boldsymbol{h_a = \frac{1}{2.304 * \varepsilon * c}} \qquad \textbf{(eq. 3)}$$

According to eq. 3, if we increase the concentration c (which can be the photoinitiator or photosensitizer in the resin), the penetration depth (h_a) will be shorter.[39] Therefore, we decided to increase the concentration of both Irgacure 819 and ITX to get thinner membranes. Noted that we cannot only increase the concentration of ITX (photosensitizer) without increasing the concentration of Irgacure 819 (photoinitiator), otherwise, there would be an insufficient amount of photoinitiator being excited. This will lead to less amount of PEG-DA being crosslinked and thus the print will collapse.

After several roof height tests (which is elaborated in sec. 4.4), we decided to fix at the concentration of 0.6 % Irgacure 819 and 0.6 % ITX. All the 3D printed control system devices are printed with this concentration of Irgacure 819 and ITX.

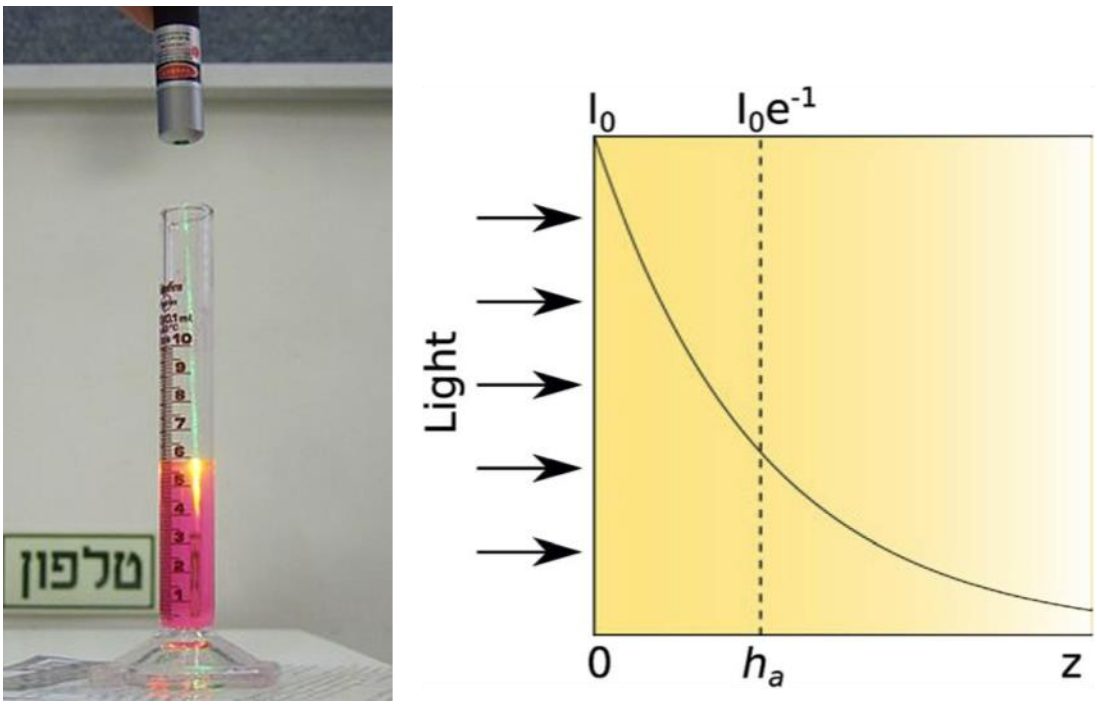

Figure 25: A photograph illustrating the penetration of light into dye (left) and graph of light intensity versus distance (right, a representation of the Beer-Lambert Law).[38,39]

4.3. 3D-printer Phoenix Touch Pro

The 3D printer, Phoenix Touch Pro Translating UV-LED DLP 3D Printer, is the first printer that we used to test our 3D prints (Fig. 26). The XY resolution of the printer is 50 µm and the Z resolution (the thinnest layer that the printer can print) is 25 µm. The light source in this printer is UV-385 nm LED, which matches the absorption peak of our PEG-DA-258 resin. The build area is 65.6 mm x 122 mm x 110 mm, which is big enough for us to put two silanized (see section 7.3) glass slides on the build plate at the same time. The Z motor control, which is the step resolution of the stepper motor, is 5 microns. The printer is connected to the computer through Ethernet cable to read the printing files. As you can see in Fig. 27, there are some tunable parameters so that we can change in the printing settings. The adherence time is the UV exposure time of the first layer (also called a burn-in layer), which forms the base of prints. The slice exposure time is the exposure time for each layer after the burn-in layer, which can be tuned down to 0.1 sec. The LED intensity is also one of the important parameters in the setting, indicating the UV energy of the light source. The higher the LED intensity is, the more energy is transferred to the resin. Noted that the build plate needs to be calibrated and match to the floor level of the vat before starting prints. The yellow hood on top can prevent the UV light from emitting out and also block the ambient light outside from the printer. Also, the

printer is suitable for multiple prints at once, which the printed device can be placed in the front, middle, and back. Limited by the projection size due to the height of the printer, the projector moves under the vat to shine UV light on these three parts separately in one layer. However, the super vat (made of polyethylene) that comes with this printer is not as durable as the PDMS vats. The super vat got worn and torn after ~10 prints and the sticking issue became severe, which sometimes led to a resin leakage problem. The sticking and leakage problem were solved after we had changed the vat to our new homemade PDMS vat. This new vat was assembled with Poly(methyl methacrylate) (PMMA) to serve as the walls and bottom to contain resins and a piece of PDMS (~ 1 mm, which the focal length should be tuned accordingly) was placed in the vat bottom.

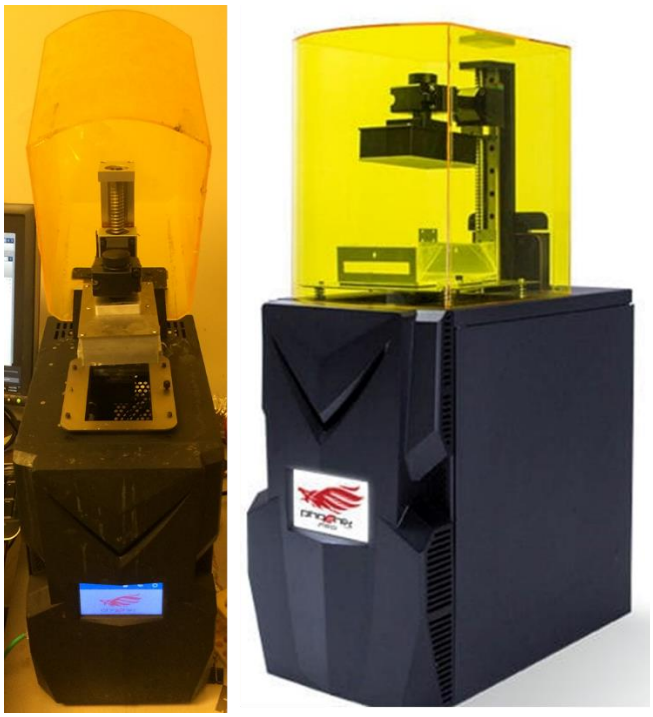

Figure 26: Photograph of Phoenix Touch Pro Translating UV-LED DLP 3D Printer.[40]

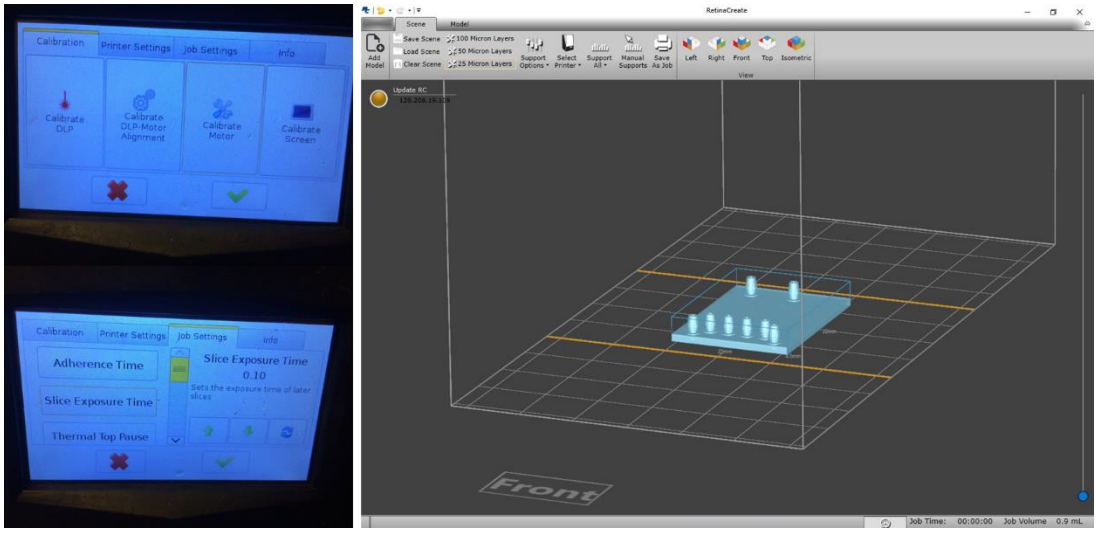

Figure 27: The control interface of Phoenix touch pro, which is on the touch screen of the printer and the printer's software – RetinaCreate user interface.

4.4. Membrane thickness testing

The structure of the Quake valve consists of a control channel on top and a flow channel on the bottom with a thin membrane layer in between. The membrane itself is basically a hanging structure in the device, which contacts the fluid in the flow channel and air in the control channel directly. The SLA 3D printer prints the device layer by layer and prints the whole structure upside down (The build plate goes down to the vat, prints the first layer and then goes up, repeatedly, so the whole device is facing down during the print, see Fig. 28). Therefore, we can know that only the big walls (which are the walls of the flow channel) on two sides of the valve seat are printed before the printer prints the membrane layer. When the membrane layer is being printed, the build plate goes down into the vat and leaves a 25-µm gap between the build plate and the bottom of the vat (which is the desired thickness of the membrane). However, if the flow channel is very shallow, the resin will fill up the whole flow channel and be trapped due to the surface tension of the resin after these previous printed flow channel layers (which are the walls and the channel) submerge into the vat. Because of the surface tension, there will be excessive amount of uncured resin staying in the flow channel. Since the UV light can travel through the trapped resin in the flow channel, excessive resin trapped between walls can be cured, causing the membrane to be thicker than 25 µm. To see the real printed membrane thickness, we designed a roof structure that has two big walls on two sides with different numbers of roof layers on top to simulate the thickness of the membrane (Fig. 29). We tested the roof heights from 25 µm to 175 µm with a 25-µm interval. With the original

concentration of Irgacure 819 and ITX (0.2 % w/w) and the default setting of LED intensity (1.00), the real thickness of the membrane is 164 µm, which has a huge difference from the set thickness- 25 µm. According to the Beer-Lambert Law above, it suggests that we should increase the concentration of the analytes, which are Irgacure 819 and ITX, in the resin. As a result, we decided to increase the concentration of Irgacure and ITX until the real thickness gets close to 25 µm. At the same time, we decreased the LED intensity to let the resin absorb less energy. Finally, we stopped at 0.6% of ITX and 0.6 % of Irgacure 819, which allows us to get a membrane as thin as 40 µm (Fig. 30) with the minimum LED intensity (0.12). We did not continue to increase the concentration of Irgacure 819 and ITX due to the color of the device. The device becomes more yellow as we add more Irgacure 819 and ITX into our resin.[37]

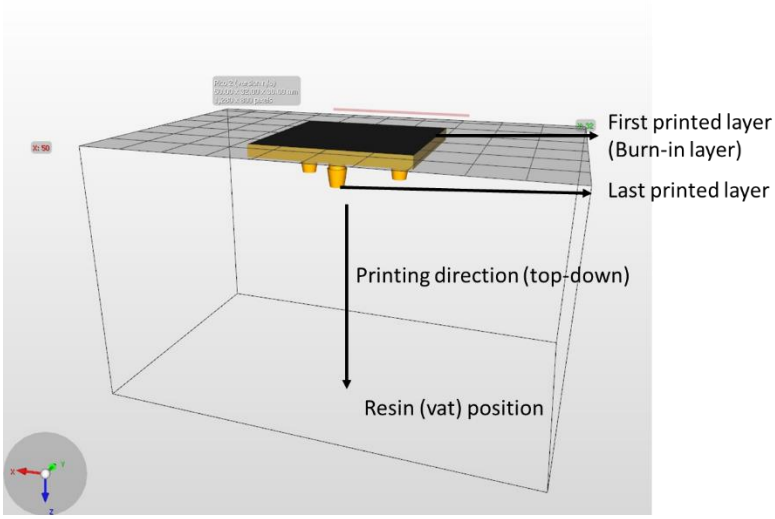

Figure 28: Schematic of the 3D printing process. A build plate is on top with a device sticking to the surface of it. The resin (vat) sits below the build plate.

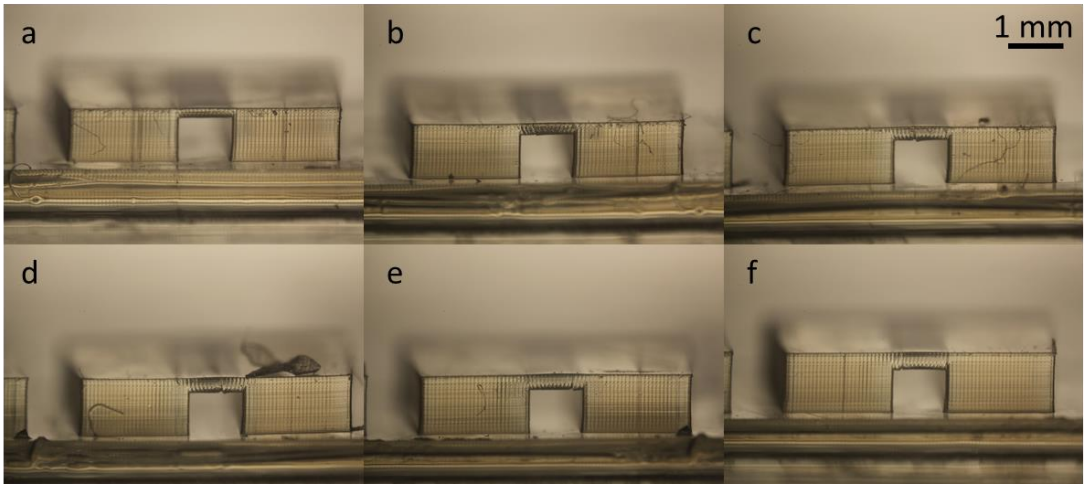

Figure 29: The printed roof structures showing different roof thicknesses. (a) 25 µm (b)

50 µm (c) 75 µm (d) 100 µm (e) 125 µm (d) 150 µm.

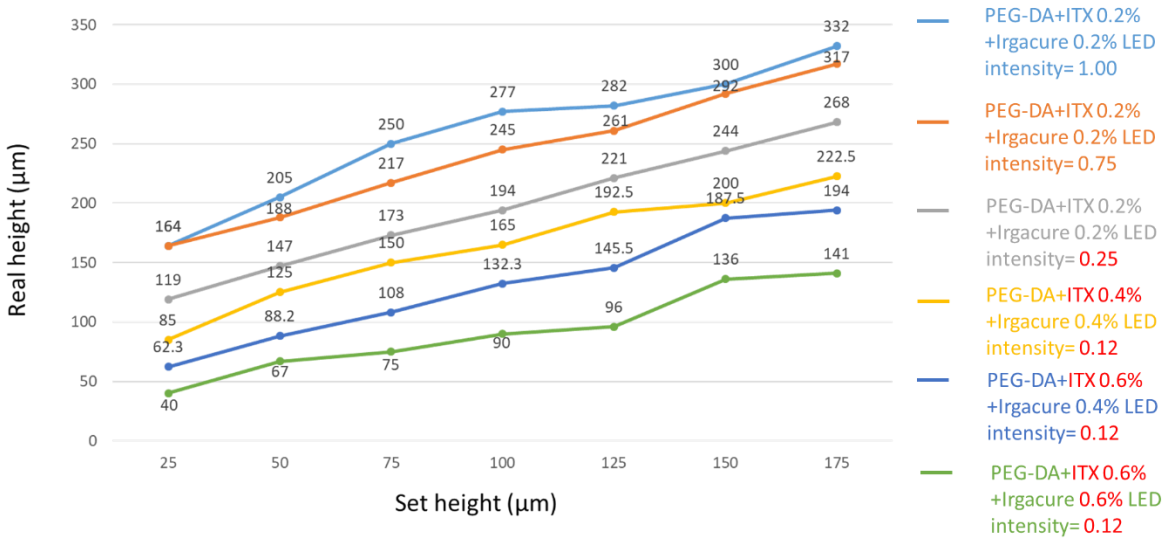

Figure 30: The real height of roofs versus the set heights. Different colors represent different concentrations of Irgacure and ITX in PEG-DA resins with different LED intensity.

4.5. Deflection test and simulation

Estimation of the membrane deflection is also one of the important tasks of building the valve. Besides assuring that the printer can print a thin and soft membrane with 0.6 % of Irgacure 819 and 0.6 % of ITX at the lowest LED intensity, we need to know the membrane deflection to decide the distance between the membrane and the valve seat. It is known that cured PEG-DA has similar mechanical properties as plastics and it does not deflect as much as PDMS. Thus, we need to bring up the valve seat closer to the membrane in order to make the membrane seal the valve seat successfully with low applied pressure. According to eq. 4, the distance that the membrane can extend is estimated with different membrane sizes, thicknesses, and Young's moduli. The simulation of the membrane deflection can help us determine the depth of the valve seat under the membrane so that we can design the initial 3D-printed Quake- style valve design with reasonable dimensions. The plots of the membrane deflection versus different variables were drawn with MATLAB by applying different parameters to eq.4. Here we designed the membrane as a disk (the reason is provided in section 5.1 and 5.2) and assumed that air pressure is applied evenly onto the membrane.

Fig. 31 shows the relationship between the deflection of the membrane and the membrane thicknesses with different valve sizes (different radius of the membrane). With the fixed

applied pressure at 15 psi, Poisson's ratio 0.3, and Young's Modulus at 2000 MPa, the deflection is larger when the radius of the membrane is bigger. Although with the radius at 2.0 mm we can have a deflection of ~200 µm when the membrane thickness is 25 µm, we decided to make the valve/membrane size smaller to save more space on the chip. Our first target was to print the membrane with ~1 mm in diameter, therefore, the deflection will be around 50 to 100 µm with the conditions set above. This simulation gives us the information that the distance between the valve seat and the membrane should be set lower than 100 µm.

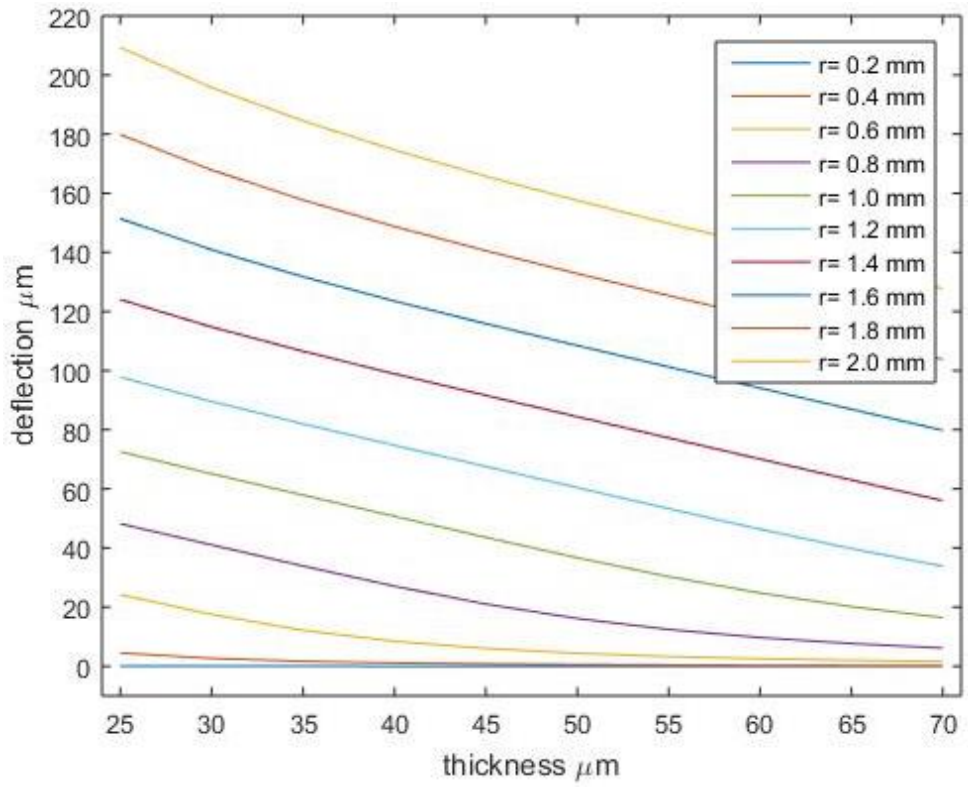

Figure 31: Membrane deflections versus thicknesses of the membrane with different cross-section areas (different membrane sizes)

In figure 32, we can see the relationship between the deflection and different membrane thicknesses with different applied pressures. The radius of the membrane is set to 2.0 mm, Young's modulus is 2000 MPa and the Poisson's ratio is 0.3. Since the maximum pressure we can get in our lab is ~15 psi, the maximum pressure in the plot is only set to 16 psi. We can observe from the plot that the membrane thickness is more dominant than applied pressure if we want to increase the deflection. For example, if we increase the pressure by 2 times (from 2 to 4 psi), the deflection will increase ~10 µm when the membrane thickness is 50 µm. However, if we decrease the membrane thickness by 2 times (from 50 to 25 µm), the deflection

will increase ~50 µm with the same applied pressure (2 psi). As a result, reducing the thickness of the membrane is much more important than increasing the pressure in the process of the valve performance optimization.

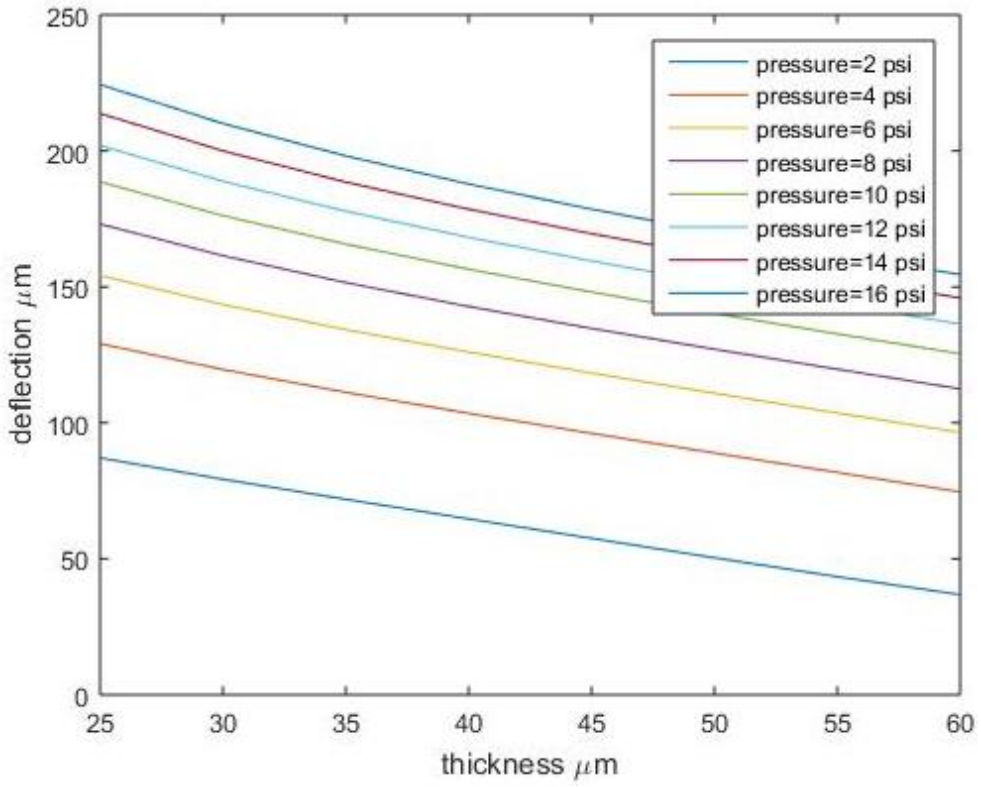

Figure 32: Membrane deflections versus thicknesses of the membrane with different pressures

The Young's modulus of the material also affects the degree of deflection. Owing to change of the concentration of ITX and Irgacure 819 in our PEG-DA resin, we would like to see how much the material's flexibility might influence the deflection. In figure 33, Young's moduli vary from 400 to 2200 MPa. The applied pressure is 15 psi, the radius of the membrane is 2.0 mm and the Poison's ratio is 0.3. It is important to decrease Young's modulus of the material to get more deflection. Nonetheless, the membrane thickness is still more dominant in this case. If the membrane thickness is decreased from 50 to 25 µm, the deflection will increase ~ 60 µm when Young's modulus is set to 2000 MPa. The deflection only increases ~50 µm, which is 10 µm less than decreasing the membrane thickness by two times, if Young's modulus is decreased by two times (from 2000 to 1000 MPa). Therefore, the simulation demonstrates the importance of the membrane thickness again, which can be controlled by changing the thickness in the design easily.

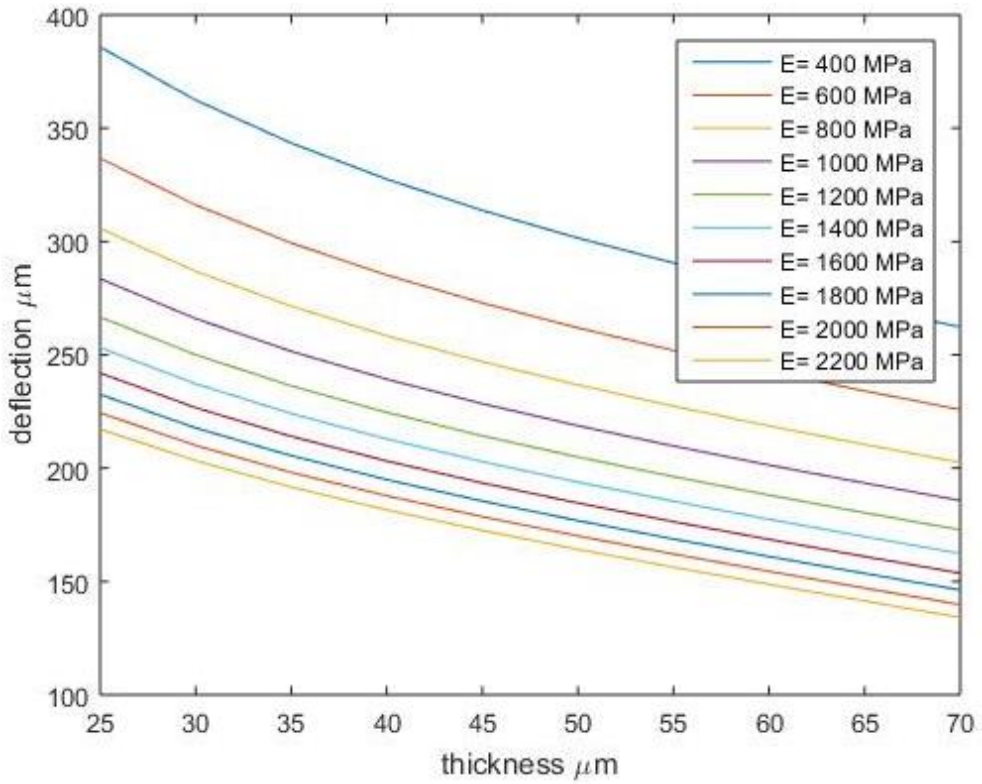

Figure 33: Membrane deflections vs thicknesses of the membrane with different Young's Moduli

5. 3D printed Quake style microvalves and micropumps

The content of this section has been published in the following paper:

Lee, Y.S., Bhattacharjee, N. and Folch, A., 2018. 3D-printed Quake-style microvalves and micropumps. Lab on a Chip, 18(8), pp.1207-1214.- Reproduced by permission of The Royal Society of Chemistry. (Available online at http://pubs.rsc.org/en/content/articlehtml/2018/lc/c8lc00001h)

5.1. Introduction

Microvalves and micropumps are fundamental components of many microfluidic systems.[2,20,41–46] Using microvalves, temporal sequences of fluids can be programmed to produce combinatorial mixtures and gradients,[47–51] droplet combinations,14 nucleic acid manipulations,[52–54] and cell culture conditions.[55,56] Additionally, microvalves allow for tuning of flow resistance[57] and microchannel topography[58] (among other operations) at a spatiotemporal scale that is inaccessible to manual manipulation. Microfluidic automation spares the costs of human labor and enables faster processing through miniaturization and parallelization.[20,59,60]

The Quake group first introduced normally-open valves with a very simple three-layer architecture made in poly(dimethylsiloxane) (PDMS): a microchannel lying orthogonally on top of another microchannel with a thin elastomeric membrane in between (Fig. 34a). One of the microchannels acts as a “control channel” that, when pressurized, causes deflection of the membrane to interrupt the flow in the orthogonal “flow channel”. Quake valves have found many applications because their design and working principle are extremely simple. Most research groups that produce Quake valves make them in PDMS from photolithographically-fabricated molds. However, the commercial ordering of photomasks, followed by photolithography and PDMS molding, is a process that typically consumes several days. Even if the photomask step is expedited by an internal service, photolithography and PDMS molding are processes that take several hours each. Moreover, stacking multiple PDMS layers to create 3D microchannels requires tedious manual labor and delicate, operator-dependent craftsmanship for aligning and bonding (i.e. Quake valves have to be made by skilled

personnel); importantly, these manual processes can have an impact on manufacturing yield and device quality.

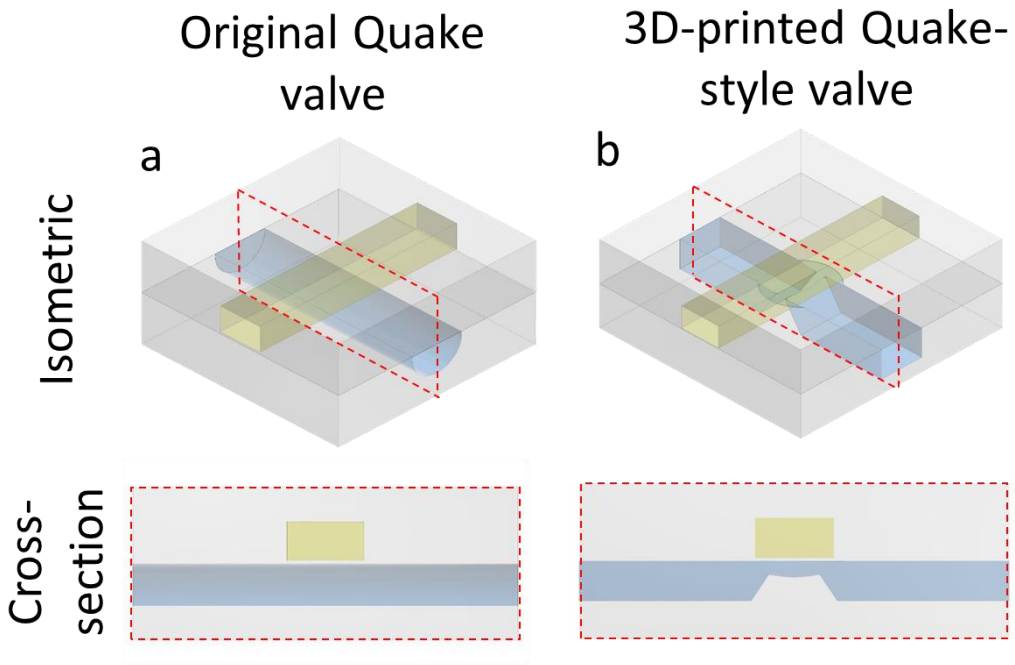

Figure 34: Isometric and cross-section views of the (a) original Quake valve design, with a semi-cylindrical seat, and (b) our 3D-printed Quake-style valve design, with a hemispherical cap seat. The cross-section views are captured from the red-dashed rectangles shown in the isometric views.

3D-printing offers an alternative to manual processing. 3D-printed micro-components such as microchannels,[31,61–64] microvalves, and micropumps[31,65,66] have become important and are widely used in the field of microfluidics owing to their compact size, easy and rapid manufacturing, and high integration ability.[3,67] One of the first 3D-printed valves was SL-printed using the commercial resin Watershed and enabled the possibility of building microfluidic perfusion systems compatible with cells.[31] Due to resolution limitations, Watershed microvalves and micropumps are much larger than PDMS ones, which leads to large dead volumes and makes the integration with other microfluidic components more difficult. Recently, Nordin et al.[68] have demonstrated 3D-printed microvalves ~1 mm in diameter which can be fabricated in a resin made of poly-ethylene glycol diacrylate (MW ~258) (PEG-DA-258) and an orange UV-absorber (Sudan I), demonstrating the suitability of this photopolymerizable resin as a 3D-printable micromechanical material (adding to its

biocompatibility demonstrated for 3D-printed microfluidics[69]). However, both our Watershed and Nordin's valve designs have a complex 3D architecture, which presents a few challenges: 1) microscopic observation of the valve operation is difficult due to the valve's 3D architecture; 2) integration of valve arrays requires 3D-piping, and 3) draining of the PEG-DA-258 precursor after printing becomes problematic as the complexity of the valve array grows.

Here we present a modified version of the Quake valve that can be 3D-printed using transparent PEG-DA-258. This modified design, which we term as a "Quake-style" valve, features a bowl-shaped valve seat (i.e. the seat is shaped as a hemispherical cap) for improved printability and operation, and offers notable design advantages in terms of microscopy and piping simplicity for future large-scale arrays.

5.2. Design and working principle of the 3D-printed Quake-style microvalve

Unlike photolithography, 3D CAD design allows for optimizing the overall symmetry of the valve seat and, consequently, the sealing ability of the valve. We first printed the original Quake-style valve (Fig. 34a & Fig. 36), consisting of a rectangular control channel placed on top of a semicircular-cross-section flow channel. However, our resin is composed of PEG-DA-258 (Young's modulus E ~ 130 MPa),[70] which is about 130 times less flexible than PDMS (E < 1 MPa).[71] As a result, the deflected PEG-DA-258 membrane (dimensions: 1000 μm × 1000 μm, membrane thickness: 25 μm) cannot seal against the bottom of the flow channel even after applying pressures greater than 10 psi. Although in principle the deflection of the membrane (for any given pressure) could have been increased by expanding its size, we decided to exploit the degree of freedom offered by 3D-printing that photolithographic fabrication does not have. Specifically, using photolithography-based processes, Quake valve channels must have constant cross-sections along the channel axis, while 3D-printing is able to generate channels with variable cross-sections. We designed the seat of the 3D-printed Quake-style valve with a bowl-shaped structure that was elevated with respect to the bottom of the flow channel so that the membrane (diam.: 1200 μm, thickness: 25 μm) could easily reach the valve seat and seal the valve upon deflection at lower control pressures (<10 psi) compared to the original Quake valve design. The curvature of the bowl shape helps create a smooth seal between the membrane and the seat. Furthermore, the flow channel partially overlaps with the valve seat in order to avoid overexposure of uncured resin. Note that this overlapping design (a necessary compromise feature) prevents the bowl from being perfectly circular. Last but not the least, the

two edges of the valve seat, which correspond to the thinnest parts of the flow channel, were ~40 μm below the membrane (Fig. 34b). The flow channel got clogged during fabrication of the control channel if the gap was smaller than 40 μm (parameter d in Table. 4). This design constraint guaranteed that the flow-channel void on top of the valve seat received the least possible dose of additional UV exposure when the additional Z-layers of the control channel walls were printed. The STL files of both two valve designs are available in ESI.†

The architecture and functioning principle of the valve are shown in Fig. 35. The Quake-style microvalve was printed with an Asiga Pico2-HD SL 3D-printer which has a projected XY pixel resolution of 27 μm. We used PEG-DA-258 resin containing 0.6% (w/w) Irgacure-819 as a photoinitiator and 0.6% (w/w) 2-isopropyl thioxanthone (ITX) as a UV photosensitizer. This mixture has been carefully optimized for resolution and biocompatibility.[37] As shown in Fig. 35a & b, the size of the 3D-printed Quake-style valve is around one order of magnitude smaller in diameter than the one that Au et al. made in Watershed.24 The valve devices were printed with 25 μm Z-layer thickness. Other than the bowl-shaped valve seat, our 3D-printed Quake-style valve basically follows the design of the original Quake valve, with a control channel on top of a flow channel (Fig. 35c & d). The membrane layer is printed as a single 25 μm-thick Z layer between the flow channel and the control channel along the Z-axis. The equation describing the relationship between applied pressure P and membrane deflection y at the center of a thin circular membrane of thickness t made of a material of Young's modulus E and Poisson's ratio v is:

$$\frac{Pr^4}{Et^4} = \frac{5.33}{1-v^2} \cdot \frac{y}{t} + \frac{2.6}{1-v^2} \cdot \left(\frac{y}{t}\right)^3 \qquad (eq.\ 4)$$

According to eqn (1), a membrane of r = 0.6 mm (diam. = 1200 μm) and E = 130 MPa deflects by y = 101.7 μm at P = 6 psi. Considering the Z-layer resolution of the printer (the printer can print in Z increments of 25 μm), we decided to design a bowl with a depth of 100 μm to ensure that the valve could be closed at 6 psi. We note that the depth of the bowl also determines the vertical gap from the edge of the bowl to the bottom of the membrane (d = 40 μm in Table. 4), which is a critical parameter because gaps lower than 40 μm result in channel clogging when the Z-layer thickness is 25 μm. Hence, although it is possible to print a valve with a bowl depth of 75 μm (which would in principle be preferable because it is predicted to close at 3.92 psi), it does not print well with the present absorptivity of our resin.

The functioning principle of the valve is shown in Fig. 35e and f. For the operation of the valve,

the control channel was pressurized with air and the flow channel was filled with blue dye (FD&C blue #1, Spectrum, New Brunswick). When zero pressure is applied to the control channel, the membrane does not deflect and the flow channel remains open; when pressure is applied, the membrane deflects. At 6 psi, the membrane contacts the bottom of the bowl-shaped structure and seals the flow channel. With 6 psi, all valves tested were completely closed without damaging or rupturing the valves. There is only a 1.7% difference of deflection distance (y) between the real membrane deflection and the predicted deflection calculated from eqn (1), showing the printer's reliability. To test the valve's durability, the valve was operated under 6 psi at a frequency of 10 Hz for over 16 hours; within that period, the valve was actuated over 500 000 times. After the 16 hour-long test, the valve could still be closed at 6 psi.

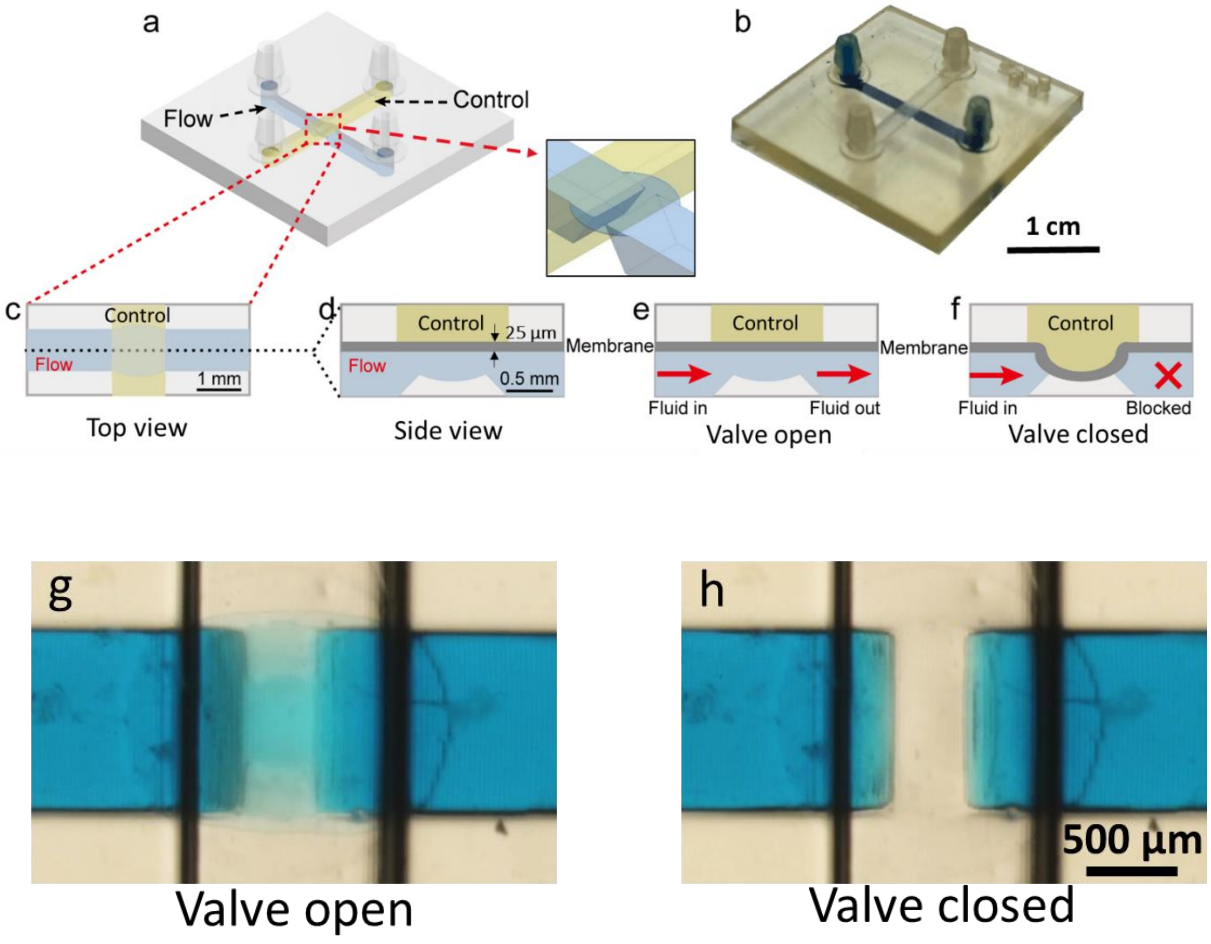

Figure 35: CAD design and the working principle of the 3D-printed "Quake-Style" valve, featuring a 1200 µm-diam. membrane. (a) Isometric diagram, showing the 3D structure of the device. (b) Photographs of a 3D-printed Quake-style valve device with no external

connections. For visualization purposes, the flow channel is filled with blue dye while the control channel, filled with air, appears transparent. (c–f) 2D schematics showing the operation of the valve, with blue and yellow identifying the flow channel and the control channel, respectively. (c) Top-view schematic of the valve. (d–f) Side-view schematics showing (d) dimensions of the valve, (e) the valve in its open state, and (f) the valve in its closed state. (g) Micrograph of the valve in its open state (0 psi) applied to the control channel. (h) Micrograph of the valve in its closed state (5 psi).

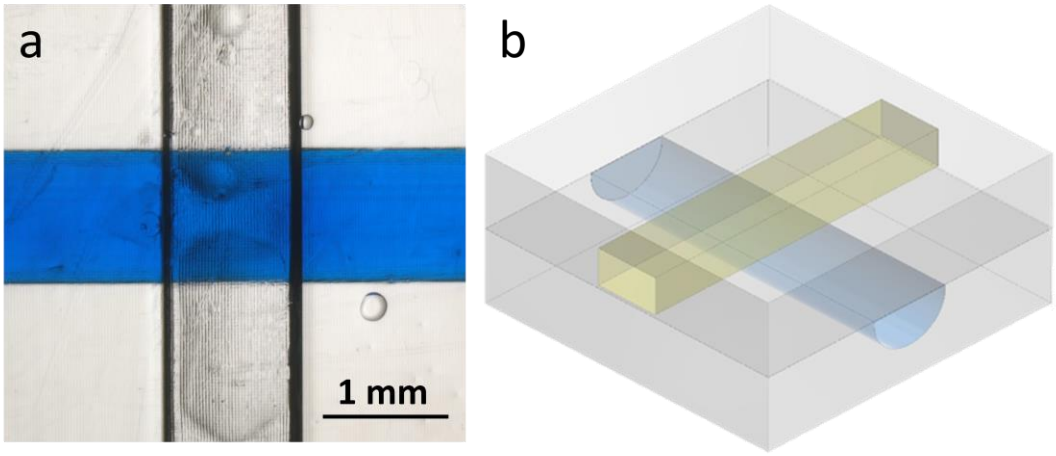

Figure 36: A valve printed with the same design as the original Quake-style valve (see Fig. 35a). (a) The pressure applied to the control channel is 11 psi, and the deflection of the membrane is barely noticeable. With this design, we were not able to close the valve upon application of air pressure in the control channel. Note that the curvature, which is the rounded bottom of the flow channel, is facing up in this device. (b) The isometric view of the 3D-printed original Quake-style.

5.3. Design steps of 3D-printed Quake style valves using Computer Aided Design (CAD)- Inventor

3D-printed design files are imported from the CAD design program (e.g. Inventor) and read by Composer, which is the accompanying 3D-printing program in the Asiga printer. Some settings such as layer thickness, exposure time for each layer, burn-in layer exposure time, build plate moving speed and waiting time after exposure can be adjusted in the program. In the process of checking files in Composer, we find out that it is important to scrutinize the shape of each layer, in this case, the most important layers would be the corresponding to the

valve seat. There are two reasons for checking the geometry of each layer. Firstly, all structures should be placed in the zero position, i.e. the bottom layer needs to show up on the first slice. Secondly, design files are required to be converted to a different file type (.stl file) for the printer to read and print. When the Inventor design file is imported into Composer, the design is sliced (rather than appearing as a continuous structure as in Inventor); these slices are used to fabricate the prints layer-by-layer by the Asiga printer. Sometimes the 3D structure of the design may not be faithfully replicated in the print, as the layer-by-layer process can miss fine structures. Thus, checking the layers that are generated by Composer can help verify the final printed structure of 3D prints prior to printing.

The 3D printed Quake style valve design can be made and visualize in a 3D design software easily. The 3D structure can be viewed from every angle and direction directly by rotating the view cube on the right upper corner. Compared to PDMS device designs that are made using photolithography, 3D printed devices designs can be visualized more intuitively without combining all the 2D layers together in a second source (which might be a piece of paper or in our mind). All the design steps are saved and can be kept track in the software. The design is able to be modified by clicking on each specific 2D sketches or changing the commands or dimensions on each 3D feature. The user interface is shown in Fig. 37.

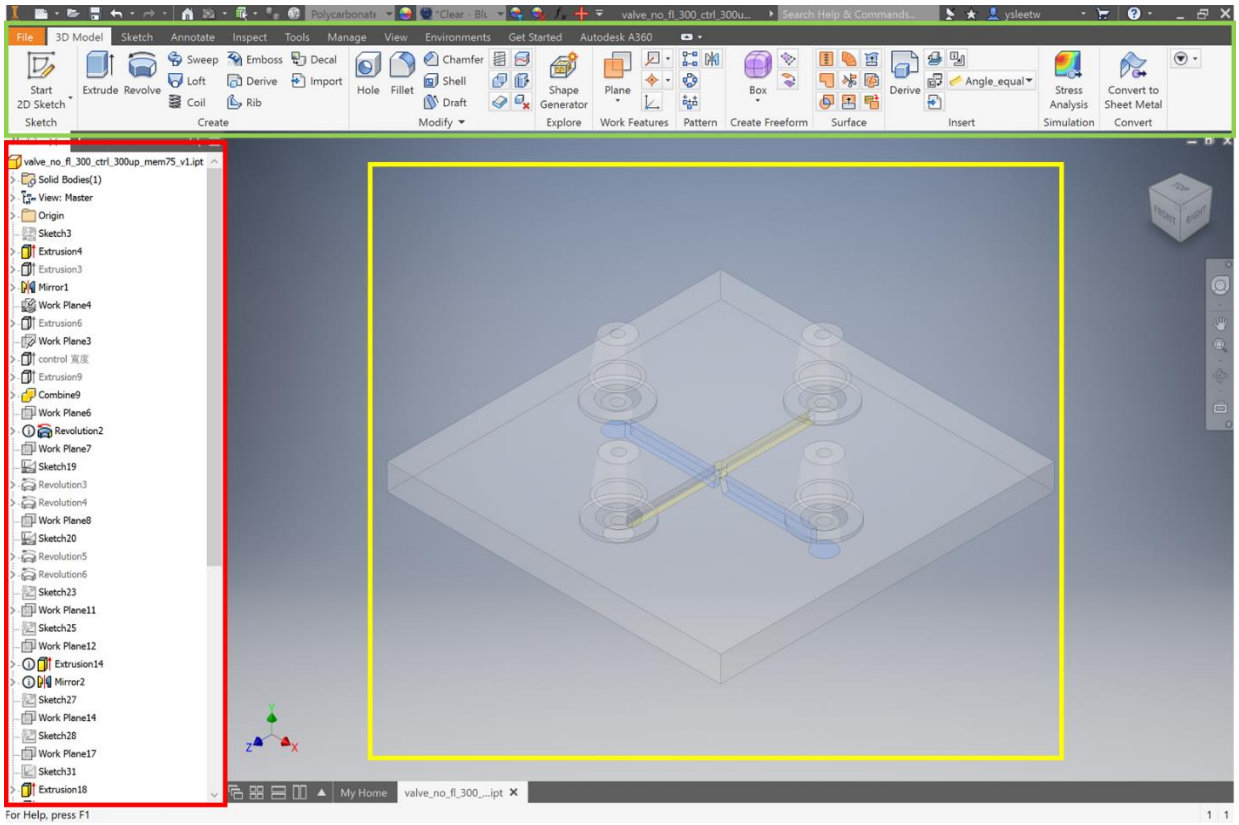

Figure 37: The user interface of Inventor in the 3D design mode. The ribbon, tabs, and panels are boxed by the green outline. The commands and icons in the red box show the design steps of the 3D model. The yellow box renders the 3D model of the design.

All 3D structures are built based on 2D sketches. In other words, we need to draw a 2D sketch before constructing 3D structures. Any kind of geometry can be made in 2D sketches including lines, circles, and polygons. After finishing the 2D sketches, we can apply different 3D commands on 2D shapes like “extrude”, “revolve” and so on to complete the 3D design process. The other feature such as constraints, 2D/3D patterns, move, copy, etc. can be used to assure the relationships between each geometry or ease and expedite the repeated design process. The simplified design process of the 3D printed Quake style valve is shown in Fig. 38.

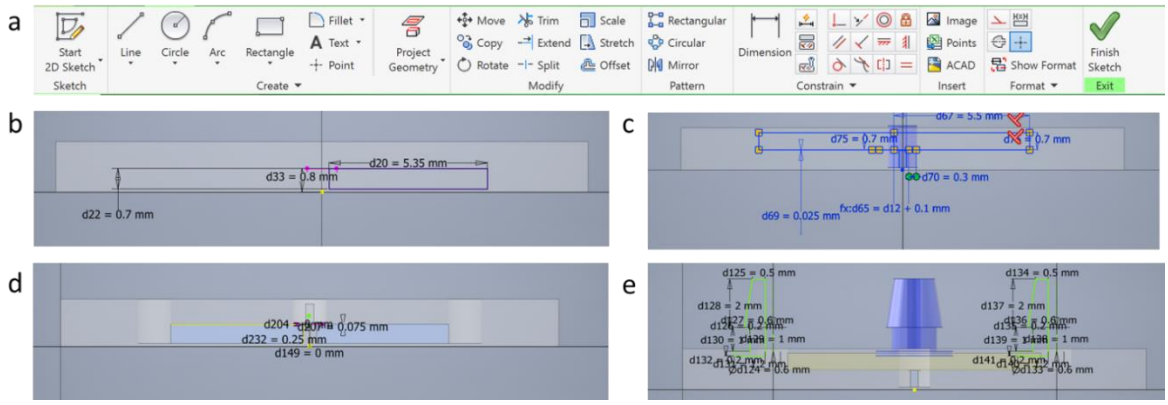

Figure 38: (a) The commands and tabs in the 2D design mode. (b) The 2D draft of the flow channel in the Quake-style valve design. (c) The 2D draft of the control channel in the Quake-style valve design. (d) The bowl shape structure of the valve seat in the Quake-style valve design. (e) The design of the connectors that connect to the flow and control channel.

6. Characterization of 3D printed microvalves and micropumps and its application

The content of this section has been published in the following paper:

Lee, Y.S., Bhattacharjee, N. and Folch, A., 2018. 3D-printed Quake-style microvalves and micropumps. Lab on a Chip, 18(8), pp.1207-1214.- Reproduced by permission of The Royal Society of Chemistry. (Available online at http://pubs.rsc.org/en/content/articlehtml/2018/lc/c8lc00001h)

6.1. Introduction

In this chapter, the functionality and performance of 3D printed Quake style microvalves and micropumps are covered. After finishing the design and prints of the valve, I did the flow rate measurement to test whether the valves can be closed when a continuous flow is applied into the flow channel. The purpose of this testing is too see if the membrane can deflect and seal against the valve seat well as air pressure is applied to the control channel. Also, the minimum applied control pressure was measured when the flow rate at the outlet of the flow channel is zero. A more accurate current measurement was done by testing the current value while letting the saline solution flow in the flow channel. A wire was connected to the inlet and outlet of the flow channel to detect the current change to see whether the flow is blocked by the valve or not. I also tested the dynamic behavior of the valve to observe if the membrane could catch up with the air pressure changes at different frequencies. With the dynamic behavior data, we knew that the membrane is still capable of being actuated even it does not fully close when higher air pressure switching frequencies are applied. Therefore, based on this property of the membrane, I combined three valves in a series to make a pump and actuate these three valves at different timing to make the fluid move peristaltically in the flow channel. With this pump performance test, I was able to get the highest pumping flow rate with a certain air pressure switching frequency on these three valves when the control air pressure is fixed. I also measured the highest pressure that the pump can drive against by applying air pressure to the outlet of the flow channel. Finally, the scalabilities of the valve, including the size and number, are demonstrated in the last part of this chapter. I was able to shrink down the valve size twice with the same valve design. The ability of making large array of the smaller version valves

(500 μm-diam.) were shown in the end of this chapter as well.

6.2. Valve performance testing- valve closing test

We characterized the fluidic resistance of the valve by measuring the flow rate and electrical current through the valve for a given head pressure (see setup schematic in Fig. 39a). We found that by applying 4 psi to the control channel, the flow rate decreased 10 times (∼12 μL min−1) compared to the flow rate when no pressure is applied (∼120 μL min−1). However, the flow was not fully stopped until air pressure greater than 5 psi was applied to the control channel (Fig. 39b). Parameters such as machine resolution, vat condition, and resin chemistry could influence the variability in flow rates observed between prints. The more accurate current measurements in Fig. 39c show that the valve does not fully close until the control pressure reaches 6 psi. The detected current value was ∼700 mA when there was no control pressure applied to the valve and it went down to a negligible ∼4 mA (0.5% of 700 mA) as the control pressure was greater than 6 psi. Idealizing the valve as a circular pipe of diameter D, the current is roughly proportional to D2, and the fluidic resistance of the pipe is proportional to 1/D2, so a closed-valve current value of 0.5% = 1/200 of the open-valve current value implies a closed-state fluidic resistance that is ∼200 times higher than the open-state fluidic resistance. It is important to keep in mind that the membrane deflection is determined by the pressure difference between the control channel and the flow channel. Thus, applying high driving pressure in the flow channel can prevent the valve from closing and even damage the membrane.

a

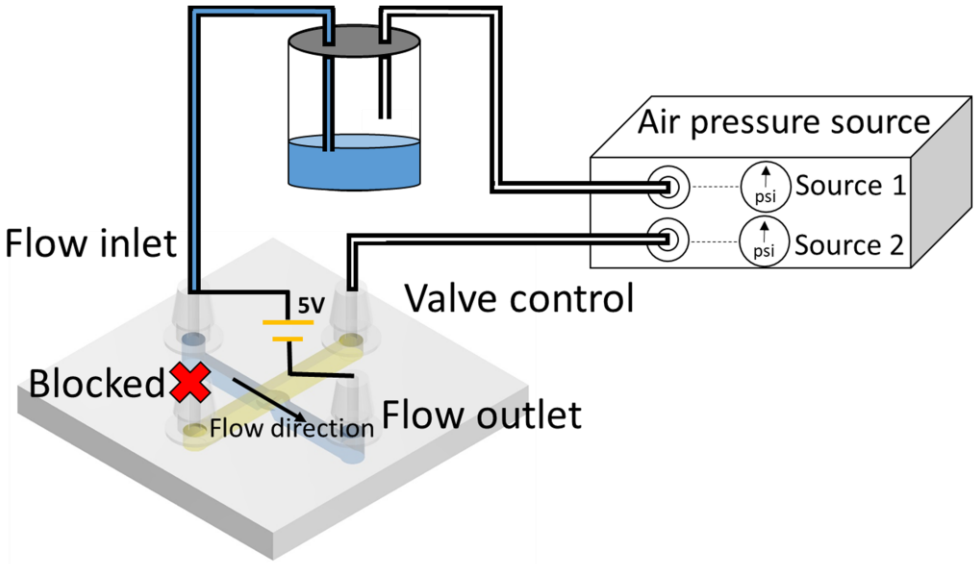
Air pressure source
psi
Source 1
psi
Source 2
Flow inlet
Valve control
5v
Blocked
Flow direction
Flow outlet

b

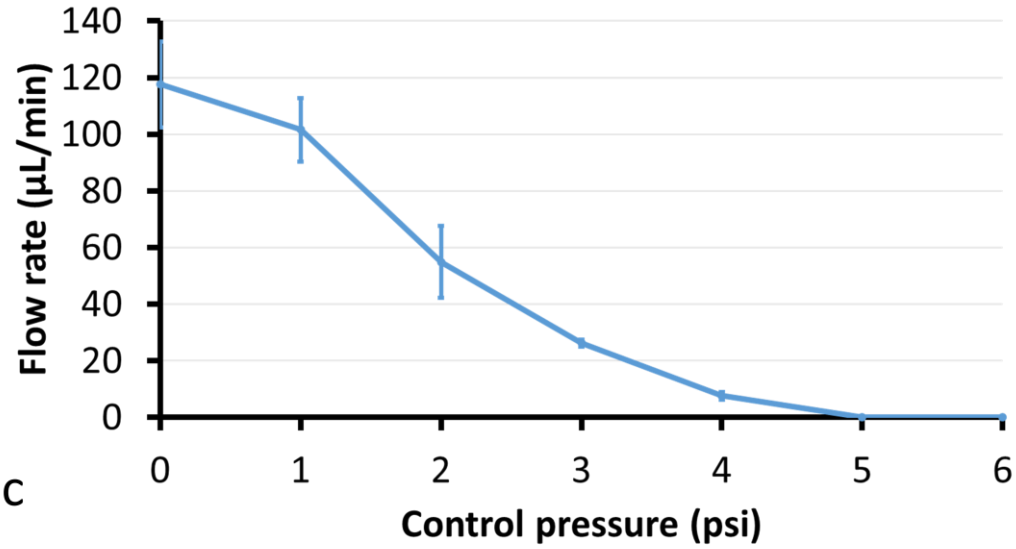
Flow rate (µL/min)
140
120
100
80
60
40
20
0
0
1
2
3
4
5
6
Control pressure (psi)

c

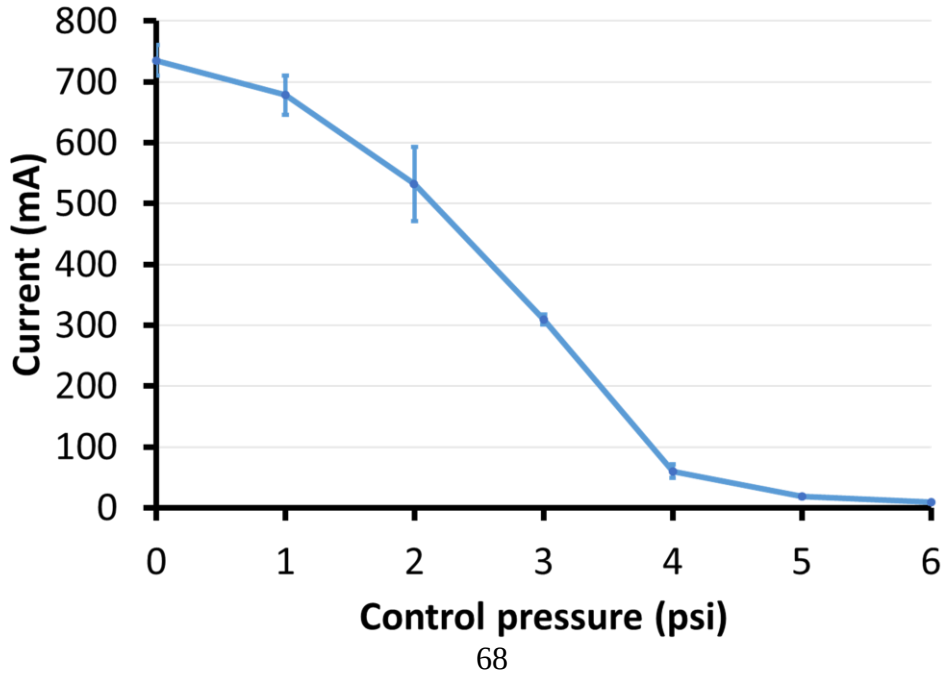
Current (mA)
800
700
600
500
400
300
200
100
0
0
1
2
3
4
5
6
Control pressure (psi)

Figure 39: Flow rate measurements with 1200 µm-diam. valves. (a) Device setup for flow rate experiments. We used a digital pressure source (Elveflow OB1 MK3 system) to control the pressure applied to the control channel. One of the digital pressure outputs is connected to a liquid bottle in order to siphon the fluid out of the bottle and into the flow channel (shown as blue in the valve's schematic diagram). The end of the control channel that is not connected to the bottle is kept blocked. Flow rates vary when different pressures are applied to the control channel. (b) Graph of the flow rate as a function of pressure applied to the Quake-style valve through the control channel. The pressure driving the flow is 0.2 psi for all data points (n = 3). Note that the fluid in the flow channel can be fully stopped when the applied pressure is above 5 psi. The error bars represent standard error of the mean. (c) Graph of the current through the flow channel as a function of the control pressures applied to the valve. A voltage of 5 V is applied to the flow channel filled with a saline solution (0.1 M KCl). The current detection setup is shown in Fig. 40a. As the control pressure increases, the current detected by the oscilloscope decreases. The current is ~4 mA when the applied pressure in the control channel is 6 psi. The pressure driving the flow is 0.2 psi for all data points (n = 3). The error bars represent standard error of the mean.

6.3. Valve performance testing- dynamic behaviors of valve

Next, we characterized the dynamic behavior of the valve by measuring the current that passes through a saline-filled flow channel while the valve is being actuated at different frequencies. The device setup is shown in Fig. 40a. A high current amplitude represents the valve open state and a low current amplitude represents the valve closed state. At 5 Hz, the valve was able to open and close as described by the high peak-to-peak current amplitude compared to higher frequencies of 20 and 30 Hz. At these high frequencies, the peak-to-peak current amplitude decreased, signifying that the valve was no longer able to fully open or fully close. At 5 Hz, the valve remained open for ~100 ms during a full cycle of opening and closing, shown by a plateau after the rising phase of the electrical current curve (Fig. 40b, black arrow). The valve took approximately 100 ms to close, of which it spent ~20 ms fully closed (Fig. 40b, white arrow). As the frequency was increased, the time period of the plateaus became shorter, meaning the valve's reaction time was not fast enough to react to the even faster changes in air pressure signal in the control channel (Fig. 40b, dashed black line). A movie of the valve

actuation at different frequencies is shown in ESI† (Movie S1).

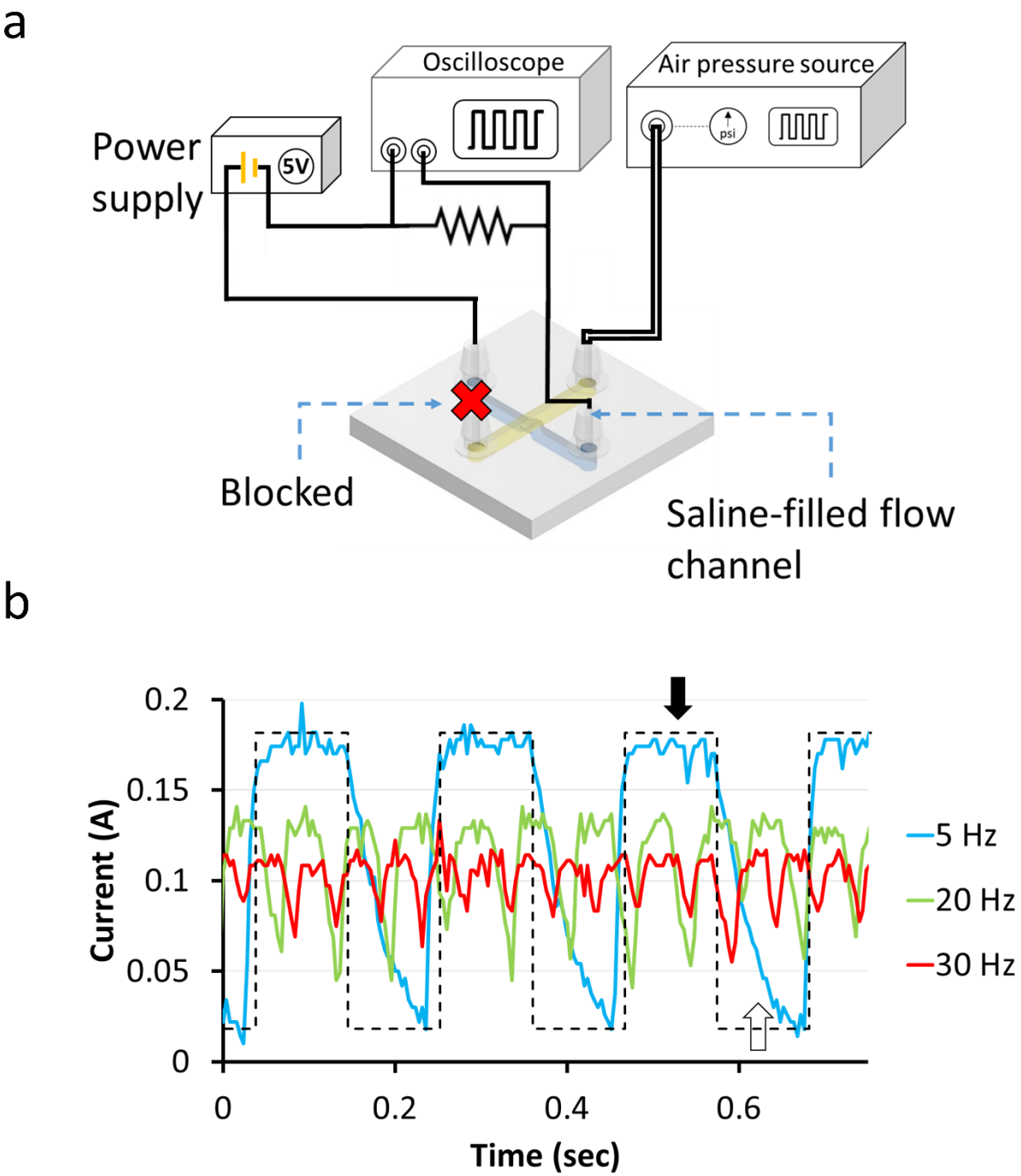

Figure 40: Measurement of valve dynamics with a 1200 µm-diam. valve. (a) The flow channel is filled with 0.1 M KCl solution. The inlet and outlet of the flow channel (colored with blue) are connected to an electric circuit, one end of the flow channel is connected to the power supply and the other end is connected to an oscilloscope. The voltage of the power supply is set to 5 V. A pressure of 5 psi is applied to the control

channel (colored with yellow). (b) Voltage changes during the valve opening and closing states at three valve actuation frequencies (5, 20 and 30 Hz). The black and white arrows show the fully open and fully closed states, respectively. The dashed line shows the ideal current change at 5 Hz assuming the valve responds infinitely fast to the pressure changes.

6.4. 3D-printed Quake-style pump design

Integrated micropumps add portability and reduce the number of external accessories in microfluidic chips.[72–74] Our 3D-printed Quake-style pumps were made by combining three valves in series (Fig. 41). A smaller valve leads to a membrane with a faster reaction time and higher resonance frequency, thereby propelling fluid more efficiently. While the higher stiffness of PEG-DA-258 compared to PDMS is a disadvantage during the deflection phase, it provides a high restoring force for the membrane to quickly return to its resting position without the application of negative pressure. The STL file of the micropump design is available in ESI.†

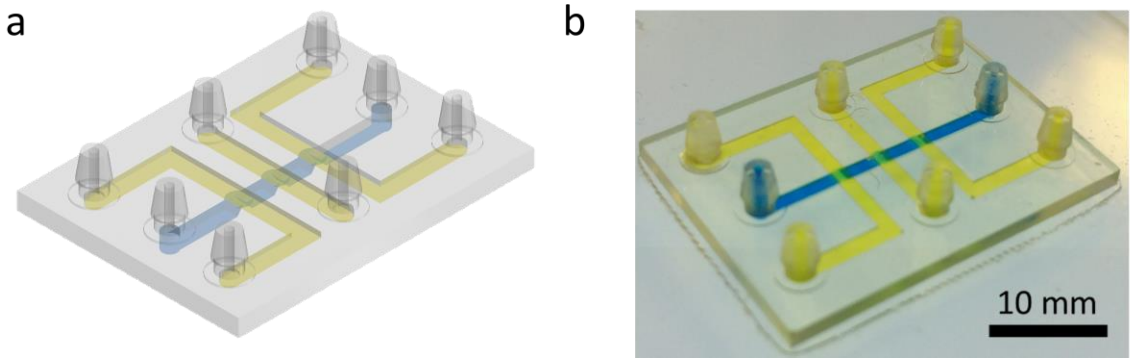

Figure 41: 3D-printed Quake-style pump featuring 1200 µm-diam. valves. (a) Isometric view of the CAD design of the Quake-style pump. (b) Isometric view of the 3D-printed Quake-style pump. The flow channel and control channels are shown in blue and yellow, respectively. The STL file of the micropump design is available in ESI.†

6.5. 3D-printed Quake-style pump performance

The pump was operated by following a standard peristaltic sequence (shown in Fig. 42a). In this sequence, there are 5 states and the switching period (T) between each state ranges from

10 ms to 500 ms. Here, pump actuation frequency (f) is defined as 1/T. Even though the valves were opened and closed almost completely with low pump actuation frequencies, the fluid movement was too slow to be observed at 5 Hz (Movie S2, ESI†). With a fixed control pressure of 7 psi, the flow rate reached a maximum of ~6.5 μL min−1 at a pump actuation frequency of 20 Hz (Fig. 42b). Although the valves did not fully close and open at a pump actuation frequency of 20 Hz, which is the same frequency at which each valve is actuated, the rapid opening and closing of the valves still displaced liquid and compensated for the lower pumping efficiency. We calculated that the amount of fluid pumped by each valve in 1 min is 32 nL at 5 Hz and 18 nL at 20 Hz. Despite the fact that the valves pumped around half the volume at 20 Hz compared to 5 Hz, in the same amount of time they opened and closed four times more often at 20 Hz compared to 5 Hz, so in total the pumping rate at 20 Hz (21.6 μL min−1) was about twice the pumping rate at 5 Hz (9.6 μL min−1). We also determined the maximum head pressure that the 3D-printed pump can overcome (maximum pump back pressure). For these experiments, we used a control pressure of 14 psi to actuate the pump and the pump actuation frequency was 20 Hz. Under these conditions, the pump was able to overcome at most a head pressure of 0.2 psi, which is equal to the pressure exerted by a 140 mm column of water (Fig. 42c); as the pressure that was applied at the outlet of the flow channel increased above 0.2 psi, the flow started to move backward (represented as negative flow values in Fig. 42c).

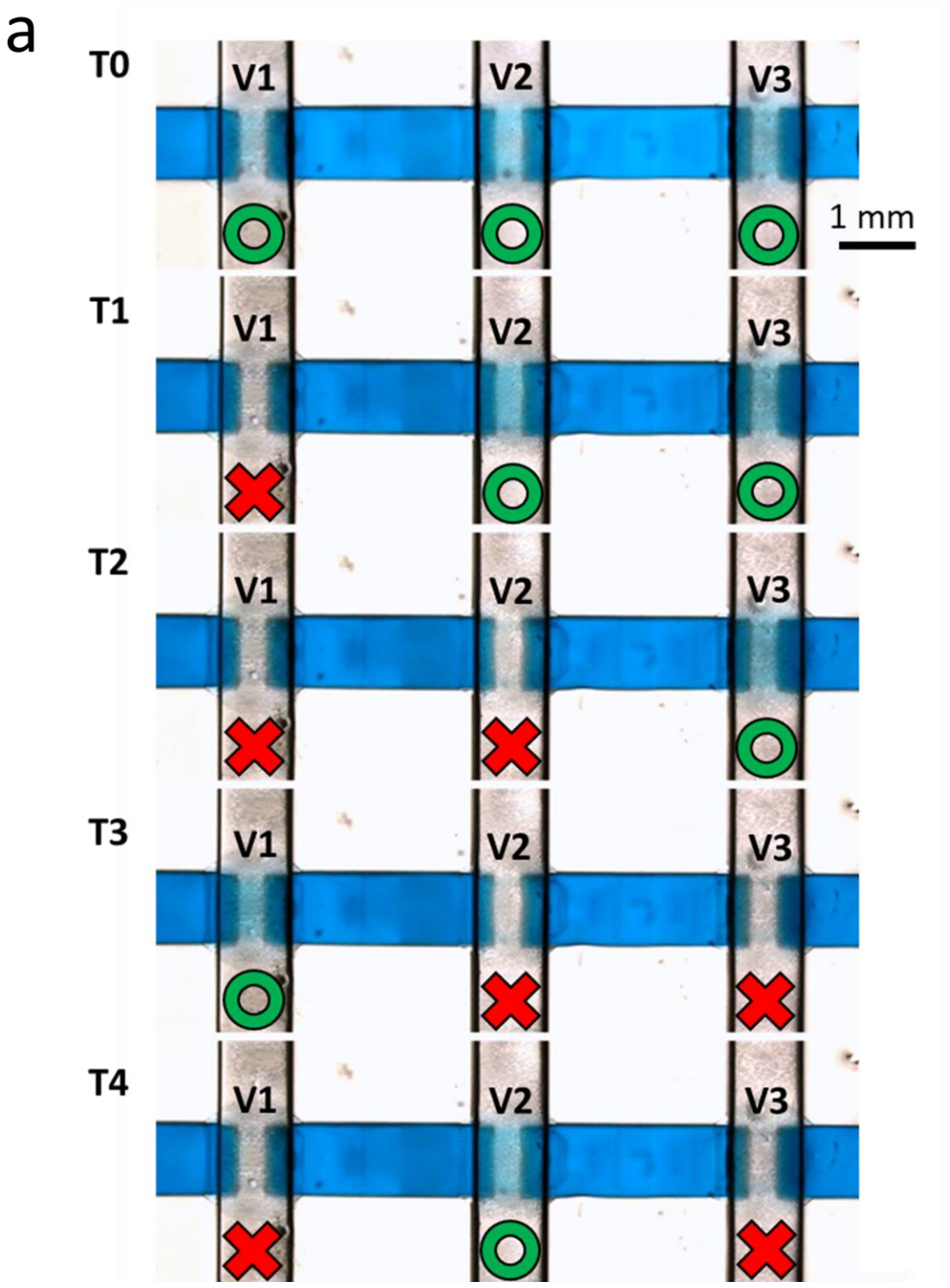
a
T0
T1
T2
T3
T4
V1
V2
V3
1 mm

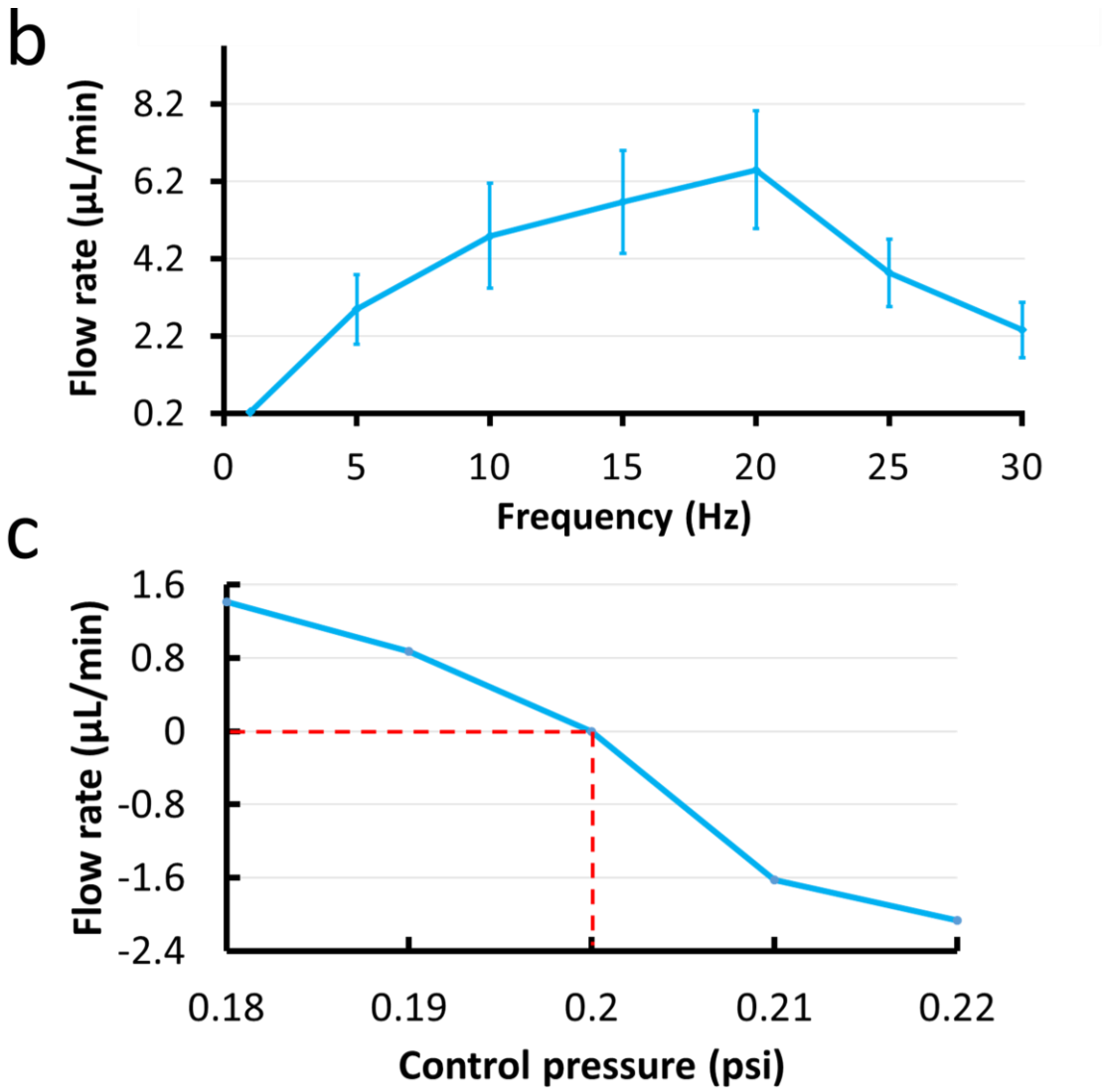

Figure 42: (a) The valve actuation sequence used to control a Quake-style pump with 1200 µm-diam. valves. In the first state (T0), all valves are open. The states denoted from T0 to T4 show each state of the 5-phase actuation. Each valve *n* (V_n) is closed in the T_n state and in the T_{n+1} state. After finishing the first round, from T0 to T4 states, the valve closing cycle repeats between the T2 state and T4 state; the red color represents the state of valve closed state and the green represents the valve open state. (b) Graph of the relationship between pump rates and pump actuation frequencies. The valve closing pressure is fixed at 7 psi. The pump has the highest flow rate when the pump actuation frequency is 20 Hz. Experiments were conducted in triplicate. (c) Graph of pumping flow rates *versus* the head pressure that the 3D-printed Quake-style pump can work against when the control pressure is 14 psi with 20 Hz pump actuation frequency. When a pressure of 0.2 psi is applied at the outlet of the flow channel, the

fluid stalls. The fluid moves forward (positive flow rates) when the head pressure is less than 0.2 psi and backward (negative flow rates) when the head pressure is greater than 0.2 psi.

6.6. Scalability of valve- 500 μm-diam. valve array

One of the powerful features of the Quake design is its scalability. We decided to test the scalability of the Quake-style design by reducing its size to a diameter of 500 μm (membrane thickness 10 μm and bowl depth 75 μm; see Table. 4) and by producing three identical arrays of 8 × 8 = 64 valves each. One of the arrays is shown in Fig. 43. Here the control channels have also been reduced to 300 μm width. We were able to print, rinse, and operate all 64 valves in all three arrays. Only 3 psi was needed to close these smaller valves. We also tested the durability of the valve array, which could be actuated at 10 Hz (3 psi of closing pressure) over 500[thin space (1/6-em)]000 times. This compact valve array not only demonstrates the scalability of the Quake-style design but also shows the high yield and reliability of the 3D-printing process.

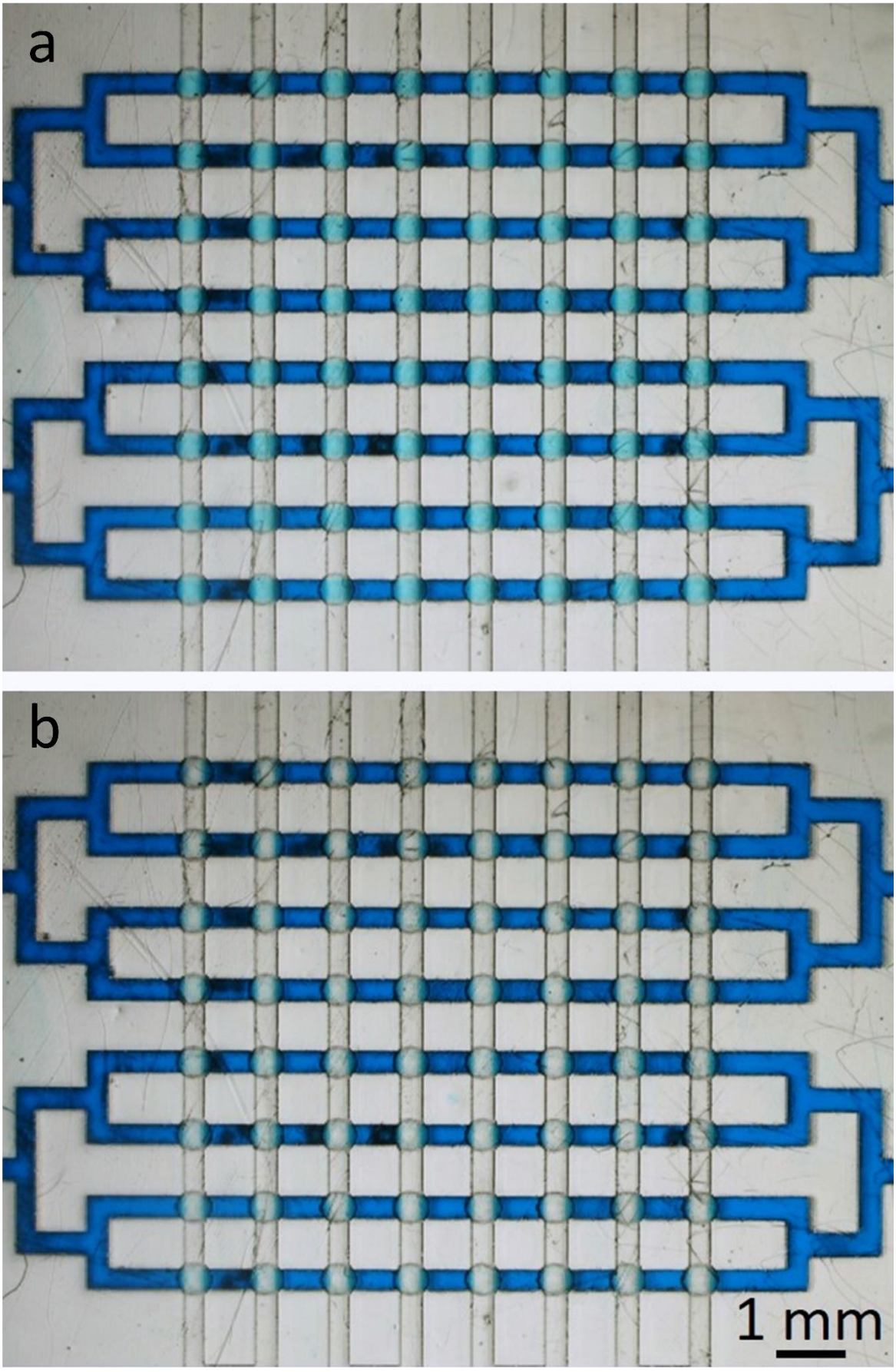
a
b
1 mm

Figure 43: The 3D-printed Quake-style microvalve array of 64 valves (500 µm-diam. valves). All the flow channels share one common inlet and outlet and all the control channels also share one common inlet and outlet. (a) All valves are open without applying any pressure to the control channels. (b) All the valves are closed by applying 3 psi to the control channels.

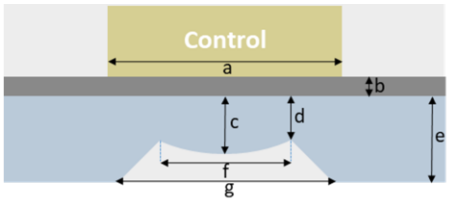

	Z-layer thickness	a	b	c	d	e	f	g	Membrane shape	Valve seat shape
Valves with 1.2 mm size	25 µm	1.2 mm	25 µm	100 µm	40 µm	700 µm	300 µm	1 mm		
Valves with 0.5 mm size	10 µm	0.5 mm	10 µm	75 µm	40 µm	700 µm	200 µm	500 µm		

Table 4: Critical dimensions in the 3D-printable Quake valve design (not to scale, see Fig. 34b for the isometric view), shown in the cross-section of the valve seat. The table shows the dimensions of two different sizes of valves. The 1.2 mm-diam. valves are shown in Fig. 35b & Fig. 41b and the 0.5 mm-diam. valves are shown in Fig. 43. The width of the control channel is = 1.2 mm (larger valves) and 0.5 mm (smaller valves). The thickness of the membrane is b = 25 µm larger valves) and 10 µm (smaller valves). The distance between the membrane and the lowest bottom of the valve seat is c = 100 µm (larger valves) and 75 µm (smaller valves), which means the membrane's maximum deflection is ~100 µm and ~75 µm for the larger valves and the smaller valves, respectively. The shortest gap between the membrane and the highest edges of the valve seat is 40 µm for both two sizes of valves; this distance determines if the flow channel will get clogged after being printed: In the case of printing larger valves, if the gap is less than 40 µm, the residual PEG-DA-258 resin in the flow channel becomes heavily photopolymerized and is hard to remove. As for smaller valves, we decided to keep the gap same distance (40 µm) to ensure that the valve seat never gets clogged. The height of the flow channel (excluding the valve seat) for both sizes of valves is e = 700 µm. The length between the two top edges of the valve seat is f = 300 µm (larger valves) and 200 µm (smaller valves). The length between the bottom edges of the valve seat is g = 1 mm (larger valves) and 500 µm (smaller valves). Both f and g should not be greater than the width of the control channel, which is a;

otherwise, the valve seat part will be exposed to too much UV light when the control channels walls are being built causing the valve seat to get clogged. In the membrane shape column, the red dashed contours indicate the membrane shape of larger valves (1200 µm-diam.) and smaller valves (500 µm-diam.). In the valve seat shape column, the red dashed contours indicate the valve seat shape of larger valves (1200 µm-diam.) and smaller valves (500 µm-diam.).

7. 3D printer and device testing setups

The content of this section has been published in the following paper:

Lee, Y.S., Bhattacharjee, N. and Folch, A., 2018. 3D-printed Quake-style microvalves and micropumps. Lab on a Chip, 18(8), pp.1207-1214.- Reproduced by permission of The Royal Society of Chemistry. (Available online at http://pubs.rsc.org/en/content/articlehtml/2018/lc/c8lc00001h)

7.1. Introduction

By means of using 3D printers, 3D printed microfluidic devices are no longer made in a clean room. The merits of 3D printing such as cleanroom free fabrication processes (only a desk is needed instead of having a room) and high manufacturability provide a great chance for more researchers and engineers to develop more different types of microfluidic devices. The development of 3D printing of this project is elaborated, for instance, the printing material we use for the 3D printed microfluidic devices, two DLP-SLA 3D printers, the setup and the connection between 3D printers and a computer, and the printer's settings. In addition, the device testing methods are also presented in this section. There are several device characterization methods covered including the flow rate measurement when the valve is closed, the dynamic behavior observation of the valve with current measurement, and the pumping rate test. All the basic device characterization methods are provided here in case a new version of the valve type is developed and needs to be tested in the future. The connection among the computer, air pressure hardware and observation platform and the configuration of the device testing setup are provided here as well.

7.2. Materials for 3D printing

We use poly(ethylene glycol) diacrylate (MW = 258) (PEG-DA-258, Sigma-Aldrich, MO), mixed with 0.6% (w/w) Irgacure-819 (photoinitiator) (BASF, IL) and 0.6% (w/w) 2-isopropyl thioxanthone (ITX, photo-sensitizer, PL Industries, PA) as the resin for making 3D printed Quake-style valves and pumps. ITX increases the absorption of the resin at the wavelengths where the spectra of ITX and Irgacure-819 overlap (~385 nm).37 According to the Beer-Lambert law, an increase in resin absorption leads to a decrease in the characteristic penetration depth at the exposure wavelength (385 nm).37 Thus, adding ITX to the resin allows us to

fabricate the 25 μm-thick membranes and the 100 μm-deep flow-channels required for the Quake-style valve design. The resin is prepared by mixing Irgacure-819 and ITX with PEG-DA-258 with a mini vortexer and put in an oven at 70 °C for 30 min to complete the dissolution of ITX, which does not dissolve readily at room temperature. After the preparation process, the resin is stored at room temperature and kept in a polypropylene container wrapped in aluminum foil to prevent exposure to ambient light. HEALTH WARNING: PEG-DA-258 resin (mixed with photoinitiator) is highly irritant and can cause severe burns and irritations. It should only be handled with gloves (double gloves for optimal protection) and in a very ventilated space (where no accumulations can occur) or inside a fume hood.

7.3. 3D-printer

We use the DLP-SL (digital light processing – stereolithography) printer Asiga Pico2-HD (Sydney, Australia) (Fig. 44 & 45) to print our microfluidic devices. This 3D-printer has an LED light source with UV wavelength 385 nm and LED power of 32.21 mW cm−2. We chose Irgacure-819 as the photoinitiator because it has an absorbance peak close to 385 nm. The XY pixel resolution of the 3D printer's projector is 27 μm, and its minimum Z plane resolution is 10 μm. The maximum build size (printable area) of the print is 51.8 mm (X) × 29 mm (Y) × 75 mm (Z). 3D-printed devices can be printed successfully by setting an appropriate exposure time and calibrating the zero position of the build plate before starting the print. To assure all printed layers are fully reacted, the build plate should not lift too fast (<0.2 mm s−1) after each layer is exposed.

The devices are printed on the silanized glass slide instead of being printed directly on the build plate to increase device transparency. Each glass slide is silanized with 3-(trimethoxysilyl)propyl methacrylate (TMSPMA, Sigma-Aldrich, MO). PEG-DA-258 is applied on the glass slide which is then placed on the build plate of the printer and exposed to UV light for ∼3 s to secure it on the build plate.34 After each print is completed, a small razor blade is used to remove the glass slide from the build plate and shave off any residue of cured PEG-DA-258 on the back side of the glass to provide a sharp and clean view of channels and valves under the microscope without any scratches imprinted on the device. The glass substrate also allows for easier removal of the print from the build plate since, in our case, the glass slide is slightly larger than the build plate. Removing the glass slide from the build plate minimizes the risk of damaging the printed device itself, and the flatness of glass slides helps the whole device sit on the microscope stage firmly and horizontally.

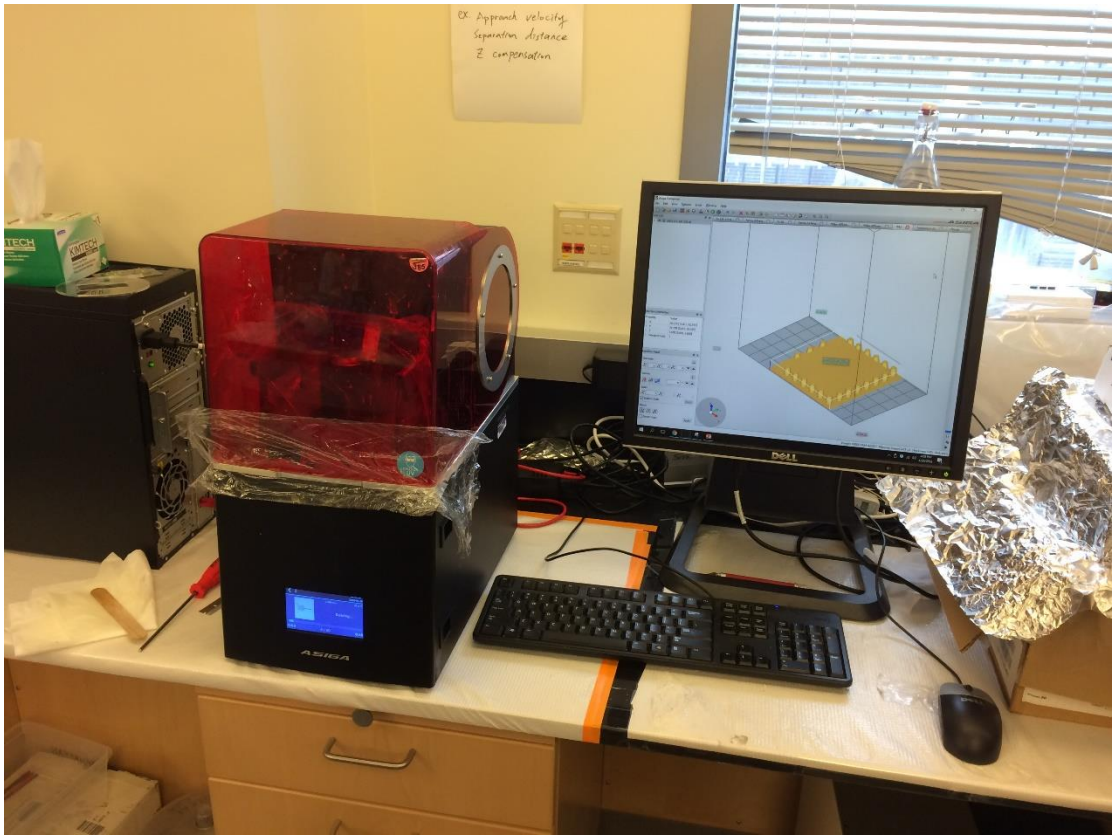

Figure 44: The Asiga's 3D printer setup. The settings of the Asiga's 3D printer are controlled by the 3D printer's software- Composer.

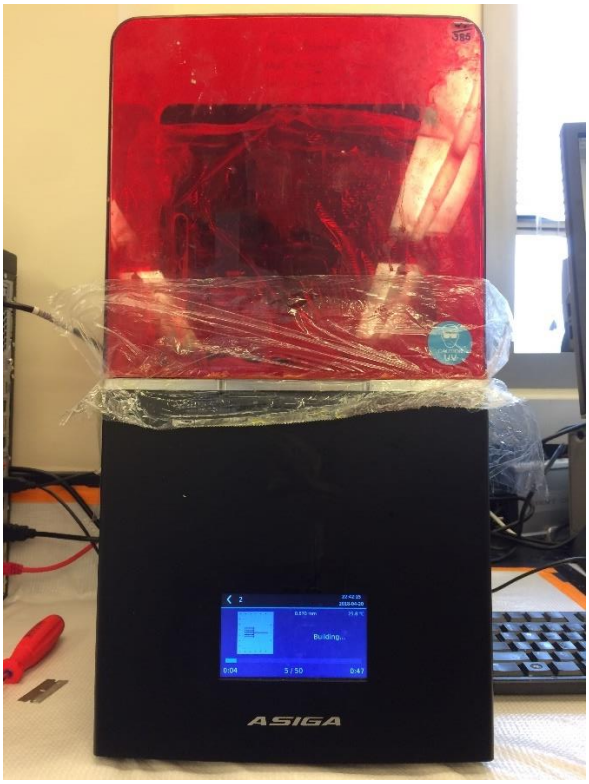

Figure 45: The Asiga's 3D printer. The screen on the printer shows the geometry of the current printed layer. Some printer settings such as Zero position, film thickness of the vat can also be changed through the touchscreen.

Some important parameters are needed to be checked before starting the print because they will affect the quality and outcome of the print and the performance of the device.

The values of each parameter can be tuned in the software of the Asiga's printer- Composer. The printing range can be changed if we want to print specific layers with different parameters. For example, we can print the membrane layer with 10 µm layer thickness and shorter exposure time and the other layers with 50 µm layer thickness and longer exposure time and when we are printing the Quake-style valve design. Also, we realized that the slider under the vat is an important feature in this printer. We need to turn on the slider and make it move slowly (~2 mm/s) during the print; otherwise, there will be a severe sticking problem which might damage the print. To prevent the sticking problem of the vat, the waiting time after exposure and separation velocity are crucial as well. The waiting time after exposure needs to be long and is 8 seconds in this case and the separation velocity of the build plate after UV exposure is set to 0.16 (which needs to be as slow as possible for delicate devices). The interface of the settings is shown in Fig. 46 & 47.

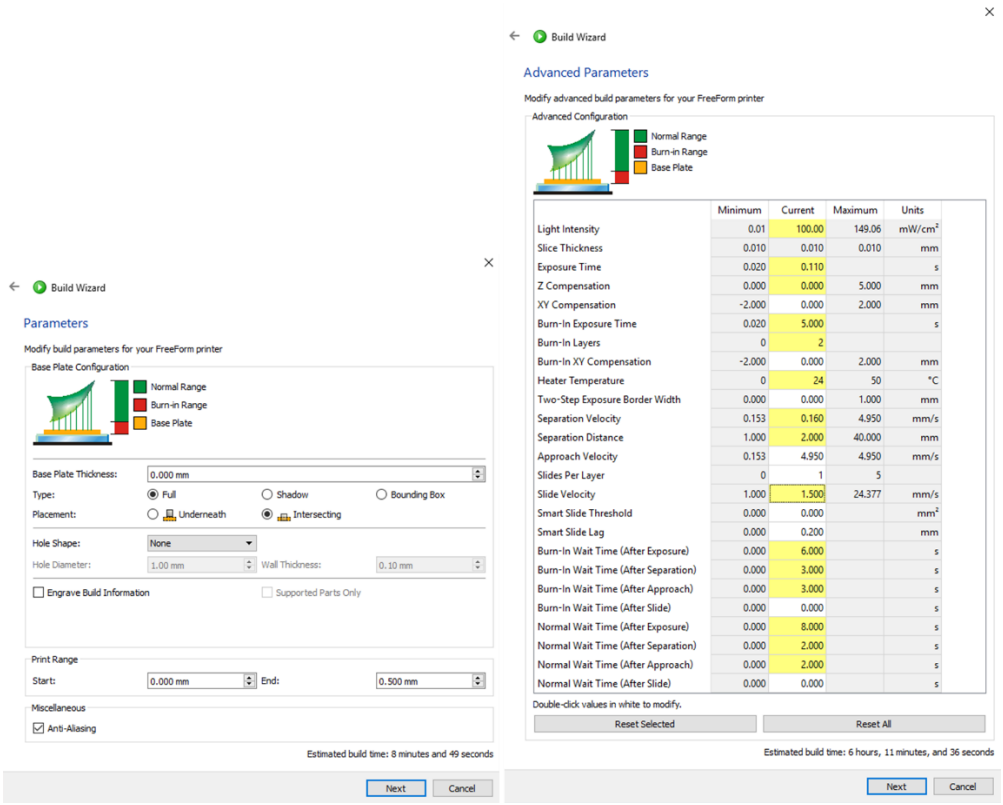

Figure 46: Build parameters for printing. The device can be separated into several prints by changing the print range. For example, the device can be printed with 25-µm layer thickness from height 0 to 0.5 mm, 10- µm layer thickness from height 0.5 to 1 mm and 50- µm layer thickness from 1 to 3.6 mm (the total height of the device is 3.6 mm, in this case). There are also some settings that can be changed like light intensity, exposure time, slide velocity, wait time after exposure and separation.

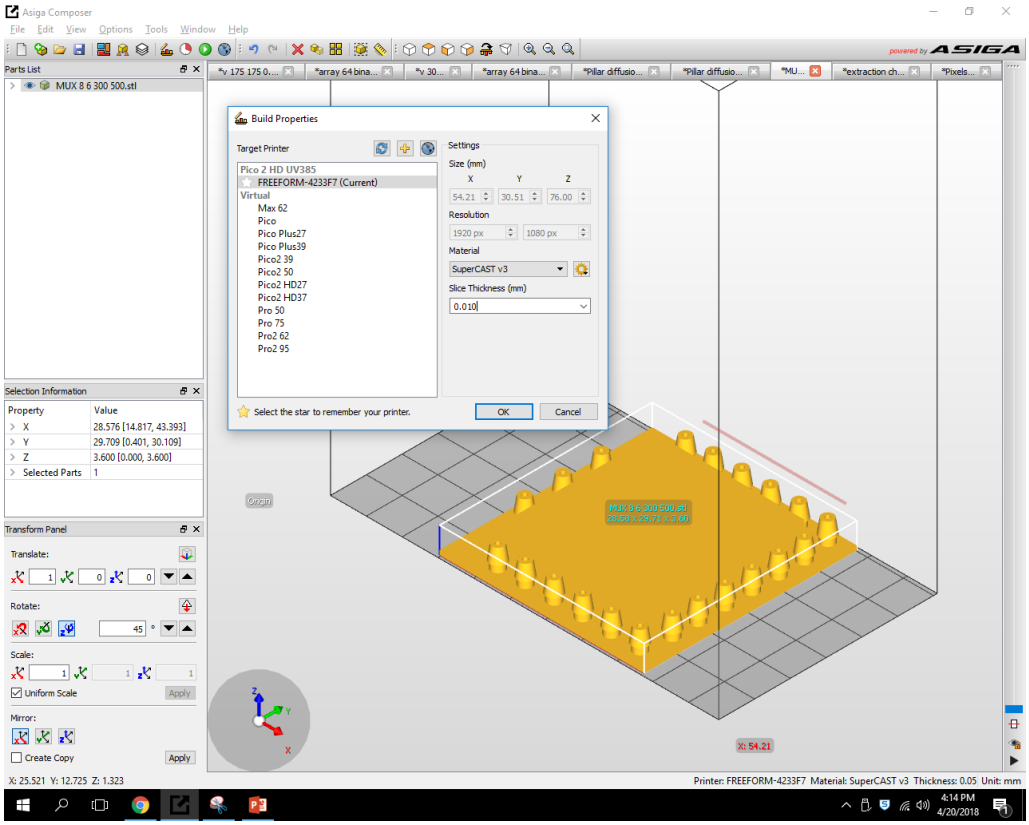

Figure 47: The slice thickness can be tuned. The thinnest layer that the Asiga's 3D printer can print is 10 µm. For our microfluidic devices, the most common thicknesses are 10, 25 and 50 µm.

The slice of each layer can be checked before starting the print. For instance, the bowl shape of the valve design is shown in the upper two photos in Fig. 48. The circle structure is smaller when the printer prints the bottom parts of the bowl shape and it becomes bigger when it prints the upper parts of the bowl shape. The membrane layer is printed in layer 81 and there is only one white layer (which means a 10- µm intact layer) printed between the last layer of the flow channel and the first layer of the control channel. The photo on the right bottom corner shows the structure of one of the control channel layers.

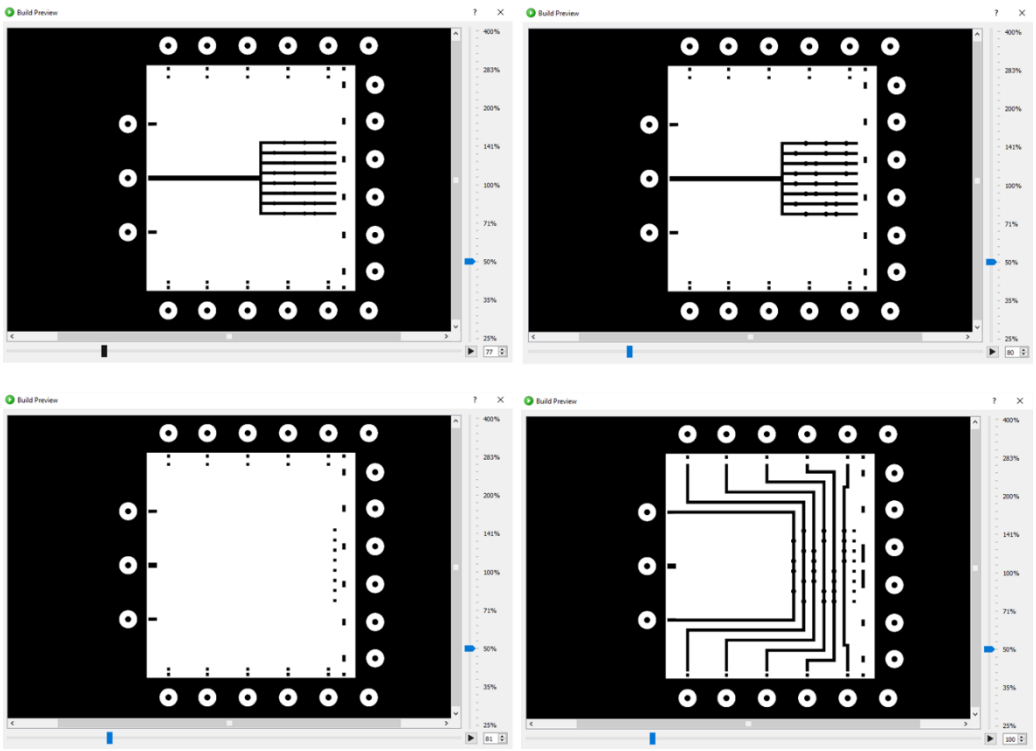

Figure 48: The slice preview of different layers.

7.4. Valve/pump device fabrication

All devices are designed using the computer-aided design (CAD) program Autodesk Inventor. The connectors, which connect tubes and channels, can be either designed together with the valve in the same 3D CAD file or created separately and assembled with the valve design into a single 3D CAD file. The finished 3D CAD files are then converted to STL (stereolithography or standard triangle language) files for the 3D print software. The STL files are provided as ESI.†

The layer thickness of each layer is 25 μm and the exposure time of each layer was set to 160 ms. We chose 25 μm as the layer thickness because it is not too thick for the membrane to seal the valve seat with high pressure. Although the Z-axis resolution of the printer is 10 μm, we were not able to reproducibly make 10 μm-thick membranes that would resist both the fabrication process (the separation from the build plate tends to tear such thin membranes) and/or the operation. The print starts with a burn-in layer, which is the base of the printed device. We set the exposure time of the burn-in layer to 4.5 s. The membrane, which is located between the control and the flow channel, is the main component of the valve structure (Fig. 34b). The valve is composed of a 25 μm-thick membrane placed between the extruded bowl-shape valve seat and the control chamber where the air pressure is applied. The shape of the

membrane is defined by the deflectable, suspended region which is bounded by two parallel lines (1 mm) on two sides and two arcs on the other two sides (r = 0.5 mm). About 30 nL is displaced when the valve is closed. The height of the control channel and the flow channel are both 700 μm. The total volume of the liquid in the flow channel is 6.54 μL.

During printing, resin remains trapped inside the channel after the roof layers are printed, so the channel must be flushed and the unpolymerized resin must be completely removed before the device is exposed to ambient light to prevent clogged channels. Considering this, connectors play a key role during the valve fabrication process, in addition to their role as inlets and outlets during operation of the device, they provide a reliable fluidic path for the removal of unpolymerized resin. Flushing can be done either under ambient light or under dark/low-light conditions. If done under ambient light, the flushing must be done swiftly (<10 s, to prevent photopolymerization of the resin in the channel caused by the ambient light), otherwise flushing should be done under low-light conditions. As soon as the printing is finished, the build plate with the printed sample on it is covered with aluminum foil, taken into a dark room and soaked in deionized (DI) water for over 3 min. A syringe filled with DI water is used to flush out unpolymerized resin in both the flow and control channels of the device. Channels are flushed carefully several times and no vacuum is applied during the cleaning step in that the vacuum could inadvertently break the membrane.

7.5. Flow rate measurements

There are one flow channel and one control channel in the valve device. The inlet of the flow channel is connected to a bottle containing blue food coloring dye. The bottle is pressurized by a computer-controlled air pressure source (Elveflow OB1 MK3) to drive the dye into the flow channel. The fluid driving pressure is fixed at 0.2 psi. To observe the flow rate, the outlet of the flow channel is connected to the silicone tubing (0.79 mm I.D., Cole Parmer). As for the control channel part, the outlet is sealed with a plastic tube cap and the inlet is also connected to the air pressure source starting from 0 psi. The air pressure is increased in increments of 1 psi in the control channel until the valve closes such that movement of the front end of the fluid in the flow channel stops. Experiments were conducted in triplicate. The whole air pressure system setup is shown in Fig. 49.

7.6. Current measurements to visualize the dynamic behavior of the valve

The flow channel of a microvalve (size: 1.2 mm-diam.) was filled with 0.1 M KCl solution as an electrolyte to provide conduction to a pair of electrodes inserted into the inlets. A constant voltage (5 V) was applied to the flow channel through connecting the inlet and outlet of the flow channel and a power supply with those electrodes (Fig. 40a). The experiment was started after assuring the current values shown on the oscilloscope are stable and there was no electrolysis observed during the test. The valve was opened and closed by applying 0 and 5 psi to the control channel, and the current changes were measured with an oscilloscope. Current changes as the valve was being closed and opened at different frequencies were recorded by the oscilloscope and plotted as a function of time to visualize the dynamic behavior of the valve. Experiments were conducted in triplicate. The whole air pressure system setup is shown in Fig. 49.

7.7. Pump flow rate measurements

For these measurements, the flow channel of the pump device was filled with blue dye. The pumping sequence was initiated after assuring that the fluid was immobile in the flow channel. The head of the fluid was set to start in front of the valve closest to the outlet and pumped towards the outlet until the fluid head arrived at the outlet. There are a total of five states in the actuation sequence of the valves, with valves open and closed at different time periods. After finishing the first cycle of the sequence, the sequence was repeated as a loop in the last three steps. Pump flow rates were measured by recording videos for each condition and analyzing the liquid displacement in the channel with ImageJ and VLC media player (the time was recorded to the first decimal place). The whole air pressure system setup is shown in Fig. 49.

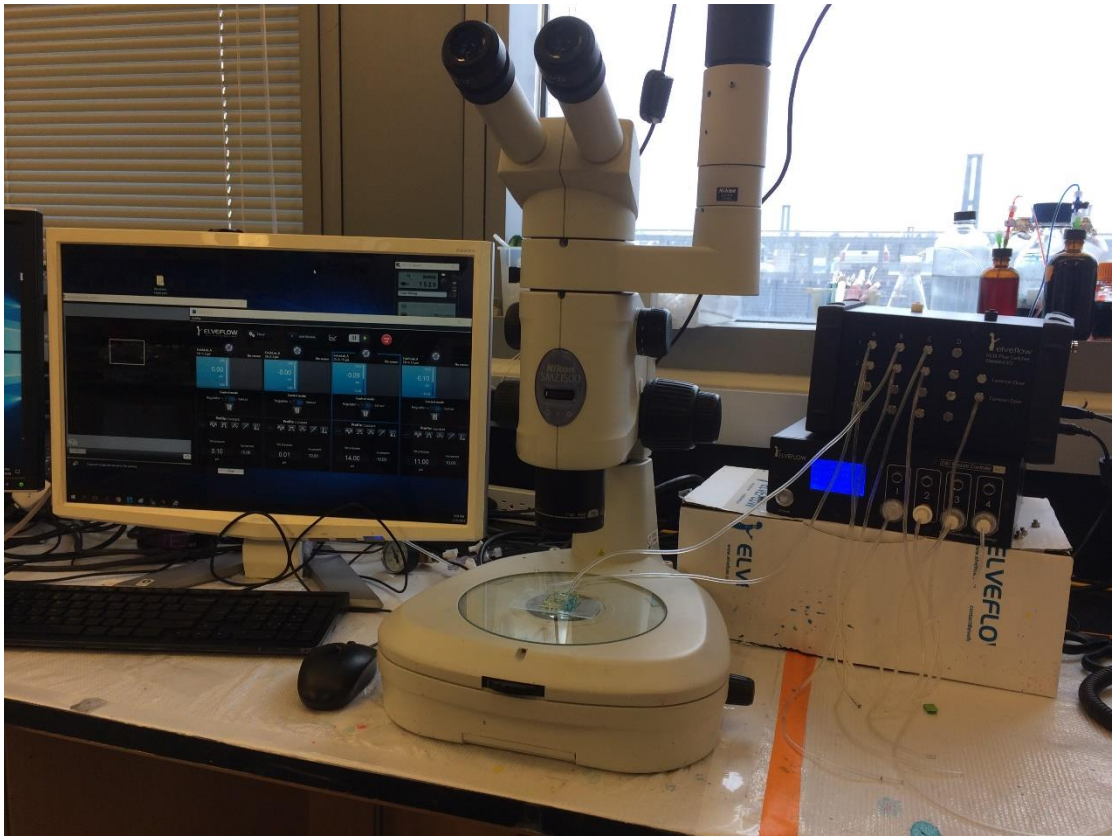

Figure 49: The interface of the air pressure control system- Elveflow. OB1 MK3, which is a pressure supply, provides positive and negative pressures (± 14 psi) to control microfluidic flow systems. MUX, which is a microfluidic flow switch matrix, can be connected to OB1 MK3 and provides up to 16 pneumatic channels with controllable on/off sequences.

8. Future Research Work

3D printing technology has been helping improve the manufacturability of microfluidic devices in terms of shortening fabrication time, reduce the cost and need of labor, simplifying design processes and decrease the difficulty of device manipulation. While time and cost are important factors in the microfluidic device development, the material properties, device quality and resolution can not be ignored. PEG-DA is a great candidate for making custom SLA 3D printer resins because it is copyright free and allows for changing mechanical properties with different concentrations of photoinitiator and photosensitizer. However, there is a limit of these additive concentrations in PEG-DA resin so that it is not as flexible and ductile as PDMS. PEG-DA is easier to be ruptured than PDMS since it is brittle (the property is more like plastic). A major task in the future is to enhance the mechanical properties by mixing with different additives (such as mixing with a high molecular PEG-DA but still maintain low porosity) or develop a whole new material which itself is more flexible and less fragile. The resolution of the printer is a key in the microfabrication development as well. It is known that the resolution of a photomask can be as high as 2 μm (XY resolution), in contrast, most the current SLA 3D printers in the market only have the resolution around 30 μm. Consequently, it is still a big challenge for a SLA 3D printer to print channels down to 10-μm in width and with 10-μm wide gaps, which restrict the numbers of components and complexity of a microfluidic system. Moreover, we observed that the resolution of a printer can have a huge impact on the device performance. For instance, the shape of the circle membrane in the 3D printed Quake style valve distorts when the diameter is 100 μm due to the limit of the XY resolution- which is 27 μm. As the size goes down, the peripheral of the circle becomes jagged, which might cause a different deformation when the membrane deflects. The Z resolution needs to improve as well. We realized that the bowl shape structure in the 3D printed Quake style valve affects the valve closing performance dramatically. The membrane does not seal against the valve seat well if the bowl shape structure is made with 25-μm Z-layer thickness compared to the 10-μm Z-layer thickness one. We anticipate that the resolution of 3D printers can be improved to print a higher quality device with better performance.

A more complex biomedical/biochemistry system can be introduced with the integration of 3D printed microfluidic control system- e.g. an automated cell culture system, multiplexer, DNA sequencing device, etc. With the using of 3D printed Quake style valve, more prototypes of these biomedical devices can be developed with a higher performance (PEG-DA is less gas

permeable than PDMS) and shorter fabrication time. The device fabrication time with PDMS grows exponentially as the complexity and the numbers of layers increase (alignment and assembly); nevertheless, the printing time only depends on the numbers of layers to be printed but not the size on the XY direction. As a result, we can take advantage of 3D printer's rapid-prototyping characteristic to develop a great number of different designs in a very short amount of time.

The other issue of the 3D printer is the printing interface between the surface of the vat and prints. Many 3D printer manufacture companies claim that their resin tray (vat) is anti-sticking, or they add some features (ex. Asiga's slider) to prevent the print from sticking to the vat. But the sticking problem still cannot be completely eradicated so that the yield of the print becomes lower when printing devices with thin layer thicknesses. Some anti-sticking features provided by the printer also creates new problems in prints, such as the scratches created by the slider under the vat and the tears and wears caused by the sheer force when the resin tray rotates. In the future, the chemical and physical properties of the vat need to be improved and customized for each resin for a better printing quality and yield.

References

1. Lee, Y.-S., Bhattacharjee, N. & Folch, A. 3D-printed Quake-style microvalves and micropumps. *Lab Chip* (2018). doi:10.1039/C8LC00001H
2. Unger, M. A. Monolithic Microfabricated Valves and Pumps by Multilayer Soft Lithography. *Science (80-.).* **288,** 113–116 (2000).
3. Bhattacharjee, N., Urrios, A., Kang, S. & Folch, A. The upcoming 3D-printing revolution in microfluidics. *Lab Chip* **16,** 1720–1742 (2016).
4. Au, A. K., Lee, W. & Folch, A. Mail-order microfluidics: evaluation of stereolithography for the production of microfluidic devices. *Lab Chip* **14,** 1294–1301 (2014).
5. https://www.elveflow.com/microfluidic-tutorials/microfluidic-reviews-and-tutorials/the-poly-di-methyl-siloxane-pdms-and-microfluidics/.
6. McDonald, J. C. *et al.* Fabrication of microfluidic systems in poly(dimethylsiloxane). *Electrophoresis* **21,** 27–40 (2000).
7. https://wallpapercave.com/old-computer-wallpaper.
8. https://www.pinterest.com/pin/310396599296448877/.
9. http://www.gene-quantification.de/lab-on-chip.html.
10. https://en.wikipedia.org/wiki/Lab-on-a-chip.
11. Whitesides, G. M. The origins and the future of microfluidics. *Nature* **442,** 368–373 (2006).
12. McDonald, J. C. & Whitesides, G. M. Poly(dimethylsiloxane) as a material for fabricating microfluidic devices. *Acc. Chem. Res.* **35,** 491–499 (2002).
13. Karkamkar, A. S. Improving the Manufacturability of Active Microfluidic Devices using Stereolithography (SL). (2016).
14. Armani, D., Liu, C. & Aluru, N. Re-configurable fluid circuits by PDMS elastomer micromachining. in *Technical Digest. IEEE International MEMS 99 Conference. Twelfth IEEE International Conference on Micro Electro Mechanical Systems (Cat. No.99CH36291)* 222–227 (1999). doi:10.1109/MEMSYS.1999.746817
15. Johnston, I. D., McCluskey, D. K., Tan, C. K. L. & Tracey, M. C. Mechanical characterization of bulk Sylgard 184 for microfluidics and microengineering. *J. Micromechanics Microengineering* **24,** (2014).
16. https://www.fluidigm.com/about/aboutfluidigm.
17. Waldbaur, A., Rapp, H., Länge, K. & Rapp, B. E. Let there be chip - towards rapid prototyping of microfluidic devices: One-step manufacturing processes. *Anal. Methods* **3,** 2681–2716 (2011).
18. Gross, B. C., Erkal, J. L., Lockwood, S. Y., Chen, C. & Spence, D. M. Evaluation of 3D printing and its potential impact on biotechnology and the chemical sciences. *Anal.*

Chem. **86,** 3240–3253 (2014).

19. https://labs.eng.hokudai.ac.jp/labo/tokeshi_lab/english/?research=miniaturized-liquid-chromatograph-based-on-on-chip-column-and-detector.
20. Au, A. K., Lai, H., Utela, B. R. & Folch, A. Microvalves and micropumps for BioMEMS. *Micromachines* **2,** 179–220 (2011).
21. Nge, P. N., Rogers, C. I. & Woolley, A. T. Advances in microfluidic materials, functions, integration, and applications. *Chemical Reviews* **113,** 2550–2583 (2013).
22. Kaigala, G. V., Hoang, V. N. & Backhouse, C. J. Electrically controlled microvalves to integrate microchip polymerase chain reaction and capillary electrophoresis. *Lab Chip* **8,** 1071 (2008).
23. https://web.stanford.edu/group/foundry/Available%20Valve%20Types.html.
24. https://www.microfluidicfuture.com/blog/microvalve-traffic-light-microfluidics.
25. Back, J. Y., Park, J. Y., Ju, J. Il, Lee, T. S. & Lee, S. H. A pneumatically controllable flexible and polymeric microfluidic valve fabricated via in situ development. *J. Micromechanics Microengineering* **15,** 1015–1020 (2005).
26. Hosokawa, K. & Maeda, R. Pneumatically-actuated three-way microvalve fabricated with polydimethylsiloxane using the membrane transfer technique. *J. Micromechanics Microengineering* **10,** 415–420 (2000).
27. Jacobson, S. C., Ermakov, S. V. & Ramsey, J. M. Minimizing the number of voltage sources and fluid reservoirs for electrokinetic valving in microfluidic devices. *Anal. Chem.* **71,** 3273–3276 (1999).
28. Tung, Y. C. & Takayama, S. Ionic liquids for microfluidic actuation: Multiplexed hydraulic valve actuation using ionic liquid filled soft channels and braille displays. in *ACS Symposium Series* **1030,** 157–173 (2009).
29. Laser, D. J. & Santiago, J. G. A review of micropumps. *J. Micromechanics Microengineering* **14,** R35–R64 (2004).
30. Grover, W. H., Skelley, A. M., Liu, C. N., Lagally, E. T. & Mathies, R. A. Monolithic membrane valves and diaphragm pumps for practical large-scale integration into glass microfluidic devices. *Sensors Actuators, B Chem.* **89,** 315–323 (2003).
31. Au, A. K., Bhattacharjee, N., Horowitz, L. F., Chang, T. C. & Folch, A. 3D-printed microfluidic automation. *Lab Chip* **15,** 1934–1941 (2015).
32. Sochol, R. D. *et al.* 3D printed microfluidic circuitry via multijet-based additive manufacturing. *Lab Chip* **16,** 668–678 (2016).
33. http://www.polysciences.com/media/catalog/product/cache/1/image/9df78eab33525d08d6e5fb8d27136e95/2/6/26279.png.
34. https://www.researchgate.net/profile/Raphael_Schneider2/publication/231224411/f

igure/fig3/AS:393322523840519@1470786805525/Scheme-2-Photoinduced-cleavage-of-Irgacure-819-and-reduction-of-gold-cations.png.
35. http://www.xtgchem.cn/upload/20110629045602.PDF.
36. https://www.sigmaaldrich.com/content/dam/sigma-aldrich/structure5/138/mfcd00055658.eps/_jcr_content/renditions/mfcd00055658-medium.png.
37. Kuo, A. P., Bhattacharjee, N. & Folch, A. High Resolution 3D-Printing of Transparent PEG-DA Microfluidic Devices. in (MicroTAS, 2017).
38. https://en.wikipedia.org/wiki/Beer%E2%80%93Lambert_law.
39. Gong, H., Beauchamp, M., Perry, S., Woolley, A. T. & Nordin, G. P. Optical approach to resin formulation for 3D printed microfluidics. *RSC Adv.* **5,** 106621–106632 (2015).
40. https://fslaser.com/Home/Landing/Phoenix.
41. Harrison, D. J. *et al.* Micromachining a Miniaturized Capillary Electrophoresis-Based Chemical Analysis System on a Chip. *Science (80-.).* **261,** 895–897 (1993).
42. Grover, W. H., Skelley, A. M., Liu, C. N., Lagally, E. T. & Mathies, R. A. Monolithic membrane valves and diaphragm pumps for practical large-scale integration into glass microfluidic devices. *Sensors Actuators, B Chem.* **89,** 315–323 (2003).
43. Laser, D. J. & Santiago, J. G. A review of micropumps. *Journal of Micromechanics and Microengineering* **14,** (2004).
44. Oh, K. W. & Ahn, C. H. A review of microvalves. *J. Micromechanics Microengineering* **16,** R13–R39 (2006).
45. Kim, J., Stockton, A. M., Jensen, E. C. & Mathies, R. A. Pneumatically actuated microvalve circuits for programmable automation of chemical and biochemical analysis. *Lab Chip* **16,** 812–819 (2016).
46. Glick, C. C. *et al.* Rapid assembly of multilayer microfluidic structures via 3D-printed transfer molding and bonding. *Microsystems Nanoeng.* **2,** 16063 (2016).
47. Hansen, C. L., Sommer, M. O. A. & Quake, S. R. Systematic investigation of protein phase behavior with a microfluidic formulator. *Proc. Natl. Acad. Sci. U. S. A.* **101,** 14431–6 (2004).
48. Li, N., Hsu, C. H. & Folch, A. Parallel mixing of photolithographically defined nanoliter volumes using elastomeric microvalve arrays. *Electrophoresis* **26,** 3758–3764 (2005).
49. Hsu, C. H. & Folch, A. Spatio-temporally-complex concentration profiles using a tunable chaotic micromixer. *Appl. Phys. Lett.* **89,** (2006).
50. Frevert, C. W., Boggy, G., Keenan, T. M. & Folch, A. Measurement of cell migration in response to an evolving radial chemokine gradient triggered by a microvalve. *Lab Chip* **6,** 849 (2006).
51. Cooksey, G. A., Sip, C. G. & Folch, A. A multi-purpose microfluidic perfusion system with combinatorial choice of inputs, mixtures, gradient patterns, and flow rates. *Lab*

Chip **9,** 417–426 (2009).
52. Hong, J. W., Studer, V., Hang, G., Anderson, W. F. & Quake, S. R. A nanoliter-scale nucleic acid processor with parallel architecture. *Nat. Biotechnol.* **22,** 435–439 (2004).
53. Ottesen, E. A., Hong, J. W., Quake, S. R. & Leadbetter, J. R. Microfluidic Digital PCR Enables Multigene Analysis of Individual Environmental Bacteria. *Science (80-.).* **314,** 1464–1467 (2006).
54. Maerkl, S. J. & Quake, S. R. A systems approach to measuring the binding energy landscapes of transcription factors. *Science* **315,** 233–237 (2007).
55. Gómez-Sjöberg, R., Leyrat, A. A., Pirone, D. M., Chen, C. S. & Quake, S. R. Versatile, fully automated, microfluidic cell culture system. *Anal. Chem.* **79,** 8557–8563 (2007).
56. Gu, W., Zhu, X., Futai, N., Cho, B. S. & Takayama, S. Computerized microfluidic cell culture using elastomeric channels and Braille displays. *Proc. Natl. Acad. Sci.* **101,** 15861–15866 (2004).
57. Lam, E. W., Cooksey, G. A., Finlayson, B. A. & Folch, A. Microfluidic circuits with tunable flow resistances. *Appl. Phys. Lett.* **89,** (2006).
58. Hsu, C. H. & Folch, A. Microfluidic devices with tunable microtopographies. *Appl. Phys. Lett.* **86,** (2005).
59. Thorsen, T. Microfluidic Large-Scale Integration. *Science (80-.).* **298,** 580–584 (2002).
60. Volpetti, F., Garcia-Cordero, J. & Maerkl, S. J. A microfluidic platform for high-throughput multiplexed protein quantitation. *PLoS One* **10,** (2015).
61. Gong, H., Bickham, B. P., Woolley, A. T. & Nordin, G. P. Custom 3D printer and resin for 18 μm × 20 μm microfluidic flow channels. *Lab Chip* (2017). doi:10.1039/C7LC00644F
62. Beauchamp, M. J., Nordin, G. P. & Woolley, A. T. Moving from millifluidic to truly microfluidic sub-100-μm cross-section 3D printed devices. *Anal. Bioanal. Chem.* **409,** 4311–4319 (2017).
63. Lee, W. *et al.* 3D-Printed Microfluidic Device for the Detection of Pathogenic Bacteria Using Size-based Separation in Helical Channel with Trapezoid Cross-Section. *Sci. Rep.* **5,** 7717 (2015).
64. Kitson, P. J., Rosnes, M. H., Sans, V., Dragone, V. & Cronin, L. Configurable 3D-Printed millifluidic and microfluidic 'lab on a chip' reactionware devices. *Lab Chip* **12,** 3267 (2012).
65. Keating, S. J. *et al.* 3D printed multimaterial microfluidic valve. *PLoS One* **11,** (2016).
66. Rogers, C. I., Qaderi, K., Woolley, A. T. & Nordin, G. P. 3D printed microfluidic devices with integrated valves. *Biomicrofluidics* **9,** (2015).
67. Waheed, S. *et al.* 3D printed microfluidic devices: enablers and barriers. *Lab Chip* **16,** 1993–2013 (2016).
68. Gong, H., Woolley, A. T. & Nordin, G. P. High density 3D printed microfluidic valves,

pumps, and multiplexers. *Lab Chip* **16,** 2450–2458 (2016).

69. Urrios, A. *et al.* 3D-printing of transparent bio-microfluidic devices in PEG-DA. *Lab Chip* **16,** 2287–2294 (2016).
70. Rogers, C. I. *et al.* Microfluidic valves made from polymerized polyethylene glycol diacrylate. *Sensors Actuators, B Chem.* **191,** 438–444 (2014).
71. Armani, D., Liu, C., Aluru, N. & Deniz Armani, Chang Liu, N. A. Re-Configurable Fluid Circuits By Pdms Elastomer Micromachining. *Micro Electro Mech. Syst. 1999. MEMS '99; IEEE Int. Conf.* 222–227 (1999). doi:10.1109/MEMSYS.1999.746817
72. Chou, H. P., Unger, M. A. & Quake, S. R. A microfabricated rotary pump. *Biomed. Microdevices* **3,** 323–330 (2001).
73. Wang, C.-H. & Lee, G.-B. Pneumatically driven peristaltic micropumps utilizing serpentine-shape channels. *J. Micromechanics Microengineering* **16,** 341–348 (2006).
74. Lai, H. & Folch, A. Design and dynamic characterization of 'single-stroke' peristaltic PDMS micropumps. *Lab Chip* **11,** 336–42 (2011).